GELATION OF REGENERATED FIBROIN SOLUTION

Submitted in partial fulfilment of the requirements
for the degree of

DOCTOR OF PHILOSOPHY

By

SHAILESH PRAKASH NAGARKAR
(Roll no 05430702)

Under the guidance of

Professor J. Bellare

and

Dr. A. K. Lele

DEPARTMENT OF BIOSCIENCES AND BIOENGINEERING
INDIAN INSTITUTE OF TECHNOLOGY, BOMBAY

2010

Thesis Approval

The thesis entitled

GELATION OF REGENERATED FIBROIN SOLUTION

by

SHAILESH PRAKASH NAGARKAR
(Roll No. 05430702)

is approved for the degree of
Doctor of Philosophy

Examiner Examiner Guide

Co Guide Chairman

Date:

Place:

Specimen ‘C’- Declaration

I declare that this written represent my ideas in my own words and where others’ ideas or words have been included, I have adequately cited and referenced the original sources. I also declare that I have adhered to all principles of academic honesty and integrity and have not misrepresented or fabricated or falsified any idea/data/fact/source in my submission. I understand that any violation of the above will be cause for disciplinary action by Institute and can also evoke penal action from the sources which have thus not been properly cited or from whom proper permission has not been taken when needed.

(Signature)

(Name of the student)

(Roll no.)

Date:-

Abstract

We have studied sol to gel transition of aqueous solutions of Regenerated Silk Fibroin (RSF) as a function of the pH, concentration and temperature. Fibroin is the structural protein of *B. Mori*. silkworm silk fibre. Fibroin can be extracted from silk fibres using several chaotropic salts; the same is then called RSF. Aqueous solutions of RSF are unstable especially at pH near the isoelectric point of fibroin, and turn into gels that are macroporous, biocompatible and possess excellent theromomechnical properties. These attributes enable the use of RSF gels as a biomaterial for cell culture and drug delivery. The present study is motivated by the fact that silk gels have potential applications as 3D scaffolds for tissue engineering. The scaffold microstructure is one of the primary characteristic that controls the environment experienced by the cells as well as dictates the mechanical properties of the gel. This thesis presents a detailed study of the RSF gel microstructure at various length scales and also throws some light on the gelation mechanism.

Silk fibroin was dissolved in lithium bromide and dialysed against deionized water to prepare RSF. Aqueous RSF solution gelled over a period of time, which depended strongly on the pH and only weakly on the temperature and fibroin concentration. Study of RSF gelation over 30 days at varying pH, concentrations and temperatures led to the development of a 'phase diagram'. Below the isoelctric pH, the gelation time varied between 10-16 hrs. Slightly above the isoelctric pH gelation time increased dramatically and gelation occurred over a period of few days to few weeks. In this study gelation was studied at pH ≤ pI, temperatures in the range 5 ^{o}C < T < 70 ^{o}C, and concentration in the range 0.5 g/L < C < 10 g/L.

The microstructure of gel was probed at various length scales ranging from molecular (1-10 nm) to mesoscopic (100-1000 nm) to macroscopic (~ few mm) using different characterization tools, namely Circular Dichorism (CD), Small Angle X-ray Scattering (SAXS), Light scattering and Confocal Laser Scanning Microscopy (CLSM). Below 10 nm the gel was made of rod like asymmetric structures. Above this length scale the structure was found to be self-similar up to about 1μm. The fractal dimension of 2 derived from scattering tools suggests random aggregation of the protein by the Reaction Limited Cluster Aggregation (RLCA) process. The secondary conformation of RSF as probed by CD changed from random coil to gel β sheet during gelation.

Kinetics of gel formation was tracked using Turbidity, Rheology, SAXS, Light scattering and CD. These studies showed that gelation involved the formation of self similar aggregates with a growth rate that increased exponentially. This supports a nucleation and growth (by RLCA) mechanism of gelation. At a molecular level protein aggregation was found to be correlated with the formation of β-sheets, the fraction of which also increased exponentially with time. This suggests that gelation is likely to be driven by β sheet formation.

Since gelation of RSF at pH > pI is a slow process, we have investigated a novel way of accelerating the gelation process. Gelation was induced using two different seeding methodologies: internal (or self) and external (or heterogenous) seeding. In both cases gelation time drastically reduced from a few days to a few hours. In the internal seeding process β sheets formed during RSF gelation at low pH were used as seeds. In the external seeding process stober silica nanoparticle were used as seeds. We hypothesized that fibroin is initially adsorbed on the silica particles whereupon it undergoes rapid conformation transition to β sheets, which further lead to RSF gelation. The gels formed via silica nanoparticles seeding were found to have enhanced mechanical properties.

Table of content

Chapter No Title Page no

LIST OF FIGURES

	per Reed model for data shown in (a).	

LIST OF TABLES

Nomenclature

β sheet	Beta sheet
$G^{'}$	Storage Modulus
D_b	Fractal dimension of elastic backbone
D_f	Fractal dimension of gel cluster
d_f	Fracatal dimension
n	Refractive Index
I_0	Incident monochromatic light
I_S	Scattered light
θ	Scattering Angle
(q)	Amplitude of wave vector
λ_0	Wavelength of light
N	Number of Particles
a	Diameter of particles
$\sigma\ (q)$	Total scattering cross section
I_r	Relative scattering intensity
M_w	Weight Average Molar Mass
$S(q)$	Structure Factor
K	Optical constant
R_θ	Rayleigh ratio
N_A	Avogadro's number
M_a	Apparent Molar mass
$G_2(t)$	Intensity Correlation function

$g_1(t)$	Auto Correlation Function
D_c	Diffusion Coefficient
A	Amplitude of mode
τ_{LS}	Decorrelation time of mode
R_h	Hydrodynamic radius
η	Solvent viscosity
k	Boltzmann's constant
γ	Shear strain
ω	Frequency
G''	Loss modulus
I	Moment of inertia
b	Parameter related to geometry of the measuring fixture
σ	Stress
$\dot{\gamma}$	Strain rate
J	Creep compliance
A	Fluorescence signal
$g(r)$	Pair correlation function
Δ	Small logarithmic decrement
Θ	Degree of ellipticity
τ	Turbidity
L	Path length
A_λ	Absorbance
K'	Optical constant for turbidity
$\Delta\rho$	Electron density difference between the particles and solvent
V	Volume of a single particle

ϕ_p	Volume fraction of particles
$P(q)$	Form factor
F_1	Form factor for homogenous sphere
R	Radius of sphere
T	Optical transmission
τ_s	Transmission coefficient of capillary
τ_{GC}	Transmission coefficient of Glassy carbon
B	Relative amplitude of the concentration fluctuations
ξ	Correlation length of the concentration fluctuations
α	Power law exponent
G_e	Elastic shear modulus of gel
η_1, η_2, G_J	Jeffery model parameters
t_g	Gelation time
t_c	Characteristic gel time
C_p	Silica particle concentration
ϕ	Volume fraction occupied by the particles
ρ_p	Density of silica particle

Acronyms

GPa	Giga Pascal
MTA	Metric ton per annum.
MPA	Mega Pascal
BMSCs	Bone Marrow Stromal Cells
RSF	Regenerated Silk Fibroin

PEO	Polyethylene Oxide
HFIP	Hexafluoroisopropanol
MSCs	Mescnchymal Stem Cells
SDS	Sodium Dodecyl Sulphate
CD	Circular Dichroism
f	Fibroin
s1-5	Sericin of five different molecular weight
kDa	Kilo Dalton
pI	Isoelectric pH
Ca	Calcium
K	Potassium
MD	Molecular Dynamics
TFA	Trifluoroacetic acid
PEG	Polyethylene Glycol
RPM	Rotation per Minutes
$Na_2 CO_3$	Sodium Carbonate
$NaHCO_3$	Sodium bicarbonate
LiBr,	Lithium Bromide
$CaCl_2$	Calcium Chloride
$Ca(CNS)_2$	Calcium cyanide
$ZnCl_2$,	Zinc Chloride
NH_4CNS	Ammonium cyanide
$CuSO_4$	Copper Sulphate
NH_4OH	Ammonium Hydroxide
$Ca(NO_3)_2$	Calcium Nitrite
MeOH	Methanol
EtOH	Ethanol

H_20	Water
β-lg	β-lactoglobulin
BSA	Bovine Serum Albumin
OA	Ovalbumin
NaCl	Sodium Chloride
RLCA	Reaction Limited Cluster Aggregation
DLCA	Diffusion Limited Cluster Aggregation
N_2	Nitrogen gas
PPM	Parts per million
3D-DLS	3D Dynamic Light Scattering
MWCO	Molecular weight cut off
RPM	Revolution per minutes
HCLH	Hydrochloric acid
NaOH	Sodium Hydroxide
GC	Glassy Carbon

Chapter 1

Introduction

1:1 Introduction to silk:

Silk is a natural fibre produced by more than 3000 species of spider and several types of worms including mites, butterflies and moths.[1] Silk is secreted by these insects in the form of a continuous filament. This filament provides structural role in cocoon formation, nest building, traps, web formation, safety lines and egg protection of the insect. Human civilizations have used silk as a textile fibre since antiquity. However research in the recent past has led us to appreciate the several interesting properties of silk fibres. For example, silk fibres are endowed with excellent toughness and stiffness, such that when combined with their low density the specific tensile strength can exceed that of steel and other man-made fibres. The excellent mechanical properties of silk combined with its biodegradability and environmental stability have, of late, attracted researchers working in diverse fields from materials science to biology, biochemistry, molecular biology, protein chemistry and bioengineering to look at silk as an engineering fibre with renewed interest.

Of all the silk spinning insects, silks from the domesticated silkworm *Bombyx mori* (*B. Mori*) and the spider Nephila Clavipes have been studied extensively because of their excellent thermo-mechanical properties and the possibility of producing them in commercial quantities. Spiders can produce silk throughout their life and use it for protection, reproduction and for aging, but silkworms can spin silk only after certain periods and during a specific stage of life. There are different types of silkworm and different breeds in each type. This classification is based on the number of generations produced per year (e.g., bivoltine versus multivoltine), larval growth rates, climate tolerance, disease resistance, silk yield and mechanical properties of silk.[2] In India four types of silkworms are found, *B. Mori* (mulberry), *Antheraea mylitta/Antheraea prolei* (Tasar), *Antheraea assama* (muga) *and Phylisomia ricini* (eri).[3] Spiders spin a wide range of silk fibres for many different purposes with high degree of variability that is determined by the physiological condition of the spider, spinning speed and temperature during spinning. The resulting fibres have surprisingly different mechanical properties. On the other hand the domestication of B. Mori has caused the insect to depend entirely on humans for feeding and protection, and correspondingly its silk has less degree of variation in its properties.[2] However, it has been shown that the mechanical properties of *B. Mori* silk can match those of spider silk if spun under controlled conditions of artificial spinning[4] as shown in Figure 1.1.

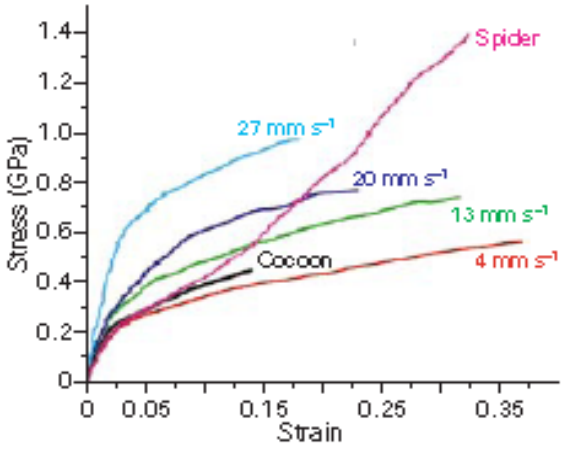

Figure 1.1: Stress strain curve for degummed single silk filament of *B. Mori*. (Shao Z. et al [4]; Reproduced with permission from Nature Publishing Group ©)

Commercial production of spider silk by deploying a large number of individual insects to spin silk or by expression of gene sequences in other organisms has been tried with limited success. In contrast a well developed sericulture industry presents a straightforward way to produce commercial quantities of silkworm silk. China has a long history of silkworm silk beginning from the 27th century BC. Silk was confined to China until the Silk Road opened at some point during the latter half of the first millennium BC. China maintained its virtual monopoly over silk for another thousand years. The Silk Road was eventually opened to western countries in the 2nd century AD. Today China is still the largest producer of silkworm silk (290 MTPA) followed by India which produces close to 77 MTPA of silkworm silk.[5]

B. Mori silk is a popular textile fibre in India. Silkworm silk has attractive features such as its pearl like gloss, velvety feel, comfortable and fashionable wear etc. The excellent mechanical properties of silk might have been realized in the early days as well. There are documented examples of the use of silk along with leather to make protective armours for soldiers especially to shield against arrows.[4] Being strong and light in weight the silk spun by insect has advantages over the other materials used for protection. The tensile strength of spider silk fiber is 1.1 GPa which is comparable to that of high strength tensile steel 1.3 GPa. On weight basis however, silk is stronger than steel because the density of silk is 1.3 g/cc while steel has density 7.8 g/cc. The strongest man-made engineering material Kevlar is three times stronger than spider silk but five times less tough and eight times less extensible

than spider silk.[6] For *B. Mori* silk Gosline et al reported a stiffness of 7 GPa, tensile strength of 0.6 GPa, extensibility 0.18 and toughness 70 MJM^{-3}.[7] J. Pe'rez- Rigueiro et al carried out careful measurements of the tensile properties on a single silk fibroin fibre.[8] They measured the diameter of the fibre accurately using SEM imaging and reported an elastic modulus value of 16±1 GPa, an tensile strength of 650 ± 40 MPa and a yield stress of 231 ± 14 MPa. It is increasingly being appreciated that these remarkable mechanical properties of silk fibre can lead to many technologically important applications in diverse fields other than textiles. For instance the ability of silk to absorb large amount of energy before failure along with high elongation strength attracts the use of these fibres in ballistic missiles.[9] It has been suggested that silk's high tensile strength can be useful in making cables or ropes for marine applications. Also, the high tensile strength and light weight fibres may find application in parachutes and hand gliders.[10]

The remarkable mechanical properties of silk fibres are a direct result of their complex self-assembled microstructure as explained in chapter 2. Moreover, such microstructure is created by an equally complex spinning process that has been perfected by insects over millions of years of continuous evolution. However silk fibres, both spider silk and silkworm silk, as spun by the natural spinning processes tend to show significant variability in properties. This is because the raw materials, namely the silk protein dope, and especially the spinning process conditions can only be controlled to a limited extent. Recently however, there have been several efforts in making silkworm silk fibres in laboratory by an artificial spinning process starting from an aqueous solution of silk.[11-13] It has been shown that the artificial spun fibres have close resemblance with the natural fibres in terms of their microstructure as well as properties.

1:2 Silk as a biomaterial:

In addition to fibres, silk and silk based materials are finding new applications in other areas. A major emerging application of silkworm silk is in making a variety of different biomaterials. *B mori* silk fibres were used as a suture for a long time, although synthetic biodegradable polymers such as poly(lactic acid) and its copolymers have nearly completely displaced silk from this application. However, there is a growing interest to explore applications of silk protein as a biomaterial for controlled release formulations and as scaffolds in tissue engineering.[14] However, some concerns have been raised regarding its

biocompatibility. It is now known that issues related to biocompatibility such as an adverse immuno response arise mainly because of sericin and also small amounts of a wax like material found on the fibre. As such pure fibroin is fully biocompatible. There is also a misconception about the non-biodegrability of silk. Many studies have reported that in fact silk is proteolytically degradable over a longer period. The degradation is mainly mediated by a foreign body response.[15, 16] Silk fibers when used as biomaterials *in vivo* show major loss of tensile strength over one year and are unrecognizable at the site within two years.[17] This shows that silk is slowly bioabsorbable *in vivo* but its rate of absorbtion depends on many parameters like implantation site, mechanical environment, diameter of fiber and variable parameters such as health and physiological status of the patient.[15, 16, 18]

Developments in the field of tissue engineering have increased the demand on various types of biomaterials to support the growth of tissues *in vitro* prior to implantation. The support material called as scaffold plays an important role as communicator between local environment and the seeded cells. The scaffold also requires properties catering to the attachment of cells, their differentiation and growth. Recent research has suggested that mechanical properties like the elastic modulus of scaffold could play an important role in the differentiation of stem cells.[19] The balance between rate of tissue growth and degradation rate of scaffold is also very important to avoid premature failure of tissue.

The combination of biocompatibility, mechanical robustness and long term bioabsorbability of a biomaterial is an essential condition for the growth of ligaments required for a high mechanical strength environment like the knee. Recently a process for making wire rope matrix of silk for autologous tissue engineered anterior cruciate ligaments using a patient’s own adult stem cells has been demonstrated. Human bone marrow stromal cells (BMSCs) were successfully attached, spread, proliferate on silk matrices.[20]

Silk based biomaterials of various sizes, shapes and microstructure can be prepared starting from regenerated silk solutions. Silk can be processed using different techniques into non woven mats, dried sponges, solvent sponges, hydogels and films.[1] Of these the three dimensional porous materials are better scaffolds for tissue engineering compared to two-dimensional films.[21] Different tissues demand different types of scaffolds. For example, porous sponge[22, 23] and hydrogels[24] scaffolds are well suited for cartilage tissue growth whereas ligament tissue requires stronger fibers.[25] Connecting tissue, endothelial tissue and

blood vessels require non-woven mats[26] while bone can be grown on sponge, films, hydrogels and non woven mats.[27-32]

Fibroin derived from *B. Mori*. silk can also be converted into other forms that are useful as biomaterials. This is done by first preparing an aqueous solution of the protein called the Regenerated Silk Fibroin (RSF) and then converting it into several valuable biomaterials such hydrogels, electrospun non-woven fabrics, sponges and films as scaffolds for tissue engineering of bone, cartilage, tendon and ligament tissue as shown in Figure 1.2.

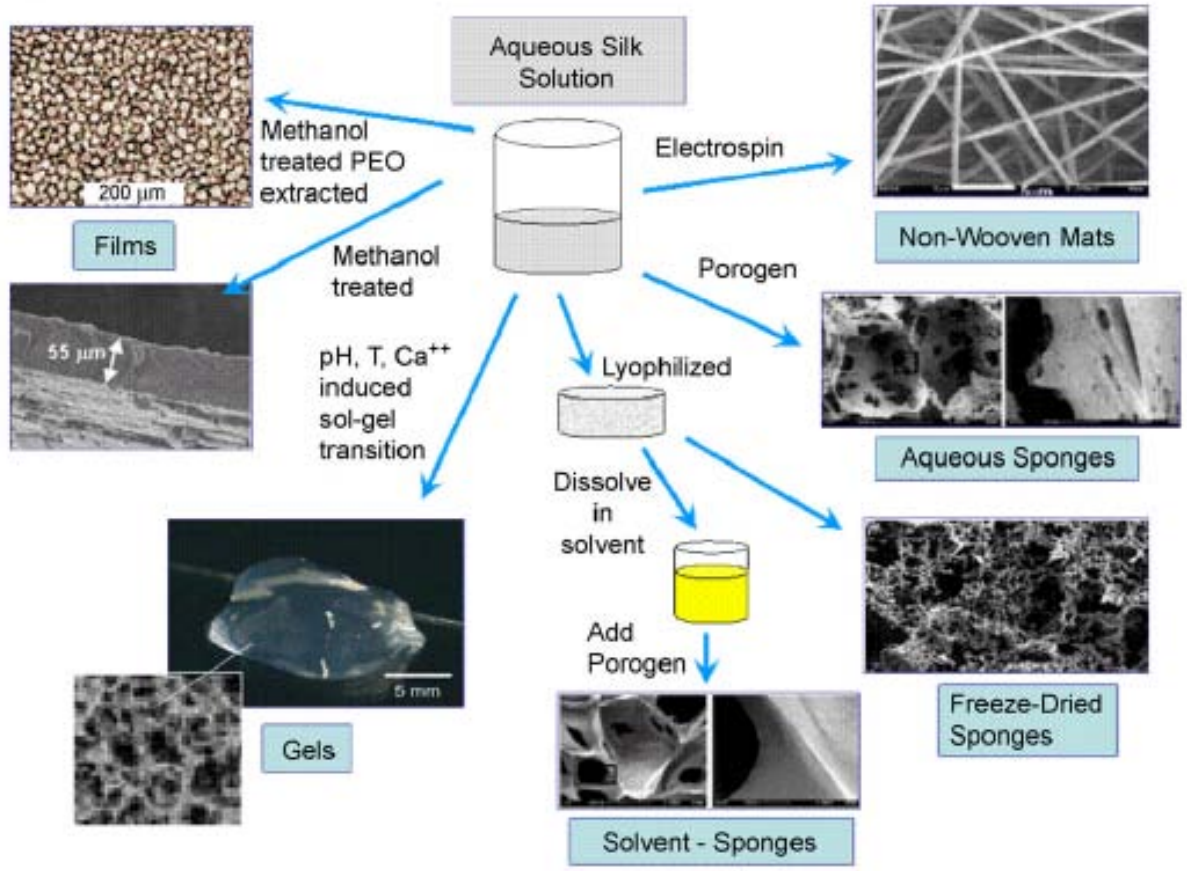

Figure 1.2: Various biomaterials prepared by processing aqueous silk fibroin solution. (Vepari C. et al [33]; Reproduced with permission from Elsevier ©)

1: 3 Motivation and objectives:

The work presented in this thesis involves hydrogels made from silk fibroin. In general, hydrogels are widely used as scaffolds for tissue engineering and as drug delivery vehicles. The main interest for using hydrogels to grow cells and tissues originates from the

fact that the mechanical properties of hydrogels, such as its compressive strength, and its internal environment, such as the amount of water absorbed in the gel, closely resemble those of the extra-cellular matrix. Kaplan D. et al have attempted bone tissue engineering from bone marrow stem cell using 3-D porous silk hydrogels as a scaffold.[34, 35] They prepared silk hydrogels from aqueous RSF solutions as well as from solutions in hexafluro isopropanol (HFIP) and studied their performance when Mesenchymal Stem Cells (MSCs) were grown in them. The water based silk hydogels had rougher topography than the HFIP derived hydrogel. Also the water based hydrogel had higher rate of enzymatic degradation, biocompatibility and scaffold remould into bone like tissue.

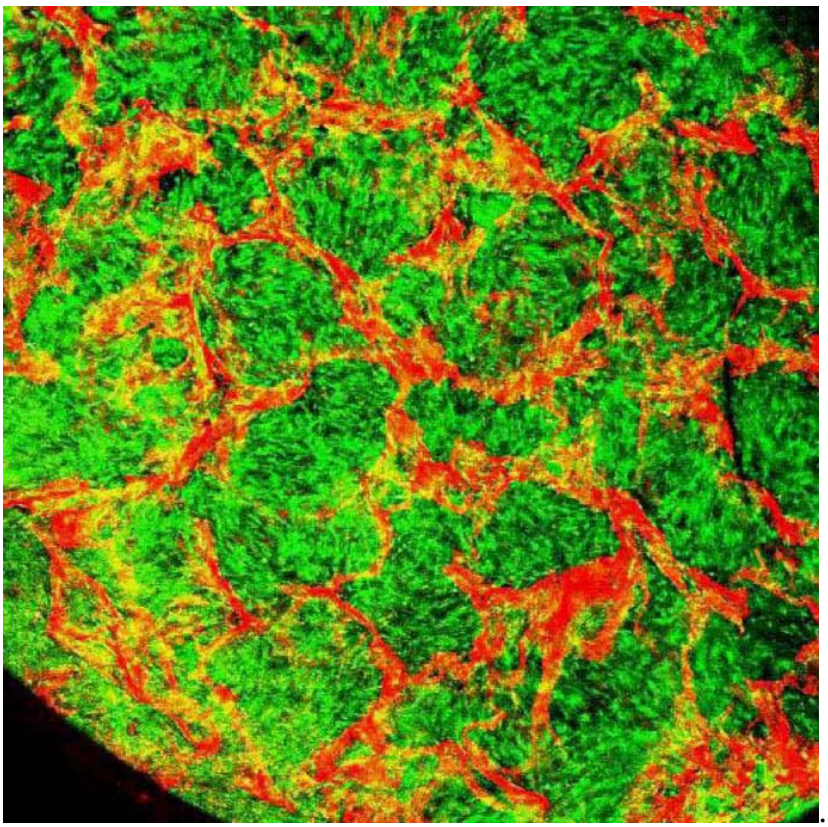

Figure 1.3: The human bone marrow derived from MSCs in 3 dimensional aqueous scaffold after 3 weeks was observed under confocal microscope. Green colour indicates live cells and red colour mostly silk fibroin and dead cells (Wang Y. Z. et al [35]; Reproduced with permission from Elsevier ©)

It has been shown that free flowing aqueous regenerated silk fibroin solutions can be converted into non-flowing gels by changing the pH, temperature, fibroin concentration and ionic strength of the solution.[36] The gels are macroporous, a feature suitable for cell

growth, and have significant content of β sheets, which makes the gels stiff. It has also been shown that the modulus of the gel can be tuned by controlling the fibroin concentration.[37] However, the physical processes underlying the formation of silk fibroin hydrogels and their morphology are not completely understood. The morphology of a hydrogel scaffold is important because it governs the topology of the local environment experienced by the cells. The morphology also dictates the mechanical properties of the gel. Furthermore the fine scale morphology of a hydrogel also ensures appropriate supply of nutrients to the growing cells. In this context the primary aims of the work presented in this thesis are

- Investigate the microstructure of fibroin hydrogels.
- Understand how the microstructure evolves during gelation.

The specific objectives of the work are

- Preparation of RSF gels at pH ≤ pI, temperatures in the range 5 ^{o}C < T < 70 ^{o}C, and in the concentration range 0.5 g/L < C < 10 g/L
- Probing the microstructure of RSF gels at different length scales namely, at the level of chain conformation, at meso-scale (i.e., 2 – 800 nm) and at micro-scale (i.e., 1 – 50 μm) using various techniques such as circular dichroism, small angle x-ray scattering, light scattering, turbidity and confocal microscopy.
- Measuring the mechanical properties of RSF gels using shear rheology and compression tests.
- Probing the time evolution of the microstructure at different length scales during gelation to gain mechanistic insights into the gelation process.
- Using the knowledge gained to accelerate the gelation of RSF solutions at pH > pI where the process is usually very slow.

The work carried out towards meeting these objectives is presented in this thesis as follows. A detailed literature survey on various topics relevant to this work is presented in chapter 2. Section 2.1 presents information on silk proteins: fibroin and sericin, including their amino acid sequence and molecular weights. Section 2.2 explains the natural and artificial silk spinning processes, and section 2.3 discusses the structure of silk fibres.

Section 2.4 summarizes literature on the process for making Regenerated Silk Fibroin (RSF) and its characterization using light scattering and SDS gel page. In section 2.5 a survey of literature on the gelation of other proteins is presented. The section discusses mechanisms of gelation and the structure of gels, and how these can be derived using various techniques.

The materials and methods used for the characterization of silk gel and for the investigation of the gelation process are explained in chapter 3. Section 3.3 provides background on the experimental techniques used for characterization and the associated data analysis. The experimental techniques used in this work are Light scattering, Rheology, Confocal Laser Scanning Microscopy (CLSM), Circular Dichroism (CD), Turbidity and Small angle X-ray scattering. Section 3.4 explains the detailed experimental protocols used in this work for all above techniques. The preparation and characterization of RSF is explained in sections 3.5 and 3.6 respectively. The preparation of RSF sol and experimental results on its stability are presented in sections 3.7 and 3.8 respectively.

In chapter 4 the main results that enable understanding of the microsture of RSF gels at various length scales from molecular to macroscopic are presented. Experimental results on CD (section 4.1.1), turbidity measurements (section 4.1.2), static and dynamic light scattering (section 4.1.3), CLSM (section 4.1.4) and small angle x-ray scattering (section 4.1.5) are presented and discussed in detail. Inferences about the microstructure of the RSF gels are drawn based on the synthesis of all this data. The elastic shear modulus and compression modulus of gels were measured and its concentration dependence is shown in section 4.1.6.

Chapter 5 is concerned with studies on the kinetics of gelation of RSF sol at various length scales using the same experimental techniques. In section 5.1.1 the results of isothermal creep measurements done on RSF sols during gelation are presented. Simultaneous measurements on turbidity and rheology are presented in section 5.1.2. The concentration, pH and temperature dependence of gelation time as also presented in this section. The evolution of fractal microstructure was tracked using light scattering and this is presented in section 5.1.3. The evolution of structure at finer length scales was also observed using SAXS and the same is discussed in section 5.1.4. Finally, studies on conformation transition observed during gelation are presented in section 5.1.5. Synthesis of all this data and the inferences drawn from them are presented in section 5.2. Section 5.3 presents the main conclusions of this part of the work.

In chapter 6 we studied gelation at higher pH 7, 8 and 9. Here two methods are explored for RSF gelation silica assist gelation explained in 6.2 and self seeding gelation explained in 6.3. The gel time measurement protocol and experimental techniques used in gelation is explained in 6.3.1. Recommendations for future work are given in section 6.4.

Chapter 2

Literature review

2.1 Silk protein:

Silk fibre is made of two different proteins – the core structural protein called fibroin and the gummy sheath protein called sericin. In *B. Mori* silk the ratio of sericin to fibroin is roughly 1:3. Fibroin is synthesized by special cells in the posterior part of the silk gland while sericin is secreted by cells lining the middle part of the gland (see Figure 2.6). During the growth of the silkworm as the fibroin moves from the posterior part to the middle part of the silk gland it gets coated with sericin. Thus a silk fibre has a core-sheath structure. Figure 2.1 shows that a single silk fiber (bave) is actually made up of two filaments (brins) of fibroin, which are coated with sericin.

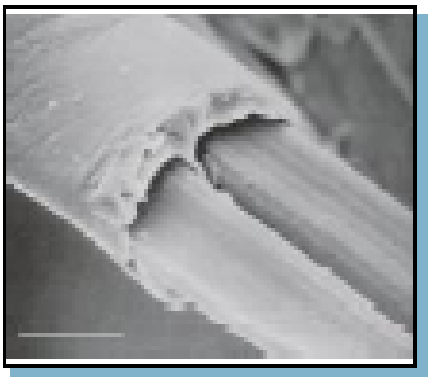

Figure 2.1: SEM micrograph of single silk fiber (Shao Z. et al [38]; Reproduced with permission from Nature Publishing Group ©)

2.1.1 Fibroin:

The structure of fibroin is discussed in greater detail here as it is relevant to the present work. Silk fibroin belongs to the class of fibre forming structural proteins; other examples of this category are keratin and collagen. A protein consists of a chain of amino acids, each of which is made of four groups. Three of the groups namely an amine group ($-NH_2$), a carboxyl group ($-COOH$), and hydrogen ($-H$), are common to all amino acids and are bound to a carbon molecule called the α-carbon. The fourth group of each amino acid, the "R" group or the side chain, varies and the diversity of silk proteins is derived from the different size, shape, charge, and chemical reactivity of this group. In addition, the interactions among the R-groups are affected by the rotation of the amino acid around the α-carbon which in turn allows the silk protein to fold in a variety of ways. Figure 2.2 shows the structure of three of the most abundant amino acids in *B. mori* fibroin.

Figure 2.2: Structure of four most abundant amino acid groups found in *B. mori* silk.

B. mori silk is composed of a light (L) (~ 25 kDa) and a heavy (H) fibroin chain (~ 350 kDa). While the L-chain of fibroin has 262 amino acid residues the H-chain has 5263 amino acid residues of which the major contribution (in mol %) comes from 42.9% glycine (G), 30.0% alanine (A), 12.2% serine (S), 4.8% tyrosine (Y), 2.5% valine(V) and 7.6% other remaining amino acids.[39] The composition of the *B. mori* fibroin is shown in Table 2.2. The H and L fibroin chains are linked to each other by a disulfide bond[40] between Cys-172 of the L Chain and Cys-c 20 (20^{th} residue of C terminus) of the H chain.[41] Recent reports also suggest the presence of P25, a glycoprotein of 30kDa, along with the H and L chain of fibroin. P25 is linked to H chain with purely physical association (mainly hydrophobic interaction) without covalent linkage.[42] The molar ratio of H chain, L chain and P25 is 6:6:1.[43]

Table 2.1: Amino acid composition for fibroin. (Sashina E.S. et al [39] ; Applied for reproduce permission)

Amino acid	Composition in mol %		
	Total	Heavy peptide chain	Light peptide chain
Glycine (g)	42.9	49.0	10.0
Alanine (a)	30.0	29.8	16.0
Serince (s)	12.2	11.3	7.9
Tyrosine	4.8	4.6	3.4
Valine (v)	2.5	2.0	7.4
Aspartic acid	1.9	0.65	15.4
Glutamic acid	1.4	0.70	0.85
Threonine	0.92	0.45	2.8
Phenylalanine	0.67	0.39	2.7
Methionine	0.37	-	0.37
Isoleucine	0.64	0.14	7.3
Leucine	0.55	0.09	7.2
Proline	0.45	0.31	3.0
Arginine	0.51	0.18	3.8
Histidine	0.19	0.09	1.6
Lysine	0.38	0.06	1.5

The amino acid sequences of the *B. Mori.* heavy fibroin chain and the light fibroin chain are available from Genbank and are given below.[44]

H-chain:

1 mrvktfvilc calqyvaytn anindfdedy fgsdvtvqss nttdeiirda sgavieeqit
61 tkkmqrknkn hgilgknekm iktfvittds dgnesiveed vlmktlsdgt vaqsyvaada
121 gaysqsgpyv snsgysthqg ytsdfstsaa vgagagagaa agsgagagag ygaasgagag
181 agagagagyg tgagagagag ygagagagag agygagagag agagygagag agagagygag
241 agagagagyg agagagagag ygaasgagag agygqgvgsg aasgagagag agsaagsgag
301 agagtgagag ygagagagag agygaasgtg agygagagag yggasgagag agagagagag
361 agygtgagyg agagagagag agagygagag agygagygvg agagygagyg agagsgaasg
421 agsgagagsg agagsgagag sgagagsgag agsgagagsg agagsgagag sgtgagsgag
481 agygagagag ygagagsgaa sgagagsgag agsgagagsg agagsgagag sgagagygag
541 agagygagag agygagagvg ygagagsgaa sgagagsgag agsgagagsg agagsgagag
601 sgagagsgag agsgagagsg agagsgagvg ygagvgagyg agygagagag ygagagsgaa
661 sgagagagag agtgssgfgp yvanggysrs dgyeyawssd fgtgsgagag sgagagsgag
721 agsgagagsg agagsgagag ygagvgvgyg agygagagag ygagagsgaa sgagagsgag
781 agsgagagsg agagsgagag sgagagsgag agsgagagsg agagsgagag sgagvgsgag
841 agsgagagvg ygagagvgyg agagsgaasg agagsgagag sgagagsgag agsgagagsg
901 agagsgagag sgagagsgag agsgagvgyg agvgagygag ygagagagyg agagsgaasg
961 agagsgagag sgagagsgag agsgagagsg agagsgagag sgagagsgag agsgagagsg
1021 agagsgagag ygagagagyg agygagagag ygagagsgaa sgagsgagag sgagagagsg
1081 agagsgagag sgagagsgag agsgagagsg agagygagvg agygagygag agagygagag
1141 sgaasgagag sgagagsgag agsgagagsg agagsgagag sgagagsgag vgygagygag
1201 agagygagag sgaasgagag agagagtgss gfgpyvahgg ysgyeyawss esdfgtgsga
1261 gagsgagags gagagsgaga gsgagygagv gagygagyga gagagygaga gsgagsgaga
1321 gsgagagsga gagsgagags gagagsgaga gsgagagsga gagsgagagy gagygagaga
1381 gygagagsga gsgagagsga gagsgagags gagagsgaga gsgagagsga gagsgagagy
1441 gagvgagyga gygagagagy gagagsgags gagagsgaga gsgagagsga gvgsgagags
1501 gagagsgaga gsgagagyga gygagagagy gagagsgags gagagsgaga gsgagagsga
1561 gagsgagags gagagsgaga gsgagvgyga gvgagygagy gagagagyga gagsgaasga
1621 gagagagagt gssgfgpyva nggysgyeya wssesdfgtg sgagagsgag agsgagagsg
1681 agagsgagag ygagygagag agygagagsg agsgagagsg agagsgagag sgagagsgag
1741 agsgagagsg agagsgagsg sgagagsgag agsgagagyg agvgagygvg ygagagagyg
1801 agagsgaasg agagagagag tgssgfgpyv ahggysgyey awssesdfgt gsgagagsga
1861 gagsgagags gagagsgaga gsgagagsga gagygagvga gygaaygaga gagygagags
1921 gaasgagags gagagsgaga gsgagagsga gagsgagags gagagsgaga gsgagagsga
1981 gagsgagagy gagagagyga gagsgagsga gagsgagags gagagsgaga gsgagagsga
2041 gsgsgagags gagagsgaga gygagvgagy gagygagaga gygagagsga gsgagagsga
2101 gagygagaga gygagygaga gagygagagt gagsgagags gagagsgaga gsgagagsga
2161 gagsgagags gagsgsgaga gsgagagsga gagsgagags gagagsgaga gygagagagy
2221 gagygagaga gygagagsga gsgagagsga gagsgagags gagagygagy gagagsgaas
2281 gagagagaga gtgssgfgpy vahggysgye yawssesdfg tgsgagagsg agagagagag
2341 sgagagygag vgagygagyg agagagygag agsgtgsgag agsgagagyg agvgagygag
2401 agsgaafgag agagagsgag agsgagagsg agagsgagag sgagagygag ygagvgagyg

2461 agagsgaasg agagsgagag sgagagsgag agsgagagsg agagygagvg agygagygag
2521 agagygagag sgaasgagag sgagagagsg agagsgagag sgagagsgag sgagagsgag
2581 agsgagagyg agagsgaasg agagagagag tgssgfgpyv anggysgyey awssesdfgt
2641 gsgagagsga gagsgagags gagagsgaga gygagvgagy gagygagaga gygagagsga
2701 gsgagagsga gagsgagags gagagsgaga gsgagagsga gagygagags gaasgagags
2761 gagagsgaga gsgagagsga gagsgagags gagagygagv gagygvgyga gagagygaga
2821 gsgagsgaga gsgagagsga gagsgagags gagsgagags gagagsgaga gsgagsgaga
2881 gsgagagygv gygagagagy gagagsgags gagagsgaga gsgagagsga gsgagagsga
2941 gagsgagags gagagygagv gagygvgyga gagagygaga gsgagsgaga gsgagagsga
3001 gagsgagags gagagsgaga gsgagagsga gsgagagsga gagsgagags gagagsgags
3061 gagagsgaga gsgagagsga gagygagvga gygvgygagv gagygagags gaasgagags
3121 gagagagsga gagsgagags gagagsgaga gsgagagsga gagygagyga gvgagygaga
3181 gvgygagaga gygagagsga asgagagags gagagtgaga gsgagagyga gagsgaasga
3241 gagagagagt gssgfgpyva nggysgyeya wssesdfgtg sgagagsgag agsgagagsg
3301 agagsgagag ygagvgagyg agagsgagsg agagsgagag sgagagsgag agsgagagyg
3361 agagsgtgsg agagsgagag sgagagsgag agsgagagsg agagsgvgag ygvgygagag
3421 agygvgygag agagygagag sgtgsgagag sgagagsgag agsgagagsg agagsgagag
3481 sgagagygag vgagygvgyg agagagygag agsgagsgag agsgagagsg agagsgagag
3541 sgagsgagag sgagagsgag agsgagsgag agsgagagyg vgygagagag ygagagsgag
3601 sgagagsgag agsgagagsg agsgagagsg agagsgagag sgagagygag vgagygvgyg
3661 agagagygag agsgagsgag agsgagagsg agagsgagag sgagagsgag agsgagagsg
3721 agsgagagsg agagsgagag sgagagygag vgagygvgyg agagagygag agsgaasgag
3781 agagagagtg ssgfgpyvan ggysgyeyaw ssesdfgtgs gagagsgaga gsgagagyga
3841 gygagvgagy gagagvgyga gagagygaga gsgaasgaga gagagagsga gagsgagaga
3901 gsgagagyga gygigvgagy gagagvgyga gagagygaga gsgaasgaga gsgagagsga
3961 gagsgagags gagagsgaga gsgagagyga gygagvgagy gagagvgyga gagagygaga
4021 gsgaasgaga gagagagags gagagsgaga gsgagagsga gagsgagags gagagsgaga
4081 gsgagagsga gagygagvga gygagyggag agygagagsg aasgagagsg agagsgagag
4141 sgagagsgag agsgagagyg agagsgaasg agagagagag tgssgfgpyv nggysgyeya
4201 wssesdfgtg sgagagsgag agsgagagyg agvgagygag ygagagagyg agagsgaasg
4261 agagsgagag sgagagsgag agsgagsgag agsgagagsg agagsgagag sgagagsgag
4321 agygagvgag ygagygagag agygagagsg aasgagagsg agagagsgag agsgagagsg
4381 agagsgagag sgagagsgag sgagagsgag agygagygag vgagygagag vgygagagag
4441 ygagagsgaa sgagagsgsg agsgagagsg agagsgagag agsgagagsg agagsgagag
4501 ygagygagag sgaasgagag agagagtgss gfgpyvangg ysgyeyawss esdfgtgsga
4561 gagsgagags gagagygagv gagygagyga gagagygaga gsgagsgaga gsgagagsga
4621 gagsgagags gagagsgaga gsgagagsga gagygagyga gagagygaga gvgygagaga
4681 gygagagsga gsgagagsgs gagagsgsga gsgagagsga gagsgagags gagagsgaga
4741 gsgagagsga gagygagygi gvgagygaga gvgygagaga gygagagsga asgagagsga
4801 gagsgagags gagagsgaga gsgagagsga gagsgagags gagagsgaga gygagagvgy
4861 gagagsgaas gagagsgaga gsgagagsga gagsgagags gagagsgaga gsgagsgaga
4921 gsgagagyga gygagvgagy gagagygagy gvgagagyga gagsgagsga gagsgagags
4981 gagagsgaga gsgagagsga gsgagagyga gagagygaga gagygagags gaasgagaga
5041 gagsgagags gagagsgags gagagsgaga gygagagsga asgagagsga gagagagaga
5101 gsgagagsga gagygagags gaasgagaga gagtgssgfg pyvanggysr regyeyawss
5161 ksdfetgsga asgagagags gagagsgaga gsgagagsga gaggsvsyga grgygqgags
5221 aassvssass rsydysrrnv rkncgiprrq lvvkfralpc vnc

L-chain

>gi|19221230|gb|AAL83649.1| silk fibroin [*B. mori*]

1 mkpiflvllv atsayaapsv tinqysdnei prdiddgkas svisrawdyv ddtdksiail
61 nvqeilkdma sqgdyasqas avaqtagiia hlsagipgda caaanvinsy tdgvrsgnfa
121 gfrqslgpff ghvgqnlnli nqlvinpgql rysvgpalgc agggriydfe aawdailass
181 dsgflneeyc ivkrlynsrn sqsnniaayi tahllppvaq vfhqsagsit dllrgvgngn
241 datglvanaq ryiaqaasqv hv

Structural analysis of the H-chain suggests that the primary structure of *B. mori* silk fibroin may be approximately divided into two types of regions: repetitive regions R(X) (X=1 to 12) each of which is internally subdivided into three smaller regions, a, b, and c and amorphous regions AY (Y=1 to 11), arranged alternately with the repetitive regions along the molecular chain. Within each repetitive region, region ‘a’ is the highly repetitive GAGAGS sequence which constitutes the crystalline part of the fibroin (94% of total chain), region ‘b’ is the relatively less repetitive GAGAGY and/or GAGAGVGY sequences consisting of the semi-crystalline parts which contain hydrophobic moieties, and region ‘c’ is similar to region ‘a’ plus an additional AAS chain. The amorphous regions contain negatively charged, polar, bulky hydrophobic and aromatic residues.[45] Figures 2.3 and 2.4 depict a schematic representation of the primary structure. The crystalline repetitive region is responsible for the secondary structure (anti-parallel β-pleated sheets) of the protein. It is widely believed that the crystalline domains are responsible for the remarkable strength of the silk fibres, whereas the amorphous domains allow the crystalline domains to orient under strain thereby introducing flexibility and further increasing the strength of the material.

Further coarse-graining of the primary sequence of the heavy chain of fibroin protein suggests a pattern comprising two large hydrophilic blocks one each at the chain ends, six smaller internal hydrophilic blocks and seven interspersed hydrophobic blocks.[46] The hydrophobic blocky sequences are ultimately responsible for the formation of strong hydrogen bonded antiparallel beta sheets in the silk fibre. The hydrophilic blocks on the other hand play an important role in preventing premature crystallization of the silk dope into insoluble beta sheets inside the silkworm’s glands.

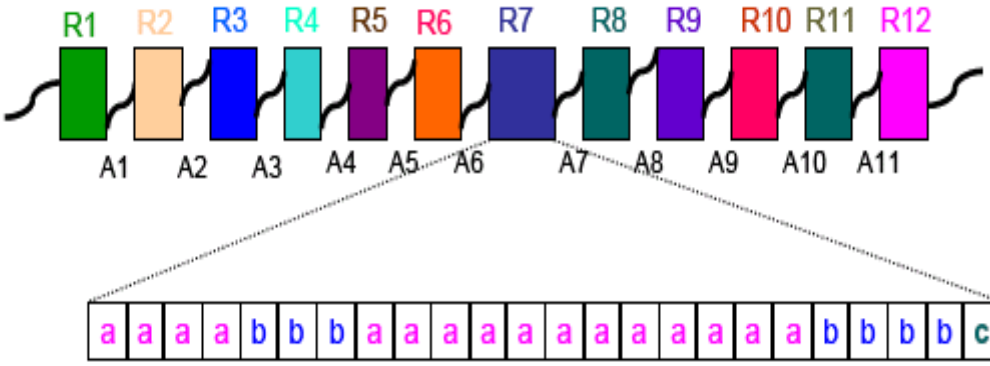

Figure 2.3: Schematic representation of the primary structure of *B. mori* silk. (Asakura T. et al [47]; Reproduced with permission from ACS Publications ©)

R (1 to 12) - Repetitive crystalline regions

a- (GAGAGS) (Hydrophobic blocks)

b- (GAGAGY) and/or (GAGAGVGY)

c- (GAGAGSGAAS)

A - Amorphous regions

Among the hydrophilic blocks, the end blocks are called the N-terminus and the C-terminus.[48] Under the conditions of pH existing in the silk spinning pathway, the N-terminus is on the average negatively charged (its isoelectric point is 4.6), while the C-terminus is positively charged (its isoelectric point is 10.5). However, it is also known that the light fibroin molecule is covalently attached to the heavy fibroin molecule via disulfide linkage at the C-terminus. Since the light fibroin chain is on the average negatively charged and is as much as five times longer than the C-terminus, one can effectively say that the fibroin complex has negative charges at either ends. Further, in the interspersed hydrophilic spacer blocks the negatively charged amino acid side chains far outnumber the positively charged amino acid side chains and hence these blocks show a uniform negative charge distribution. This charge distribution results in an overall isoelectric pH of 3.9-4.0 for fibroin.[49]

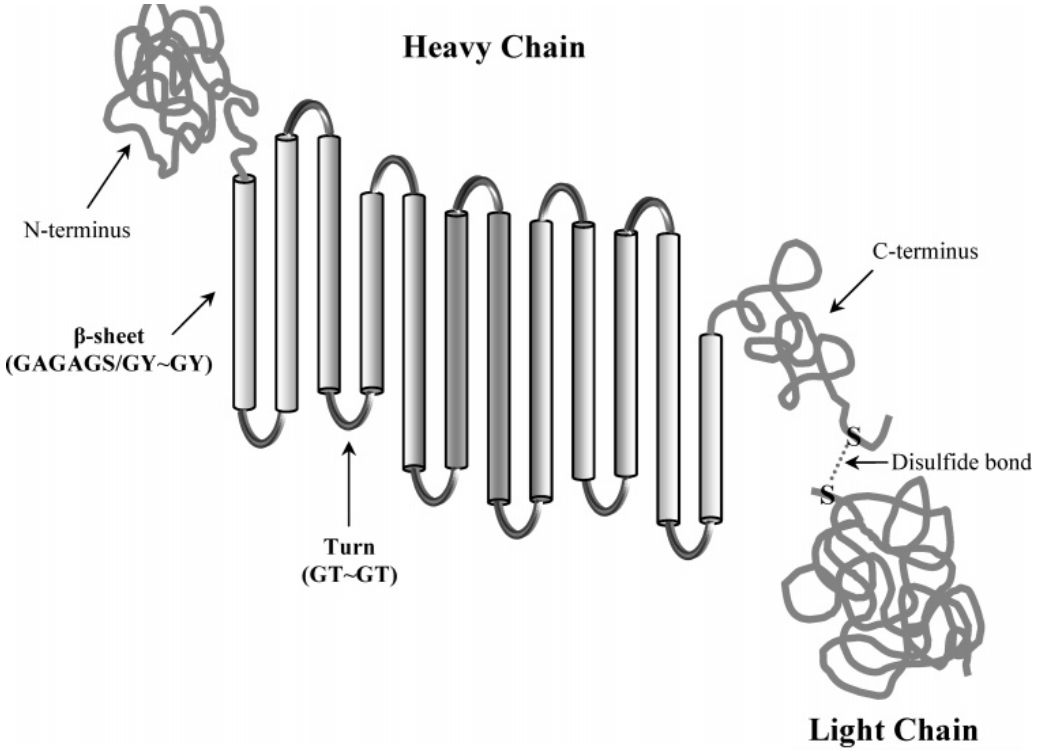

Figure 2.4: Schematic representation of H-L chain (Ha S. et al [50]; Reproduced with permission from ACS Publications ©)

The molecular weights of heavy and light chains of fibroin have been measured using various techniques like light scattering[51], SDS gel page with markers and chromatography.[52] For these different measurements the fibroin was either derived directly from the silk gland of the silkworm or from the silk fibre. In the former case the fully grown silkworm (5^{th} instar) was sacrificed to extract fibroin from various parts of the silk gland and was dissolved in 8 M Urea or 6 M Gdn. HCL solvent. Electrophoresis analysis was carried out using a polyacrylamide gradient gel (concentration ranging from 3-5%). The data suggested that the fibroin recovered from silkworm has molecular weight of 350,000 dalton. SDS gel page using polyacrylamide gel of higher concentration (up to 15%) did not show this major protein but revealed a faint band at 25,000 Da molecular weight corresponding to the light chain.

In summary, the H-chain of fibroin has a microstructure that resembles a multiblock copolymer comprising alternately placed hydrophobic and hydrophilic blocks. A unique feature of the hydrophobic blocks is that they have highly repetitive sequences of glycine and alanine, which are thought to be responsible for the formation of the tightly hydrogen bonded antiparallel beta-sheet structure in the silk fibres. The molecular weight of the H-chain is

about 350 kDa. The L-chain of fibroin has a random sequence of amino acid residues. It has a molecular weight of 25 kD and it is attached to the C terminus of the H-chain with a disulfide bond. The isoelectric point of the overall fibroin chain (H + L chains) is at a pH of about 4.0.

2.1.2 Sericin:

Sericin is the gummy sheath-forming protein of silk fibre containing 18 different amino acids as shown in Table 2.2. Because of the larger quantities of hydrophilic amino acids such as serine and aspartic acid, sericin is relatively more water soluble than fibroin. [53] It is a globular protein and comprises five different molecular weight moieties (s1, s2, s3, s4 and s5) which are synthesized in different regions of the middle silk gland.[54] The main role of sericin is to coat and bind the fibroin strands and give hardness and toughness to the cocoon.

Gamo T. et al carried out gel electrophoresis of proteins recovered from different parts of the silk gland.[54] Their data is reproduced in Figure 2.5. The letters f and s in Figure 2.5 stand for fibroin and sericin, respectively, and the numbers at the bottom indicate the regions along the silk gland as follows: (1) the posterior gland, (2) the posterior section of the middle gland, (3) the rear section of the middle section of middle gland, (4) the fore part of the middle section of the middle gland, and (5) is the anterior section in the middle gland. The molecular weights of s1 – s5 were found to vary between 8.1×10^4 and 1.34×10^5 dalton. The sericin peptide s-4 from region (4) had a molecular weight of approximately 8.0×10^4 dalton. Sericin peptides s1 and s3 secreted from the middle section of the middle gland have molecular weights of approximately 3.09×10^5 and 1.45×10^5 dalton, respectively. For peptides s-2 and s-5, secreted from the anterior section of the middle gland, their molecular weights were determined to be 1.77×10^5 and 1.34×10^5 dalton, respectively.[54]

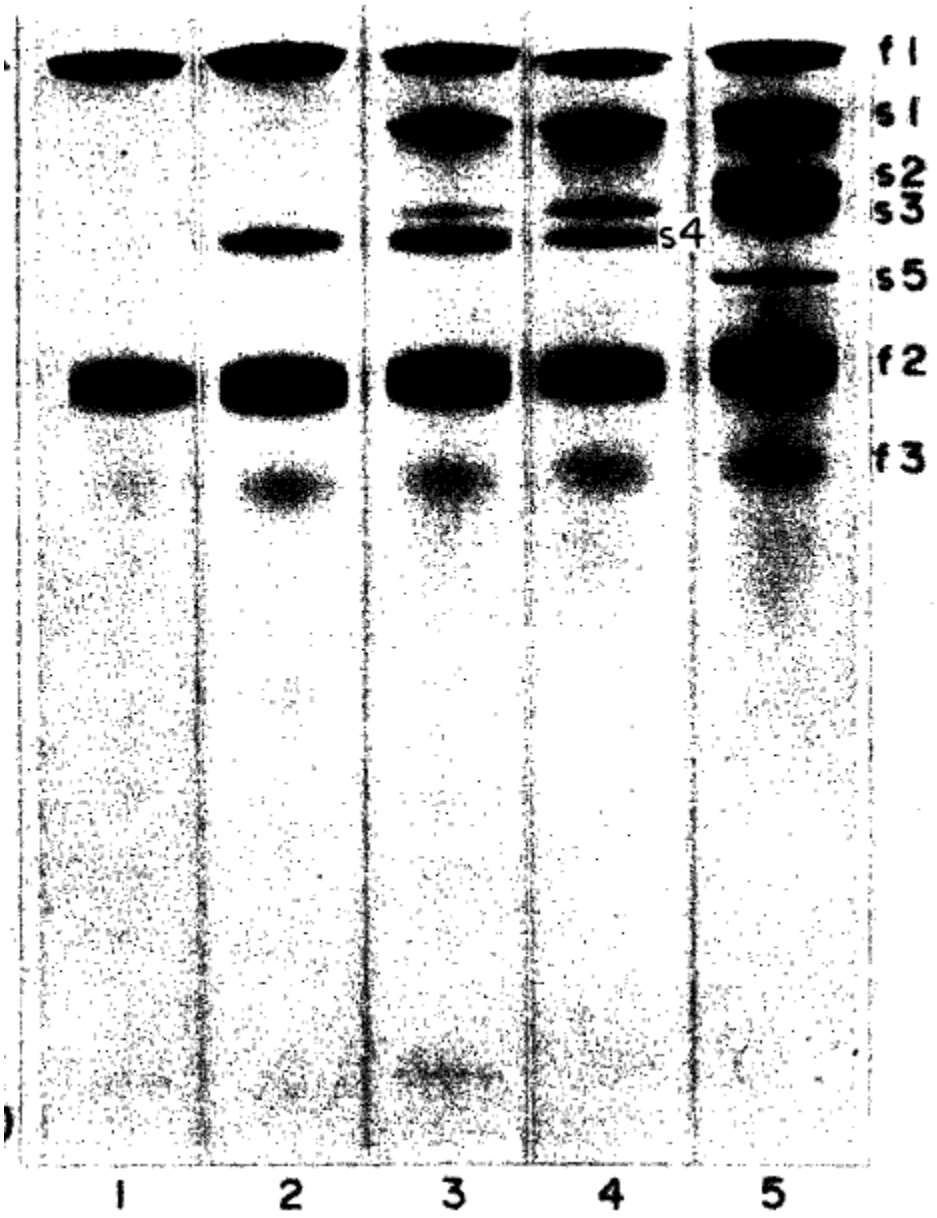

Figure 2.5: SDS gel page of sericin. (Gamo T. et al [54] ; Reproduced with permission from ACS Publications ©)

Table 2.2: Amino acid composition for sericin (Gamo T. et al [54] ; Reproduced with permission from ACS Publications ©)

Amino acid	s-1	s-2	s-3	s-4	s-5	Sericin
Glycine (g)	18	12.5	14.2	11.4	17.5	13.9
Alanine (a)	6.2	6.9	6.2	4.2	7.2	4.6
Valine (v)	3.7	2.8	1.0	3.8	0.3	3.2
Leucine (s)	2.1	1.5	0.6	2.8	2.7	1.2
Isoleucine	1.6	1.3	0.4	1.8	2.2	0.7
Serine	29.1	30.2	38.1	32.5	16.4	32.3
Threonine	8.5	8.0	4.1	11.1	4.0	8.4
Aspartic acid	13.0	12.9	12.6	11.6	13.9	14.5
Glutamic acid	5.4	5.2	10.7	6.1	10.3	4.8
Lysine	2.2	4.8	5.3	2.2	6.3	8.4
Arginine	4.0	3.9	3.0	3.6	3.5	2.3
Histidine	1.6	1.5	0.8	1.9	3.1	1.6
Tyrosine	3.3	6.8	2.1	2.8	9.0	2.6
Phenylalanine	1.5	0.7	0.4	3.4	1.2	0.4
Proline	Trace	Trace	Trace	Trace	Trace	0.4
Methionine	Trace	Trace	Trace	Trace	Trace	0.1
Cystine (half)	Trace	1.0	0.5	0.7	2.5	0.3

2.2 Natural and Artifical spinning of silk fiber:

2.2.1 Natural Silk spinning:

Fibroin and sericin are synthesized and stored in the silk glands of the silkworm. The silk glands are a pair of tubes lying one on each side of the larva as shown in Figure 2.6. Each gland is divided in three parts depending on the secretion of the protein. The posterior part, which is closed at one end, is narrow and very convoluted. The epithelial wall of this part consists of large hexagonal cells in which the main structural silk protein fibroin comprising the H- and L- chains along with the accessory protein P25 is synthesized. The fibroin moves forward into the wider, middle division which essentially plays the role of a protein reservoir. Here, the silk protein is stored in the form of a highly concentrated (~30 wt %) aqueous solution. The second protein, sericin, is synthesized in this section and forms a coat on the fibroin protein. The silk dope consisting of the two proteins moves forward without mixing into the anterior part, which becomes narrower as it approaches the final region of the gland namely, the spinneret.

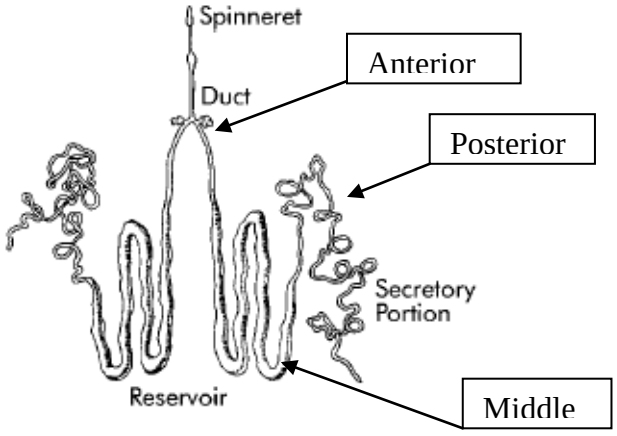

Figure 2.6: The silk spinning pathway for *B. Mori* silkworm. (Willcox P. J. et al [55]; Reproduced with permission from ACS Publications ©)

Approximately 25-28 days after hatching, a silk worm is fully grown and ready to spin silk. The silk dope from the two glands flows out through the spinneret in the form of two fine strands of viscous fluid which join in one double thread that hardens while passing through a nozzle. The thread is spun by the joint forces of drawing (from outside) and

ejection (from inside). While spiders pull on the thread during the act of spinning, the silkworm pulls the silk thread using the side by side movement of its head producing a characteristic figure of eight pattern.[56] Inside the silk gland various chemical and physical parameters such as pH, ionic concentration, diameter of the gland, shear rate, and protein concentration change along the journey of the protein from the middle division to the spinneret. The spinning process is complex and till date the mechanism of fibre formation is still not fully understood.

The interplay between the charge distribution along the fibroin chain, the changes in the pH along the silk spinning pathway from the middle division to the anterior division, and the presence of external metal ions in the silk dope such as Ca^{2+} and K^{+} are important in determining the self assembly of the fibroin chains during their conversion from a water soluble state inside the gland into a water insoluble state in the extruded silk fibre.[48] The State of liquid silk fibroin in different parts of the silk gland of *B. Mori* and changes in chemical parameters such as pH, ion concentration and water content is shown in table 2.3. The predicted pI of the N-terminus of the heavy fibroin chain in *B. Mori.* is 4.6, that of the light chain (which is bound to the C termini of the heavy chain as described earlier) is 5.06, while the pI of the interspaced hydrophilic blocks in the heavy chain is 4.03. These values indicate that the fibroin chains are uniformly negatively charged. Thus every chain is effectively a polyelectrolyte, which in an aqueous solution may be expected to attain an extended conformation due to charge repulsions. Figure 2.7 shows a schematic of the changes in pH along the various regions of the silk spinning pathway. As shown in Figure 2.7 the pH decreases from 6.9 to 5.2 from the posterior division to the middle division, and to 4.8 in the anterior part of the silk gland.

Figure 2.8 shows TEM image of a cross section of the duct region of the silk gland of *B. mori*. The observed banding is a result of bright-field image contrast arising from thicker regions of enhanced electron scattering power that appear dark, juxtaposed with thinner regions which appear lighter.[55] The pattern is characteristic of a cholesteric liquid crystal compound in the glassy state and is caused during microtoming of a solid-phase cholesteric parallel to the helical axis by a sinusoidal surface topography produced due to the preferential crack propagation along the spatially varying director field

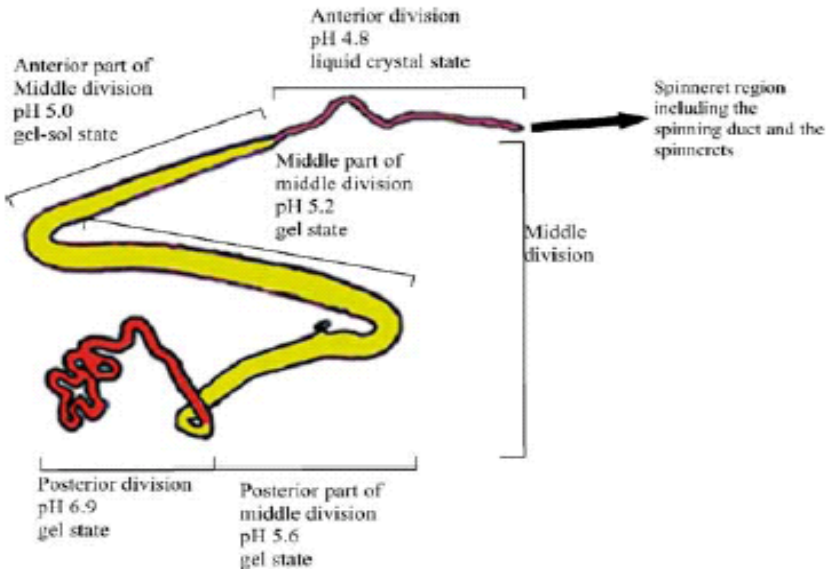

Figure 2.7: Schematic diagram of the silk gland of *B. mori*, showing the divisions in the gland and the pH and the states of the silk fibroin. (Foo C.W.P et al [48]; Reproduced with permission from Springer ©)

.

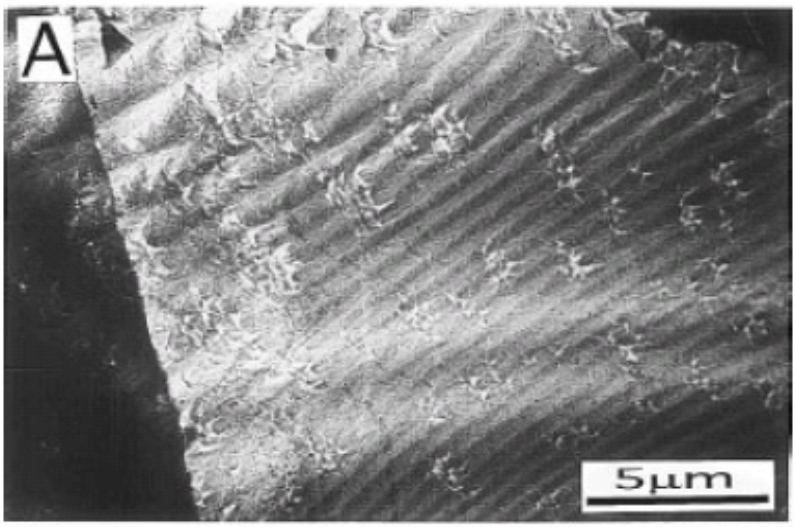

Figure 2.8: Bright field TEM image of section taken from the silk gland of *B. mori*. (Willcox P. J. et al [55]; Reproduced with permission from ACS Publications ©)

Figure 2.9 shows that the diameter of the anterior duct narrows exponentially towards the orifice. This helps to maintain a low and constant elongational flow of protein solution as it flows through the duct.[57, 58] This also helps to prevent premature silk I to silk II

transformation of fibroin during the silk spinning process inside the duct. Birefringence study on fibroin present at the start of the duct shows existence of a nematic liquid crystal texture similar to that of spider's protein (spidroin) in analogous region of duct.[59] Further down in the duct at a diameter of about 60 μm this birefringence vanishes, which is in contrast with what happens in spidroin. After that in the draw down taper region at a location of about 4 mm before the silk press there is secretion of hydrogen ions into the lumen, which further lowers the pH. This changes the protein interaction in the silk dope causing it to partially gel. The partially gelled fibroin then undergoes a unique draw down process in which it leaves the wall of the lumen as it is pulled by the downstream silk press. This drawdown is accompanied by an increase in molecular alignment of fibroin. The gel state of the fibroin is critical to the success of the draw down process. Too much of gelation can cause the fibroin to precipitate and block off the duct while too little of gelation will not result in the desirable draw down. The continuous non-birefringent layer of sericin is found to break up in the draw down taper region to form large irregular droplets suggesting that the fibroin remains in fluid state. The drawn fibroin then passes through the silk press, which is essentially a die with an elongated constriction. The silk press acts like a micropump or valve and regulates the crossectional area of duct under muscle control.[59] The shear and elongational flow imposed by the silk press causes an increase in the alignment of fibroin chains as evidenced by a further increase in birefringence. This ultimately results in the complete conversion of silk I to silk II.

A complimentary picture of structural changes in fibroin during the spinning process was suggested by Jin H.J. et al.[46] The microstructural changes are a result of the interplay between the primary structure of fibroin and changes in the aqueous environment along the spinning pathway. Due to the high pH in the posterior and middle division the fibroin molecules are in an extended conformation, and are also complexed with divalent ions to form a gel. This state changes inside the duct due to the combination of pH reduction, water absorption and flow into a compact liquid crystalline state that is stabilized by intermolecular attractive and repulsive forces. Further downstream the amphiphilic fibroin chains associate into a hairpin-type chain folded partially hydrated micellar structure comprising irregular sized globular micelles 100 – 200 nm in size. The larger terminal hydrophilic blocks form the outer shell of the micelles, while the hydrophobic blocks form the core along with the interconnected smaller internal hydrophilic blocks which remain hydrated in the initial stages

of fibroin protein assembly. The hydration of the internal blocks avoids premature β sheet (Silk II) formation. As the concentration of fibroin protein increases, the interaction between micelles increases leading to their aggregation and formation of globules of size 0.6 to 15 μm. This aggregation transforms the silk dope once again into a gel state. Shearing or elongation of the gel state in the duct may cause orientation and stretching of the globules.[46] The self assembled structure of fibroin heavy chain is shown schematically in Figure 2.10. This complex structural transformation finally results in the formation of a hierarchy of meso-scale structures in the silk fiber itself. The structure of a fractured silk fiber is shown in Figure 2.11. It shows that the core of the fiber comprises of globules, while the smooth skin comprises of sericin.

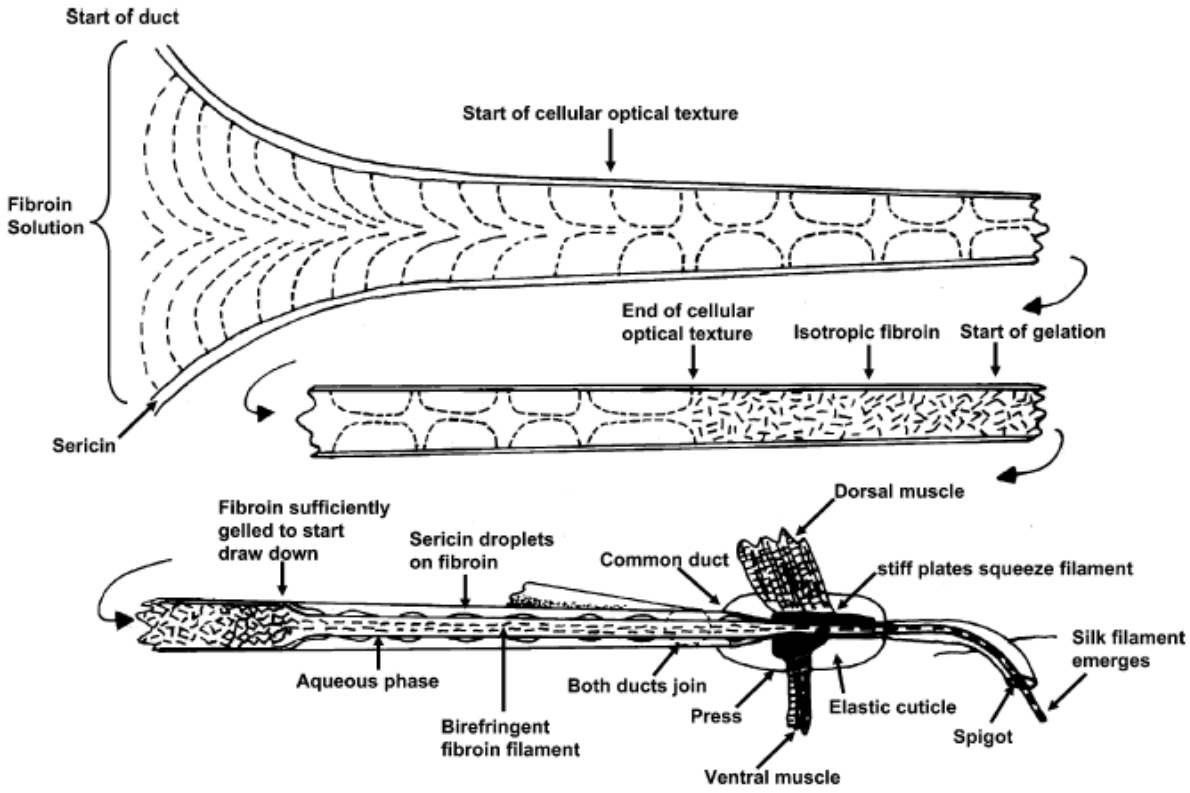

Figure 2.9: A schematic of B. Mori silkworm's duct summarising observations about the structural changes happening during spinning of silk fiber. (Asakura T. et al [59]; Reproduced with permission from ACS Publications ©)

Kataoka et al have reported in situ changes in viscosity, birefringence and wide angle X-ray scattering pattern at different parts of secretory pathways.[60] They have estimated a critical stain rate required for conversion of silk fibroin solution to β sheet.[60] Yamane et al

have done Molecular Dynamic (MD) simulation to understand silk spinning mechanism and structural transition during silk spinning. Their results suggest that structural transformations happen because of mainly two reasons: removal of water molecules from silk solution and wall shear and extensional flow of solution.[61] The dimensions of the glands and the distribution of the cross-sectionally averaged shear rates in the silk gland have been estimated at a typical spinning velocity of 1.0 cm/s and are shown in Figure 2.12.[62]

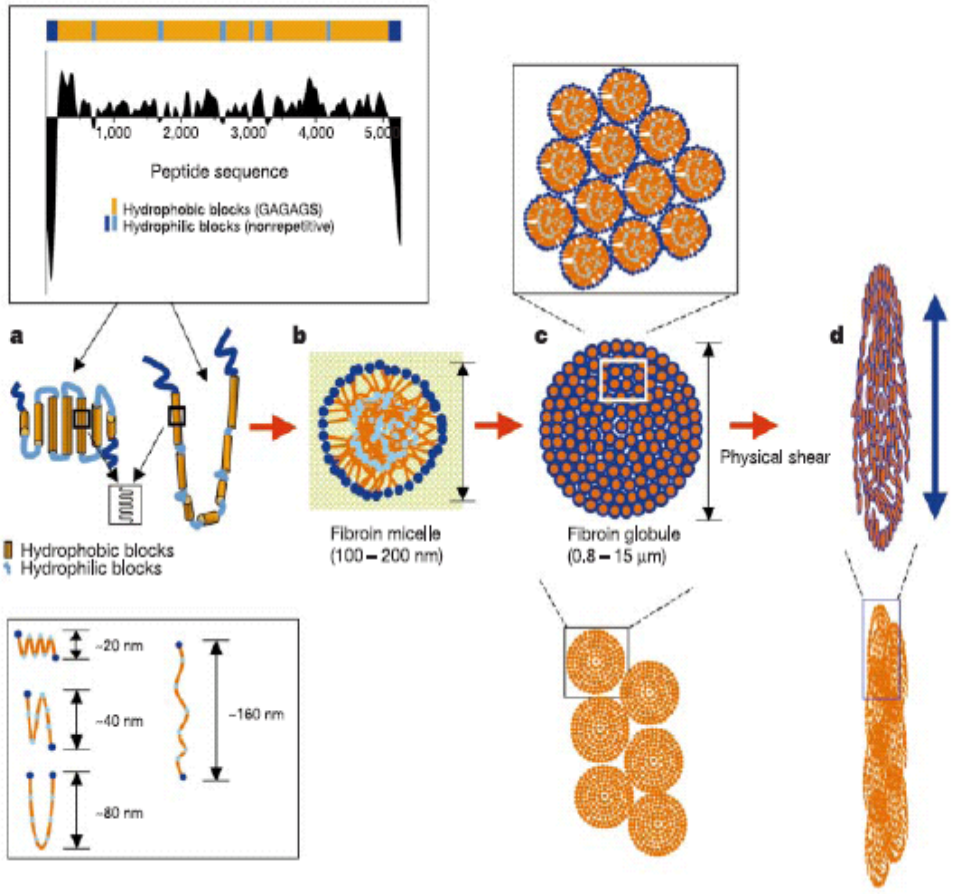

Figure 2.10: Schematic representation of the proposed model of chain folding, micelle formation, globule formation and shearing process of silk protein. (a) Blocky pattern of heavy chain fibroin in *B. mori* (b) Micelle assembly of silk fibroin in water (c) Globule formation by aggregation. (d) Elongation and alignment of globules. (Jin H.J. et al [46]; Reproduced with permission from Nature Publishing Group ©)

In summary, the spinning process converts a highly concentrated lyotropic silk dope into a strong water insoluble fibre having a complex structural hierarchy at different length scales. Several mechanistic aspects of the fibre forming process have been elucidated in

recent years by research groups from diverse disciplines. One particular aspect of the spinning process is perhaps of direct relevance to the present work. This pertains to the partial gelation of the silk dope under the action of a reduction in pH. The detailed study of gelation of aqueous fibroin solution investigated in this work might have bearing on the fiber formation process.

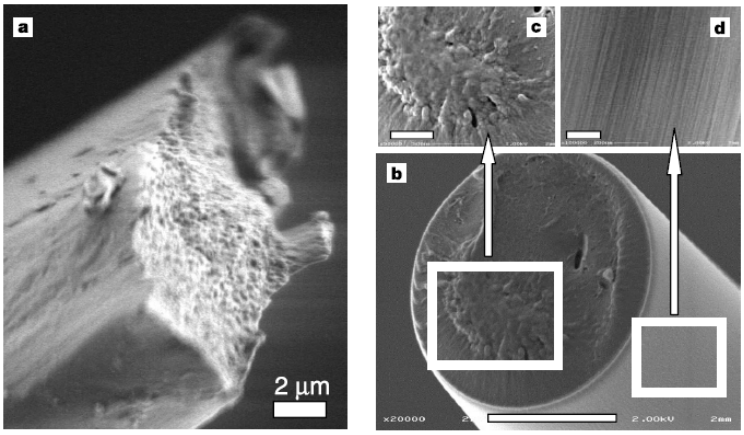

Figure 2.11: SEM image of the fracture fiber, (b) shows the micelle substrate and skin coat of aligned fibrillar structure in the absence of Sericin. (Jin H.J. et al [46]; Reproduced with permission from Nature Publishing Group ©)

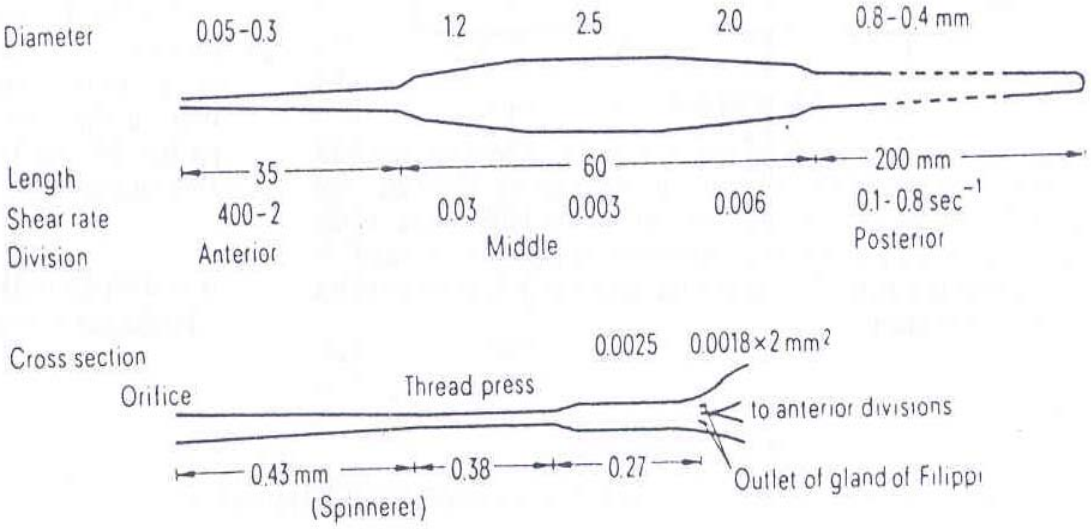

Figure 2.12: Profile of the dimension and distribution of shear rate for the silk gland and the spinneret.[63]; Applied for reproduce permission)

Table 2.3: State of liquid silk fibroin in different parts of the silk gland of *B. Mori* and changes in chemical parameters such as pH, ion concentration* and water content*. (Foo C.W.P. et al.[48]; Reproduced with permission from Springer ©)

Silk Gland	Posterior division	Middle division			Anterior division
		Posterior	Middle	Anterior	
pH	6.9	5.6	5.2	5.0	4.8
Viscosity	middle	high	high	high	Low
state	gel	gel	gel	Gel-soln	Liquid crystal
K+	-	30.2	29.5	33.3	-
Ca+	-	17.7	46.0	59.7	-
Water content	88	75	74	74	70

*Percentage are calculated on the based on atomic mass and overall composition

2.2.2 Artificial spinning:

On a related note it is worth mentioning here briefly the efforts of several reseachers who have attempted to spin fibers from aqueous silk solutions. Jelinski et al prepared 2.5 wt% *B. Mori* silk solution in HFIP and spun fibers using a microfabricated wet spinning apparatus.[64] The silk solution was pumped using a micro syring pump at a flow rate of 15 μL/s into a methanol column. The protein is insoluble in methanol hence it coagulate into fiber. This process is different in many ways than natural silk spinning process. The artifically spun fibers were mechnically tested using an Instron tensile tester and their data sugessts that they were able to achieve properties such as the maximum stress under load that were close to the naturally spun fibers.[64]

Sung- Won ha et al prepared aqeuous silk solution by dissolving fibroin in calcuim nitrate tetrahydrate and dialysing extensively. The aqueous solution of fibroin was spun using a benchtop extrusion apparatus with spinnerets of diameters 0.254, 0.381 and 0.508 mm. The solution was pressurised using nitrogen gas cylinder so that it can pass through the spinnerets with desirable spinning speed. The non solvent methol was used as a coagulant and was kept near the spinneret exit. The solution coming out of the spinneret and solidifying in the coagulant bath was passed though a downstream water bath for washing. The spun fiber was elastic in wet state but as the water evaporated it became brittle.[13] In a more recent article Sung- Won ha et al have shown that the properties of the spun fibers are dependent on the details of the spinning method. They showed that upon coagulating the silk in an acidic dope followed by drawing the fibers their modulus and strength increased considerably. They also freeze dried the dialysed silk solution into a powder, which was then redissolved into a mixture of formic acid and trifluro acetic acid (TFA) and spun using their benchtop scale extrusion apparatus.[65] The mechanical properties like tenacity of these regenerated wet spun silk were found to be better than the native silk fiber.

Xin Chen et al developed a more economical and environment friendly method of wet-spinning that can potentially be scaled up to industrial scale.[12] In this process aqueous Regenerated Silk Fibroin (RSF) solution was prepared by concentrating a dialysed silk solution using reverse dialysis against polyethylene glycol (PEG). The RSF solution was extruded into a hot ammonium sulphate solution which was used as a coagulant. Extruded fibers (I) were initially wound on a take up role of RPM 50 and then drawn down using two identical take up rolls with different RPMs, 100 and 200 to produce fiber with draw ratios II and III. Further, Fiber III was drawn manually to 1.5 times it’s lengths by steam annealing to give fiber IV. The mechanical properties like breaking stress, strain and energy of fiber IV was found to be superior to the properties of naturally spun B. Mori silk fiber.

2.3 Hierarchical structure of silk fiber:

The remarkable mechanical properties of a silk fiber are related to its meso-scale structure which consists of co-existing amorphous and crystalline domains. Structural characterization of silk suggests that peptide chains in fibroin are bound together by hydrogen bonds to form sheet like crystalline structures.[66] Typical hydrogen bonded β sheets formed between glycine and alanine, which are the predominant amino acid residues of the H-chain

fibroin, are shown in Figure 2.13. More detailed studies reveal that two different crystal structures, silk I and silk II, are present in the silk fibre.[67-69] The silk I structure is a precursor of β sheets and is found in abundance in the spinning pathway inside the silkworm. The silk I structure then changes to multiple local secondary structures to form silk II, which is found in the silk fiber.[70, 71] The silk II structure was found to have β sheet conformation. Wide angle x-ray scattering studies have confirmed the presence of β sheet crystallites in both spider dragline silk and silkworm silk cocoon.[9, 66, 69]

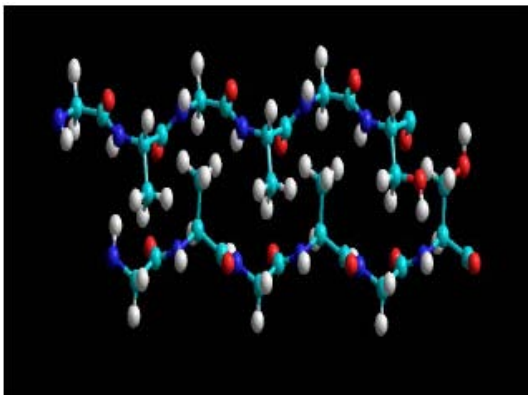

Figure 2.13: Anitiparallel β sheet structure

Thus, a schematic picture of the hierarchical structure of silk fiber is shown in Figure 2.14. A single bave of silk cocoon comprises two fibroin brins coated and bound together with a sericin coat. The fibroin filaments themselves are composed of nanofibrils, each of which has a semi-crystalline mesoscale structure comprising crystalline domains in β sheet conformations separated and connected with amorphous regions of fibroin chains. A single fibroin chain can pass through several crystalline domains since it has the microstructure of a multiblock copolymer as explained earlier. The hydrophobic blocks can associate to form the crystalline domains while the hydrophilic blocks are retained in the amorphous domains.

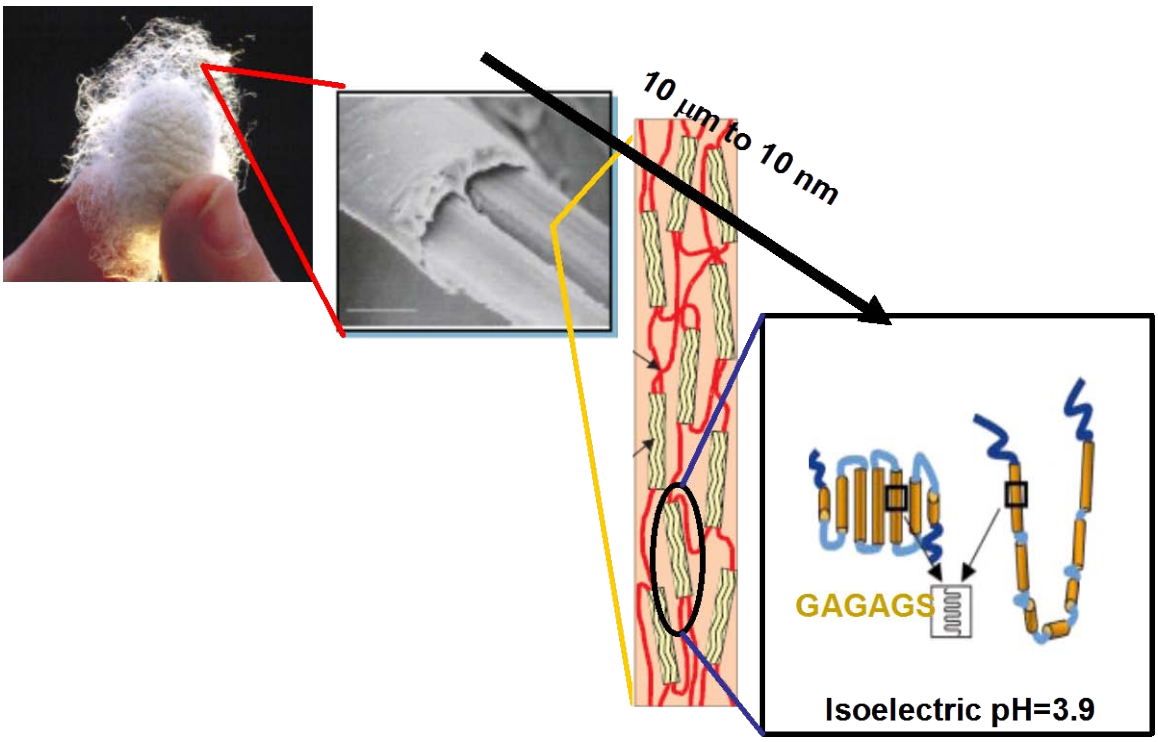

Figure 2.14: Hierarchical microstructure of silk fiber (constructed from the following references: (Jin H.J. et al [46] Shao Z. et al [4] Gosline J.M. et al [7] Altman G. et al [72] Vollrath F. Et al [6]

2.4 Regenerated Silk Fibroin (RSF):

Although insects spin silk fibers from an aqueous dope of silk proteins, once formed the fiber is insoluble in water. This is because of the presence of tightly hydrogen bonded β sheets in the fibers. In order to redissolve the fibroin in water the β sheet structure has to be destroyed. The redissolved fibroin solution is called the RSF. The preparation of RSF from silk cocoons involves the first step of removal of the sericin coat. This is called the degumming process and it uses the fact that sericin has high solubility in a hot soap solution. Consequently, Na_2CO_3 and $NaHCO_3$ are typically used for degumming. Often, a Marseille soap solution is also used. Degumming leaves a cotton-like fluffy mass of fibroin fibers which can be dissolved in concentrated aqueous, organic and aqueous-organic solution of salts such as LiCNS, LiBr, $CaCl_2$, $Ca(CNS)_2$, $ZnCl_2$, NH_4CNS, $CuSO_4$+NH_4OH, $Ca(NO_3)_2$. [39] Nearly saturated solutions of aqueous calcium chloride and ethanol CaCl2-EtOH-H20, calcium nitrate in methanol $Ca(NO)_3$-MeOH and aqueous lithium bromide and ethanol LiBr-EtOH-H_20 have been studied in more detail.[73] After complete dissolution of the fibroin in salt solution an extensive dialysis is carried out to remove the salt and thereby prepare an

aqueous silk fibroin solution. Fibroin can also be dissolved in organic solvents like hexafluroisopropanol or hexafluroacetone but only in its activated state namely, a fibroin film formed by drying a RSF solution.[74]

The molecular properties of regenerated fibroin in LiBr solution and in aqueous solution have been measured. The hydrodynamic radius of fibroin in aqueous solution of LiBr was measured using Dynamic Light Scattering (DLS).[75] The silk fiber was first dissolved in 10 M LiBr and then dialysed against 6 M LiBr to get the desired fibroin solution. DLS measurements were performed on solutions of various concentrations. In the 6 M LiBr solutions protein molecules were found to aggregate above a critical concentration of 0.7 g/L. In solutions of concentrations below the critical concentration protein molecules existed as individual chains of 9 to 10 nm size. DLS on solutions of higher concentrations showed at least two fractions viz., individual chains (high diffusion coefficient or fast mode) and aggregates (lower diffusion coefficient, or slow mode). Table 2.4 shows DLS data for the 6 M LiBr solution of fibroin. Regions A and B are respectively, above and below the critical aggregation concentration of 0.7 g/L. In aqueous solutions the protein molecules were found to aggregate easily even in very dilute solutions. In these solutions at least three different sizes of protein aggregates were observed by DLS and the data is summarized in Table 2.5.

The molecular weight of regenerated silk fibroin has been measured using SDS-gel PAGE. Silk fibroin was dissolved in $Ca(NO_3)_2.4H_2O$. MeOH and SDS gel PAGE was run on the RSF solution. Molecular weights of fractions were identified using molecular weight markers. The results (see Figure 2.15) showed a smeared and dull band above 116 kDa indicating a mixture of pepties chains and a clear band at 25 kDa. The authors suggested that the mixture of peptide chain could be the result of degradation products of the heavy chains of 350 kDa during the degumming process.[76, 77]

Table 2.4: DLS for 6 M LiBr (Hossain K. S. et al [75]; Reproduced with permission from ACS Publications ©**)**

Region	Polymer concentration C /gL^{-1}	Diffusion coefficient Dα(c)		Hydrodynamic radius $R_{H\alpha}$	
		Fast mode /10^{-7} cm^2s^{-1}	Slow mode /10^{-7} cm^2s^{-1}	Fast mode /nm	Slow mode /nm
A	0.98	1.57	0.78	10.3	210
	1.65	1.45	0.77		
	2.13	1.60	0.76		
	3.16	1.50	0.72		
	5.17	1.62	0.80		
B	0.054	1.66	1.90	9.7	90
	0.084	1.63	1.60		
	0.17	1.75	1.80		
	0.49	1.71	1.44		
	0.65	1.75	1.11		
	0.81	1.64	1.02		

Table 2.5: DLS for RSF (Hossain K. S. et al [75]; Reproduced with permission from ACS Publications ©**)**

Polymer concentr-ation C' /gL^{-1}	Diffusion coefficient D_c			Hydrodynamic radius R_H			Amplitude		
	Fast mode /10^{-7} cm^2s^{-1}	Medium mode /10^{-7} cm^2s^{-1}	slow mode /10^{-7} cm^2s^{-1}	Fast mode /nm	Medium mode /nm	slow mode /nm	Fast mode	Medium mode	slow mode
0.055	6.5	0.14	0.16	3.1	18	130	0.14	0.27	0.59
0.006	7	0.12	0.22				0.13	0.31	0.56
0.20	7.5	0.13	0.19				0.10	0.30	0.60
0.41	8.0	0.12	0.18				0.12	0.32	0.56
0.61	8.9	0.15	0.19				0.13	0.29	0.58
1.15	8.8	0.16	0.20				0.11	0.34	0.55
2.39	9.1	0.15	0.18				0.06	0.21	0.73
4.76	8.1	0.12	0.15				0.11	0.42	0.47

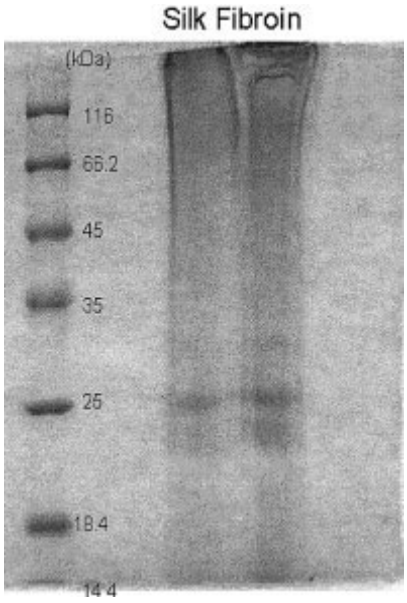

Figure 2.15: SDS gel page of regenerated silk fibroin (Iridag Y. et al [76]; Applied for reproduce permission)

2.5 Gelation of proteins:

Since the main interest of the present work is investigation of the gelation of regenerated silk fibroin it is instructive to understand the work done on gelation of other proteins. Among proteins the gelation of globular proteins has been studied much more extensively than fibrous proteins. The gelation of globular proteins such as β-lactoglobulin (β-lg),[78] casein,[79] egg white protein,[80] lysozyme,[81] ovalbumin (OA),[82] and bovine serum albumin (BSA)[83] has been studied for more than a decade. The structure and mechnism of gelation is important as it finds application in food industry.[84] Globular proteins form gels on heating due to change in their conformation. It has been shown that globular proteins first undergo unfolding (or denaturation) and then form linear fibrils, which randomly assosiate to form a gel when the protein concentration is above a critical value C*.[85, 86] The denaturated proteins form colloidal aggregates because of non covalent interactions namley van der Waals attractive forces, electro static interactions, hydrogen bonding and hydrophobic interactions. These interactions and the resulting aggregation process as well as the structure of the gel depends on the pH, concentration of protein, temperature and ionic strength.

At room temperature the globular proteins are mainly present in dimer state. As the temperature is increased the dimer state breaks and forms monomer but protein gets

denatured. The denatured protein then forms aggregates, which further assosiate to form fractal networks. The aggregation rate increases with temperature and decreases with concentration of protein but the struture of gel is independent of temperature and concentartion of protein. The schematic of gelation of β-lg at pH and 0.1 M NaCl is shown in Figure 2.16.[87]

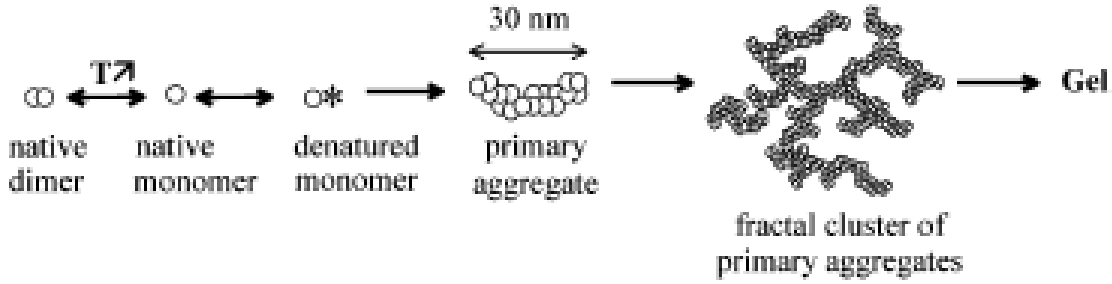

Figure 2.16: Schematic of gelation of β-lg.(Pouzot M. et al [87]; Reproduced with permission from ACS Publications ©)

Different gel structures have been observed for β-lg below and above its isoelectric pH (pI). At pH 2 which is below the pI of β-lg finely stranded transperent gels are formed whereas at pH 7 which is above the pI densely branched aggregates are formed resulting in turbid gels.[84] These two differnt types of gels are formed due to different types of associations between the protein molecules. Clearly at pH 2 there is lesser extent of assosiation between molecules than at pH 7, where the formation of dense domains leads to micro-phase separated protein aggregate.[88] Figure 2.17 shows cryo TEM image of β-lg below and above isoelectric pH and at low and high ionic strength. Figure (a) shows rigid linear aggregates and (b) shows flexible aggregates and formed at pH 2 and 0.01 and 0.1 M respectively. Figures (c) and (d) show aggregates formed at pH 7. At low ionic strength elongated aggregates are observed and at high ionic strength larger aagregates are formed by random aggregation of small aggregates formed at pH 7.[89]

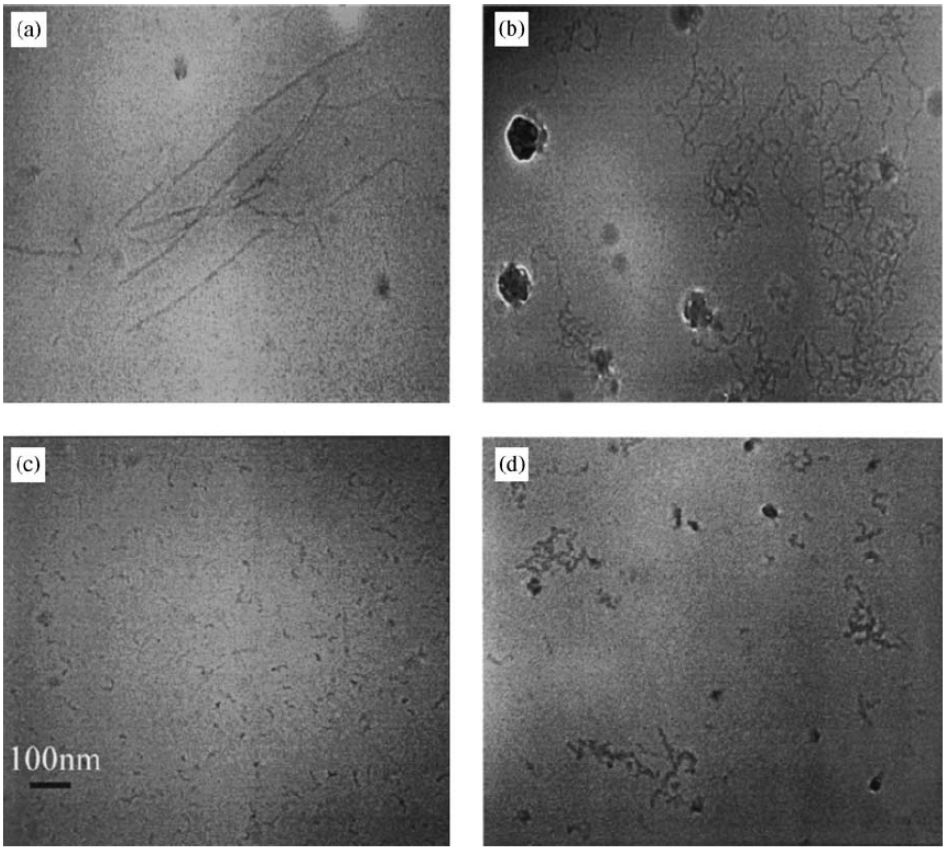

Figure 2.17: Cryo TEM of β- lg aggregates at pH 2 (a,b)and pH 7 (c,d) and 0.001 amd 0.1 M NaCl. (Durand D. et al [89]; Reproduced with permission from ACS Publications ©)

The elastic modulus determined using rheological study is sensitive to the structure of gel. Pouzot M. et al have done rheological measurements on β- lg gels at various concentrations and studied the evolution of structure by probing elastic modulus G' as function of time. This is shown in Figure 2.18. The concentration dependance of G' after gel has been formed at 80 ^{o}C for 24 hrs is shown in Figure 2.18. The concentration dependance follows 4.5 power law for G' ($G' \propto C^{4.5}$) for C > 20 g/L concentartion as shown in Figure 2.19. Similar concentration dependance ($G' \propto C^{4.5}$) has been observed by Verheul and Roefs for whey protein gel containg 70% β- lg prepared at 68.5 ^{o}C for 20 hrs.[90] A stronger concentration dependance ($G' \propto C^{6.1}$) for β– lg gel having concentration 25-60 g/L heated at 80 ^{o}C for 1 hr was observed by Renard D. el al.[91]. Thus G' depends on heating time and temperature. Based on the structural information of fractal networks Shih et al[92] explained the relationship between G' and concentration as follows

$G' \propto C^n$ where $n = \frac{3+D_b}{3-D_f}$, where 2.1

D_b =Fractal dimension of elastic backbone

D_f = Fractal dimension of gel cluster

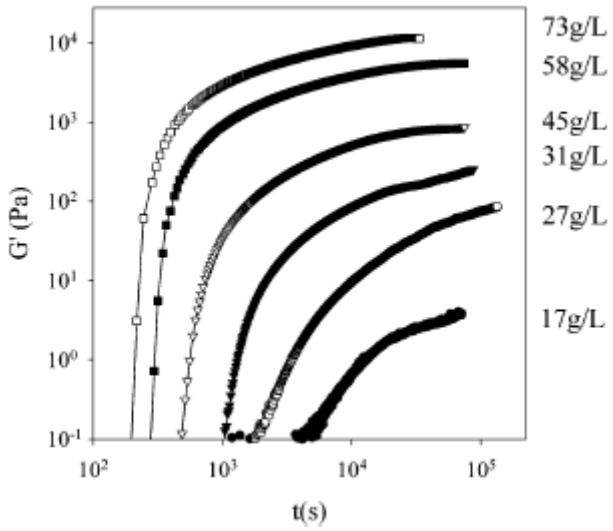

Figure 2.18: Time evolution of gel storage modulus of β-lg at 80°C at various concentrations (Pouzot M. et al [87]; Reproduced with permission from ACS Publications ©)

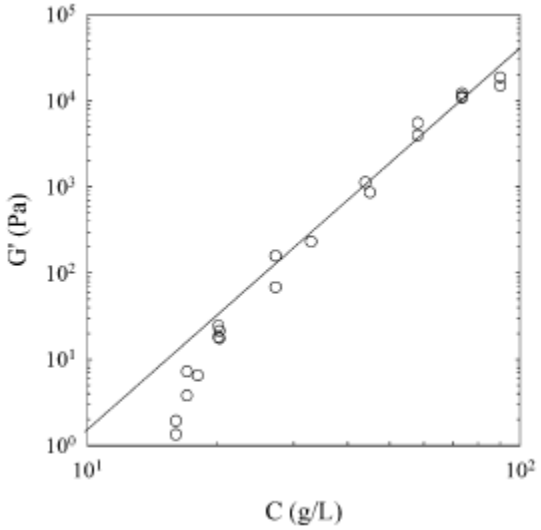

Figure 2.19: Concentration dependance of the storage modulus of β-lg gel after heating at 80 °C for 24 hrs. The solid line has slope 4.5. (Pouzot M. et al [87]; Reproduced with permission from ACS Publications ©)

Komla A. et al studied β- lg microstrure using confocal micrcosopy. They have shown that the gel microstructure is homogeous below 0.2M NaCl concentration (low ionic strength).[93] The system became hetergenous upto length scale of several microns at higher NaCl concentration (high ionic srength). Confocal images of their gels are shown in Figure 2.20. The pair correlation function g(r) was calculated using pixel intensities; an example is shown in Figure 2.21. The images show that protein gels were formed by connecting aggregated protein domain. At short distances g(r) changes only slightly which corresponds to homogenity, while at larger distances, g(r) decreases sharply which coresponds to size of aggregates. The form of decay of g(r) represents the shape of the domain and the way they are connected. The g(r)-1 of all concentrations of salt superimposed on each other by vertical and horizontal shifts as shown in Figure 2.22.

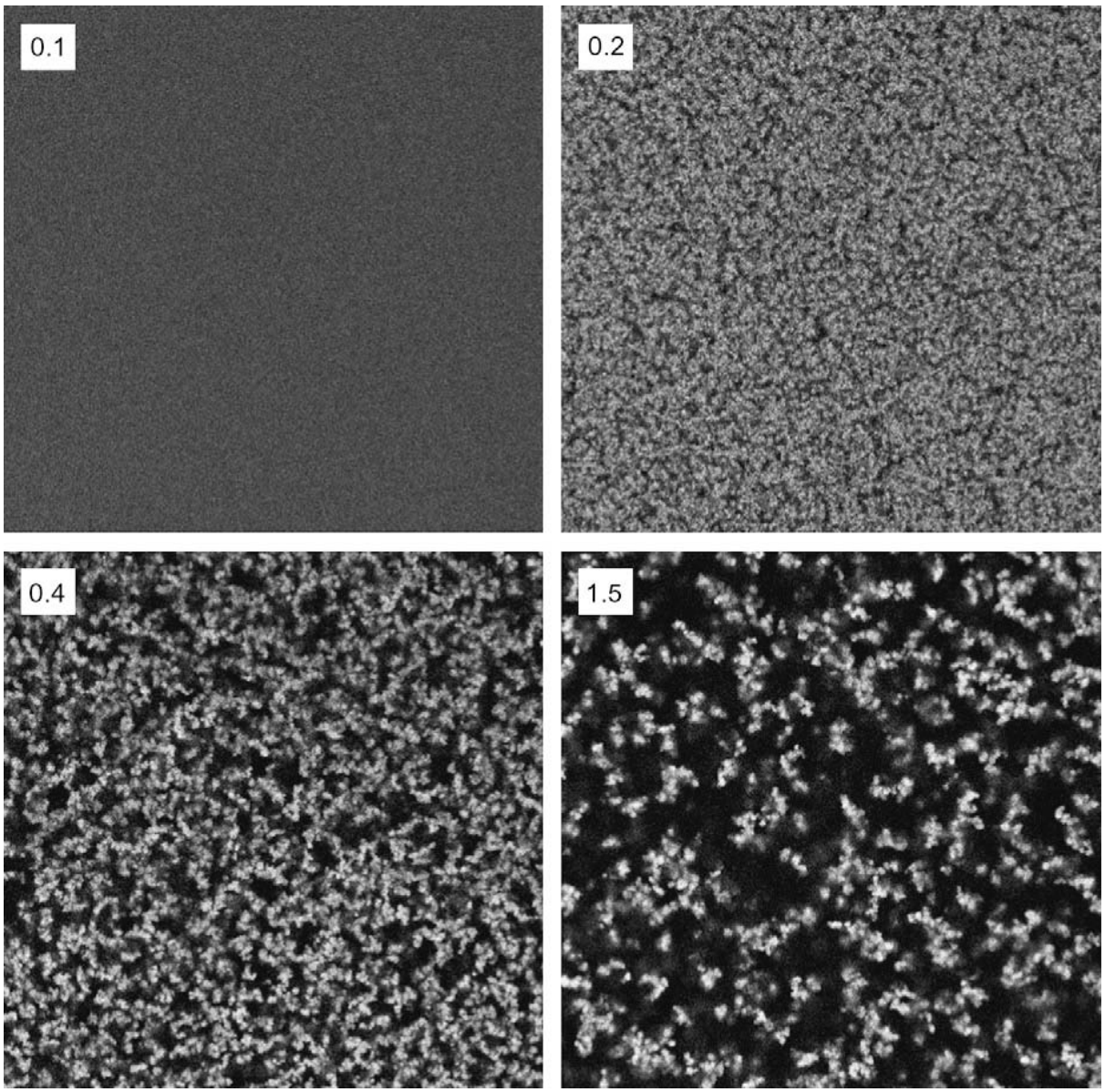

Figure 2.20: CLSM images of β- lg gel of concentration 100g/L and pH 7 at different ionic strength indicated on top of each figure. (Ako K et al [93]; Reproduced with permission from Elesvier ©)

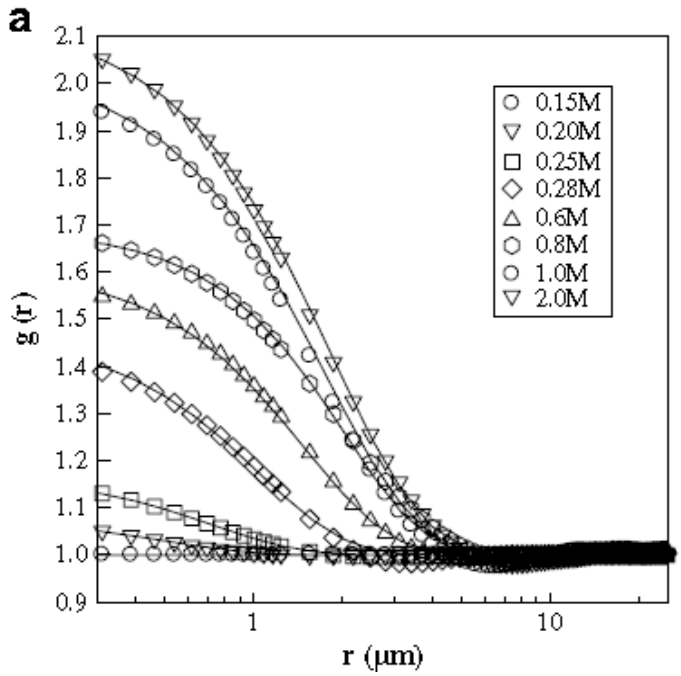

Figure 2.21: Pair corelation function of β- lg gel of concentration 100 g/L at pH 7 and different ionic srength. (Ako K et al [93]; Reproduced with permission from Elesvier ©)

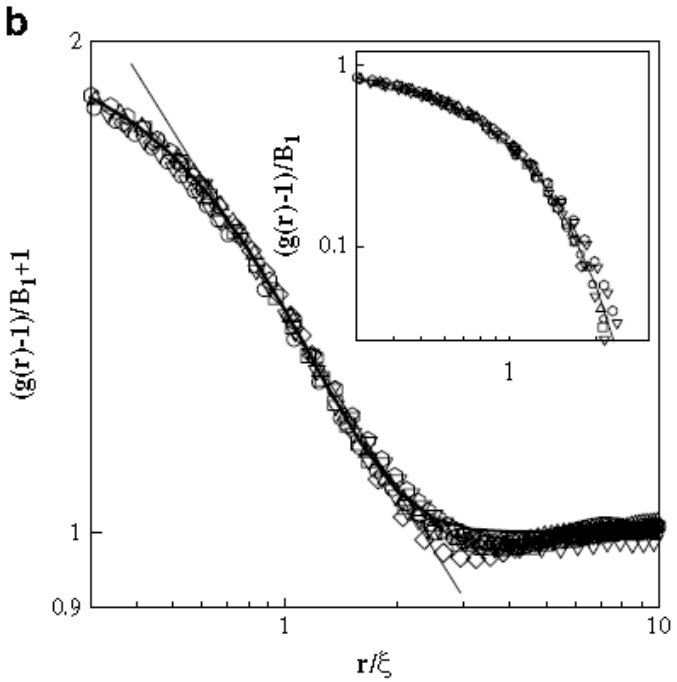

Figure 2.22: Superimposition of pair corelation functions of β- lg gel for different ionic strengths. (Ako K et al [93]; Reproduced with permission from Elesvier ©)

The fractal dimesion (d_f) of a gel gives useful information about structure of the colloidal aggregates and the mechanism of gel formation. Fractal dimension of colloidal aggregates can be determined using various techniques like light scattering, rheology, microscopy, small angle X-ray scattering and neutron scattering. Conventional light scattering has the limitation of working with only dilute solutions.[94] Howerver, the recently developed cross correlation dynamic light scattering technique can be used to study the structure of turbid gels as well.[87, 95]

The colloidal aggregation process is considered to be cluster-cluster type aggregation. In this process, particles or molecules diffuse in a medium, contact in a random way with probability *p* and stick to each other to form aggregates. Aggregates themselves diffuse and form larger aggregates by linking with other aggregates or invidual particles or molecules. Two different cluster-cluster aggregation processes have been reported namely, reaction limited cluster aggregation (RLCA) and diffsuion limited cluster aggregation (DLCA). These processes can be distinguished on the bases of the *p* value; the case $p<<1$ refers to RLCA while $p\sim1$ indicates DLCA.[96] Aggregates formed in RLCA process are found to be more coarse or open space aggregates than those formed in DLCA. There is a correlation between the type of cluster-cluster aggregation process and the fractal dimesion (d_f) based on many theoretical and experimental results. Aggregates grown in RLCA process have d_f = 2.0-2.2 and those grown in DLCA process have d_f=1.7- 1.8.[78, 97-99]

Colloidal aggregates of β-lg were analysed using different tecniques viz., small angle light sacttering, ultra small angle light scattering and small angle neutron scattering. The combined scattering data is shown in Figure 2.23. A power law dependence of the scattered intensity on the wave vector q was observed over the range $2 \times 10^{-4} < q < 2 \times 10^{-1}$ nm^{-1}, which implies that the aggregates have a fractal structure over at least three orders of magnitudes from about 30 nm upto several microns. The blue points in figure indicate the scattering from native protein. The green line indicates the apprent molecular weigh of primary aggregates of β-lg. The weight avarage molecular weight of the fractal aggregates spanned 10 upto greater 10^7 g/mol.

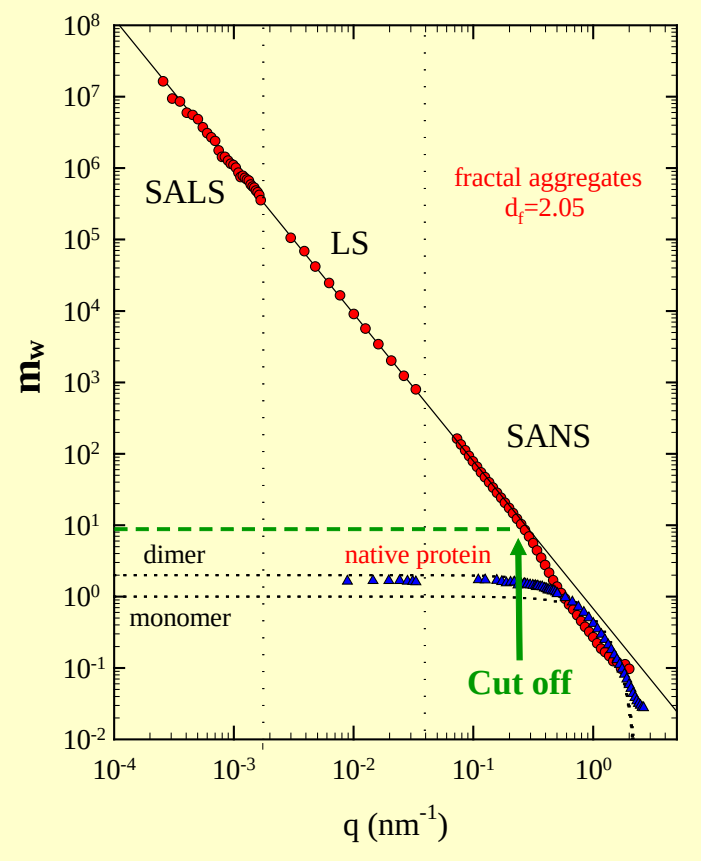

Figure 2.23: Fractal struture of β-lg observed at various length scale

(10000 to 0.1 nm). (Personal commucation with Prof. D. Durand)

As mentioned earlier, the focus of the present work is to investigate the gelation of regenerated silk fibroin (RSF) solution. These gels are potentially interesting biomaterials since they can be used as 3D porous scaffolds for tissue engineering.[100] The RSF solution is inherently metastable and turns into gel state under isothermal storage conditions. Gelation is accompanied by the formation of thermodyanamically stable β sheets.[101], [49] Kim et al have shown that RSF gels have macroporous structure and their compression modulus can be tuned by changing protein concentration.[37] Gelation of RSF is a slow process and its rate increases with decrease in pH.[101] There are only a few reports on the microstructure of RSF gels and on the mechanism of gelation.[49, 100, 101]

Ayub et al in 1993 studied fibroin gel using infra red spectrosopy (IR), circular dichroism (CD), scanning electron microscopy (SEM) and x-ray.[49] CD showed that the protein had random coil conformation in the solution and β sheet conformation in the gel. Similar conformation change was detected using Fourier transform infra red spectroscopy

(FTIR). X- ray studies on dried silk gel showed crystalline structures formed from β sheets, while an electron micrograph of a freeze dried gel showed a porous network structure. Based on these results, Ayub et al suggested that silk gelation is driven by hydrophobic interchain interactions leading to the formation of hydrogen bonded β sheets that give stability to the structure of the gel.[49]

Matusmoto et al studied the gelation of Regenerated Silk Fibroin (RSF) solution as a function of different paramters like concentration, pH and temperature. The time evolution of gelation was investigated by tracking changes in the optical density, and FTIR and CD spectra.[101] The gel time was measured from the changes in optical density. The authors observed a strong pH dependance on the gelation time of the RSF solutions; the gel time increased with increase in pH. Based on their data, they suggested the following mechanism of gelation. Changing the pH from neutral to acidic causes protonation of the carboxyl group present on the side chains. This decreases the charge replusions and thereby increases the hydophobicity of the fibroin, resulting in strong hydophobic interactions and more physical cross links which accelerates the gelation process. Upon changing the pH from neutral to basic in the range 6 to 9 pH, both carboxylic and amino groups are charged. The attractive electrostatic interactions between the oppositely charged groups does induce gelation but at a rate slower than at acidic pH. Above pH 9, the basic amino groups and the acidic carboxyl groups start deprotonating. This increases the repulsive electrostatic interactions between the carboxyl groups leading to longer gelation time. A schematic representation of these interactions as a function of pH is shown in Figure 2.24.

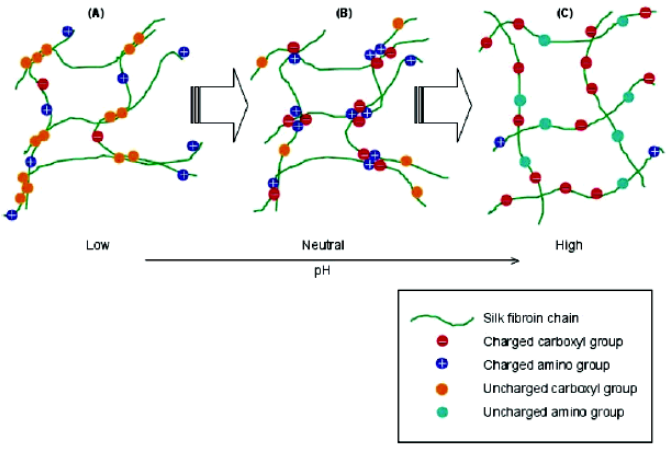

Figure 2.24: Schematic pH dependent interaction of fibroin chain (Matsumoto A. et al [101]; Reproduced with permission from ACS Publications ©)

The secondary structural change during RSF gelation was tracked using FTIR and CD. These techniques suggested that the random coil conformation of fibroin in solution changed to β sheet conformation in the gel. The authors estimated the percentage of β sheets formed during gelation. Their study suggested that in the initial stages of gelation there are fewer β sheets and the gel is being formed due to relatively weak interactions so that the gelation process could be reversible at these early stages. However at later stages the gel becomes more stronger with the formation of large number of β sheets and correspondingly the gelation becomes irreversible. The schematic of gelation mechanism proposed by Matsumoto is shown in Figure 2.25.

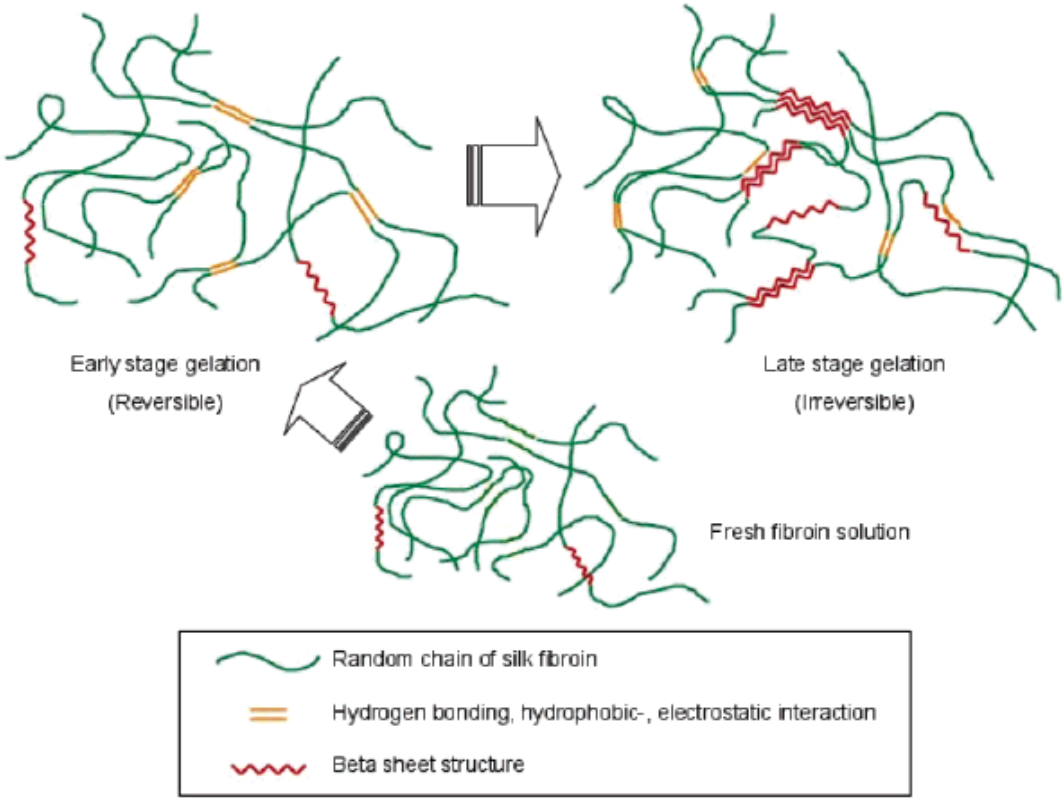

Figure 2.25: Schematic of fibroin gelation (Matsumoto A. et al [101]; Reproduce with permission from ACS Publications ©)

It is evident from the above studies that the structure of silk fibroin gel has thus far been characterized only at a molecular length scale by tracking the formation of β sheet structures. As discussed earlier, globular protein gels have self-similar meso-scale structures that are formed by cluster-cluster aggregation processes. The fractal dimensionality of the gels is determined by the mechanism of aggregation. The rate of gelation and its temperature

dependence is largely determined by whether there is a denaturation of protein involved during gelation. These detailed aspects have not been studied for a fibrous protein like silk fibroin. A study of the structure of the gel, the gelation rate and mechanism can be important in terms of our ability to design better tissue engineering scaffolds. Also, the study could have implications on the partial gelation process that is supposed to occur in the natural silk spinning process during the reduction of pH to values close to the pI of the fibroin chain.

2.6 Summary:

In this chapter, reviews of literature on several topics that are pertinent to the scope of work of this thesis have been presented. The topics reviewed here included the structure of proteins that make the silk fibre, the structure of silk fibre as it is formed in the natural silk fibre spinning process used by silkworms, the processes to make regenerated silk solution, and investigations on the gelation of proteins other than silk.

Chapter 3
Materials and Methods

This chapter provides details of materials used to prepare RSF gels and brief background about the characterization techniques used to understand the microstructure of the gels at different length scales over the range 2 nm – 50 μm. The chapter also provides about experimental protocols and data analysis procedures that are pertinent to the results presented later in chapters 4, 5 and 6.

3.1 List of materials used:

- Cocoons of bivoltine *B. Mori* silkworms were kindly supplied by the Central Silk Research and Training Institute (CSTRI), Mysore, India. The silkworms were reared under controlled conditions in the sericulture laboratory of CSTRI.
- $NaHCO_3$ (S. D. Fine chemicals, India) and LiBr (> 99% purity, Sigma Aldrich, Germany) were used as supplied. Cellulose acetate dialysis bags of cut off molecular weight equal to either 10 kDa or 12.4 kDa were purchased from Sigma Aldrich.
- Deionized water (MiliQ, Millipore Inc.) of pH 6.9, resistivity 18.2 MΩ cm and TOC less than 10 ppb was used for preparing the RSF solution.
- 0.1N HCL (S. D Fine chemicals, India) was used for the adjustment of pH.
- Rhodamine b isothiocyanate obtained from Aldrich was used for tagging protein molecules for the confocal microscopy experiments.
- Silicon oil (GE Silicones) was used to avoid evaporation of water during rheological tests.
- 4mm diameter quartz tubes were obtained from Sigma Aldrich and were used for light scattering experiments and 2 mm quartz capillaries were used for SAXS experiments.
- 0.1mm quartz sample holder was used for Circular Dichroism experiments.
- Molecular weight markers: a Lactalbumin (14 KDa), Carbonic Anhydtase (30 KDa), Egg Albumin (54 KDa), Bovine Serum Albumin (76 KDa), Phosphorylase (96 KDa), Frutose 6 phosphate Kinafe (84 KDa), b galoctosidase, Alcohol dehydrogenase (170 KDa), Myosine, rabit muscle (200 KDa)

3.2 List of methods employed:

- A preliminary vial tilting method (flow/no-flow test) was used to observe the state of the sample. If the sample flows it is categorized as a sol; if it does not flow it is a gel.

- Rheological tests such as isothermal dynamic oscillatory time sweep tests and isothermal creep tests were performed during gelation of RSF to quantify the state of the RSF in terms of its macroscopic mechanical response.
- Confocal laser scanning microscopy was used to image and quantify the microstructure of RSF gel over length scales of 1 – 50 μm.
- Light scattering (static and dynamic) experiments were performed on: (i) RSF solutions to measure the size and molecular weight of fibroin chains, (ii) RSF gels to measure its meso-scale microstructure, and (iii) RSF solutions during gelation to probe the development of meso-scale structure.
- Small angle X-ray scattering experiments were performed on the RSF gel to measure its fine scale microstructure over a length scale range of approximately 2 – 20 nm and to track the development of such structure during gelation.
- Circular dichrosim (CD) was used to monitor the change in conformation of fibroin during gelation of RSF.
- SDS gel electrophoresis was used to determine the molecular weight of fibroin.

3.3 Background: Experimental techniques and data analysis methods:

Since the techniques of light scattering, confocal laser scanning microscopy, rheology and circular dichroism were used in this work to a considerable extent to determine the microstructure of the RSF gel and to study the gelation process they are discussed in more detail in this section relative to other techniques.

3.3.1 Light Scattering Theory:

Light scattering is a physical process in which an incident light is deviated (i.e., scattered) from a straight path by localised non uniformities in the medium through which it passes. These non uniformities are essentially the fluctuations of the refractive index 'n' in the medium. Such local fluctuations take place because of the random (Brownian) motion of the molecules or particles (also called the scatterers) of the medium. The schematic of a typical light scattering setup is shown in Figure 3.1. An incident monochromatic beam of light of intensity I_0 hits the particles in the sample and gets scattered. The detector measures the intensity I_s of the scattered light as a function of the scattering angle 'θ'.

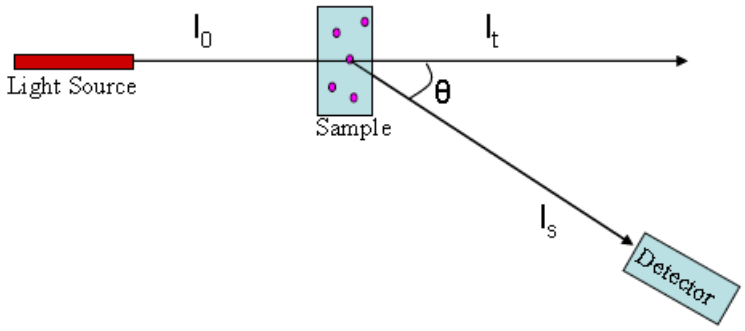

Figure 3.1: Schematic of a light scattering experiment.

Depending upon the nature of interaction between the beam and the sample the analysis of the scattered intensity gives us information about the properties of the scatterers such as their particle size, polydispersity and molecular weight.[102]

The scattered intensity $I_s(q)$ is given by,

$$I_s(q) = Na^6\sigma(q) \qquad 3.1$$

where, N = the number of particles, a = diameter of the particle, $\sigma(q)$ = the total scattering cross section and q is the amplitude of the scattering vector, which is defined as the difference between incident beam vector and the scattered beam vector $\vec{q} = \vec{k}_i - \vec{k}_s$.

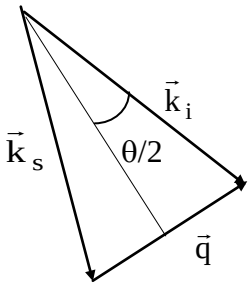

Figure 3.2: Definition of q.

The amplitude of the wave vector of the incident and the scattered light is practically the same. If the angle between the incident and the scattered light is θ, then the amplitude of the scattering vector is:

$$q = \frac{4\pi n}{\lambda_0}\sin(\theta/2) \qquad 3.2$$

where n = refractive index of the sample and λ_0 = wavelength of light

The length scales that can be resolved with scattering experiments are approximately of the same order of magnitude as the reciprocal of the scattering vector q. Equation 3.2 then implies that smaller the wavelength λ_0 of the radiation the smaller are the structures that can be investigated with a scattering experiment. Thus, x-ray scattering and neutron scattering experiments, which employ radiations of smaller wavelengths, are commonly used to investigate crystal structures, small particles such as micelles or micro emulsions, or local structural properties in polymers, while laser light scattering is often the method of choice for the characterization of colloidal systems. Two different light scattering experiments can be performed to give information about the size and molecular weight of the scatterer. Static light scattering experiment is carried out to determine parameters like the molecular weight and gyration radius of the scatterer, while dynamic light scattering is performed to know the hydrodynamic size of the scatterer.

3.3.1.1 Static light scattering (SLS):

In a SLS experiment the mean scattered intensity is measured as a function of the scattering vector q, which is experimentally available through a variation of the angle of observation θ. From the measured scattered intensity the relative excess scattering intensity (I_r) is determined as the total scattered intensity I minus the solvent scattering I_{sol} divided by the scattering of a standard such as toluene I_{st}. In dilute solutions I_r is related to the weight average molar mass (M_w) and the z-average structure factor ($S(q)$) by[103]

$$I_r = K.C.M_w S(q) \qquad 3.3$$

I_r is experimentally calculated using

$$R_\theta = \frac{I - I_{sol}}{I_{st}} \left(\frac{n}{n_{st}} \right) R_{st} \qquad 3.4$$

R_θ = Rayleigh ratio

I = Intensity of light scattered by sample

I_{sol} = Intensity of light scattered by solvent

I_{st} = Intensity of light scattered by standard (toluene)

n =Refractive index of sample

n_{st} =Refractive of standard (toluene)

R_{st} =Rayleigh ratio of standard (toluene)

In eq 3.3 C is the solute concentration and K, defined below, is an optical constant that depends on the refractive index increment.

$$K = \frac{4\pi^2 n^2 \left(\frac{dn}{dc}\right)^2}{\lambda_0^4 N_A} \qquad 3.5$$

n = refractive index of toluene

$\frac{dn}{dc}$ = refractive index increment

λ_0 = wavelength

N_A = Avogadro's number

$S(q)$ describes the dependence of I_r on the scattering wave vector. For dilute solutions ($c \to 0$) the particle scattering factor is given by

$$S(q) = \left[1 + \frac{q^2 R_g^2}{3}\right]^{-1} \qquad 3.6$$

At higher concentrations, intermolecular interactions influence the scattering intensity so that an apparent molar mass M_a can be obtained by extrapolation to $q = 0$.

3.3.1.2 Dynamic Light Scattering:

Particles suspended in a liquid are not static, but are in fact under constant motion (the so-called Brownian motion). As a result in a scattering experiment the phase relations of the light scattered by different particles change randomly and also the number of particles in the

scattering volume fluctuates. Both effects lead to a fluctuation of the scattering intensity as shown schematically in Figure 3.3

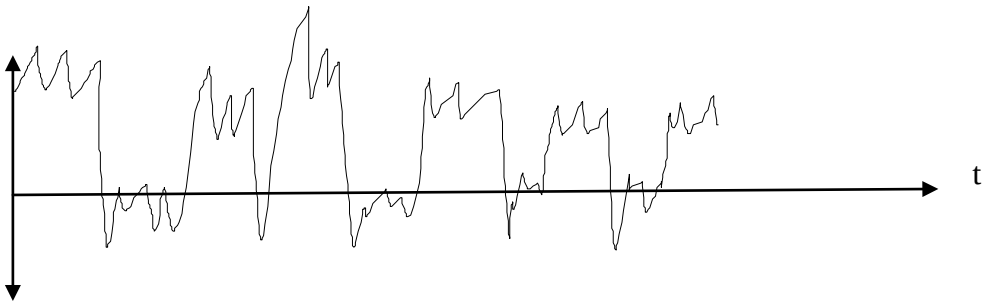

Figure 3.3: Typical light scattering data plotted intensity against time.

It is possible to directly measure the spectrum of frequencies contained in the intensity fluctuations arising from the Brownian motion of particles. These intensity fluctuations give information about the diffusion process in terms of a correlation function**.** The best way to measure this is to use a device called a digital correlator. A correlator is basically a signal comparator. It is designed to measure the degree of similarity between two signals, or one signal with itself at varying time intervals. Thus correlation can be of two types: auto correlation when the signal is compared with itself and cross correlation where two different signals are compared and correlated. If the intensity of a signal is compared with itself at a particular point in time and a time much later, then for a randomly fluctuating signal it is obvious that the intensities are not going to be related in any way, i.e. there will be no correlation between the two signals (see Figure 3.4). However, if the intensity of signal at time = t is compared to the intensity a very short time later ($t+\delta t$), there will be a stronger correlation between the intensities of the two signals. The period of time δt is usually very small (nanoseconds or microseconds) and is called the sample time of the correlator. Figure 4b shows the correlogram, i.e. correlation function, which decays with time.

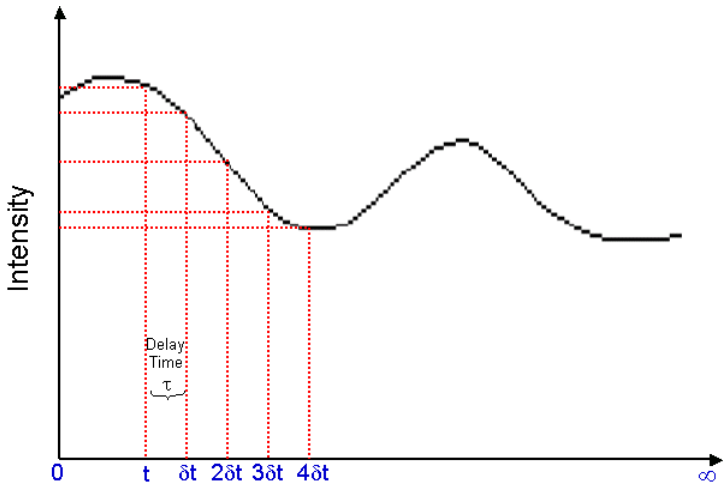

Figure 3.4: Calculation of correlation function from light scattering data.[104]

The intensity correlation measured by the correlator is given by

$$G_2(t) = \langle I(0)I(t)\rangle \tag{3.7}$$

where $I(0)$ and $I(t)$ are the measured intensities at zero time and a short time t later. The normalized electric field autocorrelation function, $g_1(t)$, is calculated from the measured intensity correlation function, $G_2(t)$, using the so-called Siegert relation[105]

$$g_1(t) = \left[\frac{G_2(t)}{\langle I^2\rangle} - 1\right]^{0.5} \tag{3.8}$$

For a dilute solution of monodisperse particles $g_1(t)$ is an exponential decay given by

$$g_1(t) = \exp\left(-Dq^2\tau\right) \tag{3.9}$$

The relaxation time τ represents the time it takes for a particle to diffuse over a distance close to q^{-1} with a diffusion coefficient D. For a solution containing polydisperse sized scatterers $g_1(t)$ can be written as[106]

$$g_1(t) = \int A(\tau_{LS})\exp(-t/\tau_{LS})d\tau_{LS} \tag{3.10}$$

where $A(\tau_{LS})$ is the amplitude of the mode and τ_{LS} is the decorrelation time of the mode. When q^2-dependent relaxation modes are observed caused by the relaxation of the

concentration fluctuations of a macromolecule, the cooperative diffusion coefficient can be calculated from the average relaxation rate as $D_c = \frac{\langle \tau_{LS}^{-1} \rangle}{q^2}$. At low concentrations when interaction becomes negligible the z-average hydrodynamic radius, R_h, can be calculated using the so-called Stokes-Einstein relation,

$$R_h = \frac{kT}{6\pi\eta D_c} \qquad 3.11$$

with η the solvent viscosity, k the Boltzman's constant and T the absolute temperature

3.3.2 Rheology Theory:

Rheology is the science of flow and deformation of matter. Rheological measurements are done by imposing a well defined deformation, shear or extensional, and measuring the stress response of the fluid. This is called strain-controlled rheometry. Alternatively, a shear stress or an extensional stress is imposed on the fluid and the corresponding strain response is measured. This is called stress-controlled rheometry. Linear viscoelastic fluids are materials which exhibit simultaneously the characteristics of a Newtonian viscous fluid (i.e., constant viscosity) and a Hookian elastic solid (i.e., constant modulus).

3.3.2.1 Small amplitude oscillatory shear experiment:

When a sinusoidal shear strain $\gamma = \gamma_0 \sin(\omega t)$ of small amplitude γ_0 and frequency ω is imposed on a viscoelastic fluid the stress response is composed of in-phase and out-of-phase components and is given by

$$\sigma(t) = G'(\omega)\gamma_0 \sin(\omega t) + G''(\omega)\gamma_0 \cos(\omega t) \qquad 3.12$$

In eq 3.12the coefficients G' and G'' represent the elastic (or storage) and viscous (or loss) moduli of the fluid. They represent respectively the stored and dissipated components of the energy input into the fluid by the imposed mechanical deformation. A particular experiment carried out in this work is called the time-sweep experiment in which a sinusoidal strain of constant amplitude and frequency is imposed on the sample, and the evolution of its response in terms of G' and G'' is measured as a function of time. If $G'' > G'$ then the fluid is

predominantly viscous but if $G' > G''$ then the fluid is predominantly elastic. Change from a viscous to an elastic character may be expected as a fluid gels with time. In the present work this experiment is used to track the gelation of RSF. Gel point may be defined as the point where $G' = G''$ or when there is a rapid rise in the moduli.

3.3.2.2 Creep test and creep ringing phenomenon:

The response of a viscoelastic fluid to an imposed step stress is dominated by viscous character at long time and elastic character at short time. Consequently, at times greater than a characteristic response time of the material, its creep compliance typically increases linearly with time. At short times the inertia of the system (measuring fixture plus rheometer drive) couples with the elasticity of the material, and for certain fluids this results into a damped oscillatory response of the creep compliance. This phenomenon, called creep ringing, has been observed for biopolymer gels[107] and colloidal gels[108], and has been reviewed recently.[109] The inertial effects are unavoidable in stress controlled rheometry and they were thought to limit measurement ability in a creep test at shorter times. However useful visocoelastic properties of the fluid can in fact be extracted from creep ringing data.

The creep behavior of a viscoelastic fluid can be effectively described by a generalized Jeffery model, which is essentially a combination of multiple Jeffery modes organized in series as shown in Figure 3.5. Each mode contains three elements: a viscous element (dashpot) arranged in series with a Voigt-Kelvin mode, which consists of an elastic element (a Hookean spring) in parallel with another dashpot.

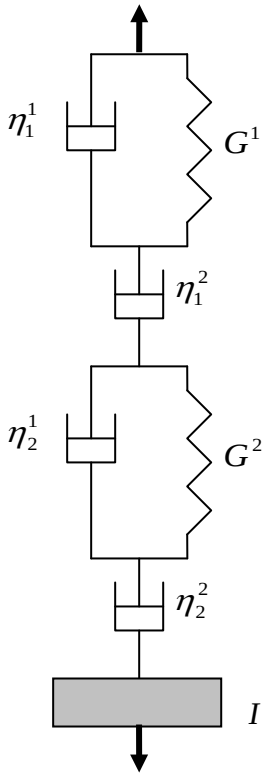

Figure 3.5: Schematic of Jeffery model

The governing equations that describe the creep response of the generalized Jeffery's model on application of a stress (σ_0) are [109]

$$\frac{I}{b}\sum_i \frac{d\dot{\gamma}^i}{dt} = \sigma_0 - \sigma \tag{3.13}$$

$$\sigma + \tau_1^i \frac{d\sigma}{dt} = \eta_2^i\left(\dot{\gamma}^i + \tau_2^i \frac{d\dot{\gamma}^i}{dt}\right) \tag{3.14}$$

Here I is the moment of inertia of the system, b a parameter related to the geometry of the measuring fixture, σ the stress in each Jeffery mode (note that all modes share the same stress when arranged in series), and $\dot{\gamma}^i$ the strain rate of the i^{th} mode. $\tau_1^i = \frac{\eta_1^i + \eta_2^i}{G^i}$ and $\tau_2^i = \frac{\eta_1^i}{G^i}$ are respectively the relaxation time and retardation time of the i^{th} mode, and η_1^i, η_2^i and G^i are respectively, the viscosities of the two dashpots and the elastic modulus of the spring comprising the i^{th} mode as shown in Figure 3.5.

In general the solution to the coupled equations 3.13 and 3.14 is not analytically tractable. However, there is an analytical solution available for a single mode[108, 109] and is given by

$$J(t) = \dot{\gamma}_J\, t - B_J + e^{-A_J t}\left[B_J \cos\left(\omega_J t\right) + C_J \sin\left(\omega_J t\right)\right] \qquad 3.15$$

Here,

$$\dot{\gamma}_J = \frac{\sigma_0}{\eta_2} \qquad 3.16$$

$$A_J = \frac{G_J + \eta_1\eta_2 b/I}{2\left(\eta_1 + \eta_2\right)} \qquad 3.17$$

$$B_J = \frac{\sigma_0}{G_J}\frac{\eta_1 + \eta_2}{\eta_2}\left[\frac{2A_J I}{\eta_2 b} - 1\right] \qquad 3.18$$

$$C_J = \frac{A_J}{\omega_J}\left(B_J - \frac{\dot{\gamma}_J}{A_J}\right) \qquad 3.19$$

$$\omega_J = \sqrt{\frac{G_J b}{I}\frac{\eta_2}{\eta_1 + \eta_2} - A_J^2} \qquad 3.20$$

It can be shown from eq (3.15) that at very short times $J(t) \approx \frac{b}{2I}t^2$ and at long time $J(t) \approx \dot{\gamma}_J t$. At intermediate times the last term in eq (3.15) produces an oscillatory response when, $G_J > A_J^2 \frac{I}{b}\left(\frac{\eta_1 + \eta_2}{\eta_2}\right)$. The moduli of sample can be estimated using Struick's formula [109]

$$G' \approx \frac{I\omega_*^2}{b}\left[1 + \left(\frac{\Delta}{2\pi}\right)^2\right] \qquad 3.21a$$

$$G'' \approx \frac{I\omega_*^2}{b}\left(\Delta/\pi\right) \qquad 3.21b$$

which is applicable for small logarithmic decrement Δ and negligible sample inertia. Here ω_* is the experimentally determined creep ringing frequency. The logarithmic decrement can be calculated using

$$\Delta = 2\ln\left[\left(J_1 - J_2\right)/\left(J_3 - J_2\right)\right] \qquad 3.22$$

and is typically found to be $\Delta < 2\pi$. In eq 3.22 J_1, J_2 and J_3 are the compliance values of the first peak, first valley and second peak of the creep ringing data.[109]

3.3.3 Confocal Laser Scanning Microscopy (CLSM):

Confocal microscopy is a useful instrument for visualizing fluorescent or fluorescently tagged molecules or particles. A confocal microscope selectively collects fluorescence from thin focused optical sections of sample. It is also possible to image a series of thin optical sections at different penetration lengths inside the sample and reconstructing the series into a three dimensional structure of the sample. Several types of confocal microscopes are available but the most commonly used one is a confocal laser scanning microscope (CLSM). This microscope scans the sample with a focused laser and collects emitted fluorescence signal with a photodetector which is generally a photomultiplier tube. CLSM can resolve features of size several hundred nanometers and above.

Information from a CLSM image can be quantified by calculating the pair correlation function $g(r)$ of the fluorescence signal (A) at coordinates $\vec{\mathrm{i}}$ and $\vec{\mathrm{j}}$

$$g(r) = \frac{\sum_{i=1}^{n}\sum_{j=1}^{m} A_i.A_j}{\sum_{i=1}^{n} A_i.\sum_{j=1}^{m} A_j} \qquad \text{with} \qquad r = \left|\vec{i} - \vec{j}\right| \qquad 3.23$$

This function is equal to the pair correlation function $g_c(r)$ of the molecular or particle concentration fluctuations in the sample if the right precautions are taken.[93]

$$g_c(r) = \frac{< C(0).C(r) >}{C^2} \qquad 3.24$$

3.3.4 Circular Dichroism (CD):

CD refers to dichroism which occurs when left and right circularly polarized light passes through a chromophore. In the case of proteins and peptides the optically active centre i.e. chiral carbon plays the role of a chromophore. When the left and right circularly polarized light passes through the sample, if one of the out coming lights is absorbed to a greater extent than the other then the resultant radiation becomes elliptically polarized. CD spectrophotometer is the instrument which records the CD spectrum and does not recombine the right and left component but detects them separately. It gives dichorism either in terms of the difference in absorbance of two components A or ellipticity in degrees (θ'). These two parameters are related to each other $A*32.98= \theta'$.[110] Generally, in most of biological work the ellipticities are very small and can be in the order of 10 millidegrees. This means that the difference in absorbance is only about $3x10^{-4}$ absorbance unit. Hence careful attention and good experimental practice is required for acquiring reliable data.

A CD spectrum is recorded when the dichroism is measured as a function of wavelength. A protein molecule possesses a number of chiral carbons which give different CD signals. In the far UV region (240-180 nm), the CD spectrum gives information about the secondary structure of protein molecules such as a helix and a β sheet where as in the near UV region (320-260 nm) it gives information about the tertiary structure of protein.

The most conventional CD instrument has Xeon arc as a light source which gives good output over the range of 178-1000 nm. This is a useful wavelength range to detect all structural and conformational information of proteins. The light is circularly polarized using a modulator which consists of a piezoelectric crystal tightly coupled with a thin plate of quartz. The alternating electric current coming from the piezoelectric crystal induces structural changes in the quartz plate which transmits circularly polarized light. The light is then passed through a quartz sample holder of known path length. The detector is a photomultiplier tube and is placed after the sample holder. It is also necessary to flush the instrument with Nitrogen gas (N_2) continuously to avoid ozone formation from oxygen and to minimise the damage to optical components. The N_2 atmosphere allows us to work below 175 nm wavelength.

3.3.4 Turbidity:

Turbidity (τ) is a measure of the total volume average scattering of light passing through a sample. Turbidity can be calculated as

$$\tau = \frac{-1}{L}\left(2.303 \times A_{\lambda}\right) \qquad 3.25$$

where $A_{\lambda} = -\log_{10}\left(I / I_0\right)$ is the measured optical density (or absorbance) in a spectrophotometer and L is the path length of the light passing through the sample. In dilute solutions the turbidity is proportional to the weight average molar mass and the integral of the structure factor over all scattering angles:

$$\tau = K'CM_w \int_0^{2\pi} \int_0^{\pi} S(q)\left(1+\cos^2\theta\right)\sin\theta d\theta d\varphi \qquad 3.26$$

In eq 3.26 K' is an optical constant that is slightly different from K defined in eq. (3.5) At higher concentrations M_w should be replaced by the apparent molar mass M_a.

3.3.5 Small Angle X-ray Scattering (SAXS):

X-ray is another electromagnetic radiation having wavelength in the range of 100 - 0.1 nm. The principle of x-ray scattering is similar to that of light scattering except that scattering of x-rays occurs as a cause of electron density difference between the constituents of the specimen. X-ray scattering techniques using a typical Cu source that emits x-rays at a wavelength $\lambda = 1.54$ Å can probe structures of size in the range of 0.1 to 150 nm. Smaller structures (0.1 – 1 nm) are probed by measuring scattering at larger angles (Wide Angle X-ray Scattering, WAXS) while larger structures (1 – 100 nm) are detected by Small Angle X-ray Scattering (SAXS). Data is obtained in the form of a spectrum of I (scattered intensity) versus q, where q is the magnitude of the scattering vector given as $q = 4\pi/\lambda \sin\theta/2$, θ being the scattering angle. The scattered intensity is a function of scattering vector q and it can be represented as

$$I(q) = \Delta\rho^2 V_p \phi_p P(q) S(q) \qquad 3.26$$

where $\Delta\rho$ is the electron density difference between the particles and the solvent, V_p is the volume of a single particle, ϕ_p is the volume fraction of particles, $P(q)$ is the single particle form factor and $S(q)$ gives a measure of the inter-particle correlations and is known as the structure factor. In very dilute solutions where the inter-particle correlations are absent, the scattered intensity can be assumed as the form factor of the sample.[111]

The form factor amplitude for a homogenous sphere can be calculated using following eq.

$$F(q,R) = \frac{3[\sin(qR) - qR\cos(qR)]}{(qR)^3} \quad 3.27$$

where R is the radius of the sphere. For $qR >> 1$, $F \sim q^{-2}$.

For thin rod like structure the form factor can be calculated using eq. 3.28

$$F(q) = 2Si(qL)/(qL) - 4\sin^2(qL/2)/(q^2L^2) \quad 3.28$$

$$Si(x) = \int_0^x t^{-1}\sin t dt \quad 3.29$$

where L is the length of the rod. For $qR >> 1$, $F \sim q^{-1}$.

3.4 Experimental protocols used in this work:

3.4.1 Rheology:

Rheological measurements were performed with MCR 301 rheometer (Anton Paar, Austria) using a cup and bob fixture (bob 16.66 mm outside diameter, cup 18.01 mm inside diameter, and sample volume of 4.7 ml) inserted in a peltier environmental system maintained at 25^{oC}. A thin film of silicon oil of 1000 cp viscosity was used to cover the sample surface to prevent evaporation of water from the sample during the test.

Isothermal oscillatory shear measurements were done with an imposed strain of 0.2% and a frequency of 1 Hz to determine the storage modulus (G') and loss modulus (G''). That the 0.2% strain is in the linear response regime for the sample before and after gelation was confirmed separately. Creep tests were performed by applying a small stress (0.2 Pa for 0.5, 1.0 and 1.5 g/L sols, and 2.0 Pa for 7.5 g/L sol) for a period of 215 s. The tests were repeated

every 3 hours until the creep compliance of the sample showed little change between consecutive tests, which took approximately 24 h.

3.4.2 Confocal Laser Scanning Microscopy:

Images of silk gel samples were taken with a Leica TCS-SP2 CLSM (Leica Microsystems Heidelberg, Germany). Two different water immersion objective lenses were used: HCx PL APO 63x NA=1.2 and 20x NA=0.7. The theoretical resolutions of these lenses were 0.3 µm and 0.5 µm, respectively, in the x-y plane. This implies approximately that one pixel corresponds to 300 nm and 500 nm respectively for the two lenses used in this work. Fibroin was labelled with fluorochrome rhodamine B isothiocyanate, by adding a small amount of a concentrated rhodamine solution to the RSF sol before gelation. The rhodamine concentration needs to be sufficiently high to give a significant signal, but not so high that it modifies the structure of protein gels. The possible influence of rhodamine on the structure was investigated by measuring RSF gel solutions containing different amounts of rhodamine. It was found that the RSF gel was not significantly influenced by rhodamine for concentrations up to at least 5 ppm (g/g) at which a sufficiently large signal was observed. So the concentration of rhodamine in the RSF sol was limited to a maximum of 5 ppm. Solutions were inserted between a concave slide and a coverslip and then hermetically sealed. The samples were maintained at the desired conditions overnight to ensure complete gelation of the RSF. Incident light was emitted by a laser beam at 543 nm which excited the rhodamine. The fluorescence light was recorded between 560 and 700 nm. The images of samples were taken at a single plane which was close to the surface.

3.4.3 Light scattering and turbidity:

All RSF samples used for light scattering studies were prepared in dust-free environment inside a laminar hood. Membrane filtration of solutions was avoided because of the shear sensitivity of RSF. Static and dynamic light scattering measurements on freshly dialysed RSF solutions were made using an ALV-5000 multibit, multitau, full digital correlator in combination with a Spectra-Physics laser emitting vertically polarized light at λ = 532 nm. The temperature was controlled by a thermo-stat bath to within ± 0.1 °C. Dynamic light scattering was also performed on some dilute RSF sols during gelation at ambient temperature and pH 2 with a 3D-DLS equipment (LS Instruments) employing a J.D.U. Uniface laser of 628 nm wavelength. Samples were held in a quartz cylindrical sample cell of

4 mm diameter. Measurements were made at angles between 15 and 115 degrees. At each angle the scattered light intensity data was collected for 1 min. Two such readings were taken and the average intensity was reported. Static light scattering was done on gel samples prepared in quartz cylindrical sample cell at pH 2 to 4, temperature 20 to 70 ^{o}C and various concentrations.

Optical transmission (T_r) measurements were done at 20 °C using a UV-Visible spectrophotometer Varian Cary-50 Bio (Les Ulis, France). The path length was either 1cm or 1mm depending on the sample turbidity.

3.4.4 X-ray scattering:

Small angle x-ray scattering experiments were done with a Bruker Nanostar equipment equipped with a rotating copper anode generator operating at 45kV and 100 mA, a three-pinhole collimation system and a two dimensional multiwire detector. Silk sols were filled into quartz capillaries of 2 mm diameter and sealed with paraffin. Data was acquired and circularly averaged to convert to one dimensional format (intensity versus wave vector) using the Bruker software. The scattered intensity of sample is corrected using equation 3.30

$$I_{corr} = I_s - \tau_s . I_{BG} \qquad 3.30$$

I_{corr} = Corrected intensity of sample

I_s =Scattered intensity of sample

τ_s = Transmission coefficient of capillary

I_{BG} = background scattering

$$\tau_{s=} \frac{I_{S-GC} - \tau_{GC} Is}{I_{GC} - \tau_{GC} I_{BG}} \qquad 3.31$$

τ_{GC} = Transmission coefficient of Glassy carbon

I_{GC} = Scattering Intensity of Glassy carbon

3.4.5 Circular Dichroism:

CD spectra were obtained for a 0.5 g/L RSF solution at pH 2 and at ambient temperature with a Jasco 810 circular dichroism spectrometer using a quartz sample cell of path length 1 mm. Samples were scanned over a wavelength range of 190 nm to 260 nm at a scan speed of 20 nm/min with three accumulations.

3.5 Preparation of Regenerated Silk Fibroin (RSF) solution:

The preparation of aqueous RSF solution involved three steps: degumming, dissolution in an aqueous LiBr solution and dialysis. One hundred *B. Mori* silk cocoons were first boiled in 5 litres of a 0.5 wt-% solution of $NaHCO_3$ for half an hour. In this process the sericin is removed and the silk cocoons lose their shape to form a cotton-like fluffy mass of fibers. The boiling process was repeated once more with a fresh solution of $NaHCO_3$ to ensure complete removal of sericin and other wax like materials. The resulting fibroin fibres were washed thoroughly with excess water to remove $NaHCO_3$. In principle the residual sericin content, if any, of the silk fibroin can be quantified by amino acid analysis.[112] However, such analysis was not carried out in this work due to lack of requisite facilities in the laboratory. Degummed silk fibroin was then dissolved in 9.3 M LiBr at ambient temperature to obtain a 10 wt% solution. Complete dissolution took approximately 24 hours. This solution was dialyzed against de-ionized water for 48 hours using cellulose acetate dialysis bags of MWCO= 10 or 12.4 kDa. The de-ionized water was frequently changed; the first change was made after 3 hours and thereafter every 9 hours. The presence of bromide ions in the de-ionized water was tested using a simple silver nitrate test; the presence of bromide ions caused visible precipitation of silver bromide. There was no precipitate observed after the first three changes of de-ionized water which ensured nearly complete removal of LiBr in as far as this simple test can measure. The presence of trace amounts of Li^+ can in principle be measured using X –ray photoelectron spectroscopy.[37] However, this was not checked due to non-availability of the requisite facility.

Some experiments were also done by dissolving the degummed fibroin in an aqueous 10 wt% $Ca(NO_3).4H_20$ solution followed by dialysis. The freshly dialyzed RSF prepared in this way was used for gel electrophoresis studies. Also, some RSF solutions were prepared

for light scattering studies by diluting the 9.3 M LiBr solutions down to 4.7 M and 2.3 M LiBr solutions.

The dialyzed aqueous RSF solution was centrifuged at 15000 RPM for 20 minutes. The pH of the freshly dialyzed RSF was found to be 8.2. The protein concentration (C) of the RSF was determined by measuring the absorption at 272 nm in a UV-visible spectrophotometer (Shimadzu Scientific Instruments, Japan) and using the molar extinction coefficient 11.8 mol/L/cm.[113] Dialyzed solution was always stored in refrigerator at 5-7^{o} C. Typical fibroin concentration of a freshly dialysed RSF was found to be about 40 g/L and the same was used to prepare sols for all sol to gel phase transition studies.

3.6 Characterization of freshly dialyzed RSF:

3.6.1. SDS-PAGE (Sodium Dodecyl Sulphate Polyacrylamide Gel Electrophoresis):

Molecular weights of the heavy and light fractions were measured using gel electrophoresis (SDS-PAGE). Two polyacrylamide gels prepared by using 6 mol% and 12 mol% bisacrylamide were used for gel electrophoresis. Gels of two different crosslinking densities were required in order to resolve the bands corresponding to the light and heavy chain fractions of the fibroin molecule. Figure 3.6 shows the results of the SDS-PAGE experiments. Also shown on each gel are distinct bands of molecular weight markers. The 12% gel showed a clear band for the light chain fraction of fibroin. The molecular weight, determined qualitatively from comparison with marker bands, was approximately 25kDa, which is in agreement with the reported molar mass of the light chain fraction of fibroin.[6] This indicates that the light chain fraction remained intact during the regeneration process. The 6% gel on the other hand showed a smear starting from the well and stretching down to a significant distance along the gel. A closer look showed that a relatively darker band at a location corresponding approximately to 350 kDa was visible in the smear. This molecular weight is in agreement with the reported molar mass for the heavy chain fraction.[46] Smear patterns similar to the one shown in Figure 3.6 have also been reported earlier for regenerated fibroin solutions.[114] Smear can be caused by the presence of salt or due to adsorption of the protein on the gel matrix. On the other hand the presence of smear could also imply a broad distribution of molecular weight. In our case the molecular weight distribution corresponding to the observed smear length ranged from values much higher than 300 kDa to about 150 kDa. The lower molecular weight species could be formed due to degradation of

the fibroin during the regeneration process. It may be noted that the cocoons were boiled in alkaline water for 60 min, and some degradation can happen during this process. The higher molecular weight species could be formed due to aggregation as discussed below.

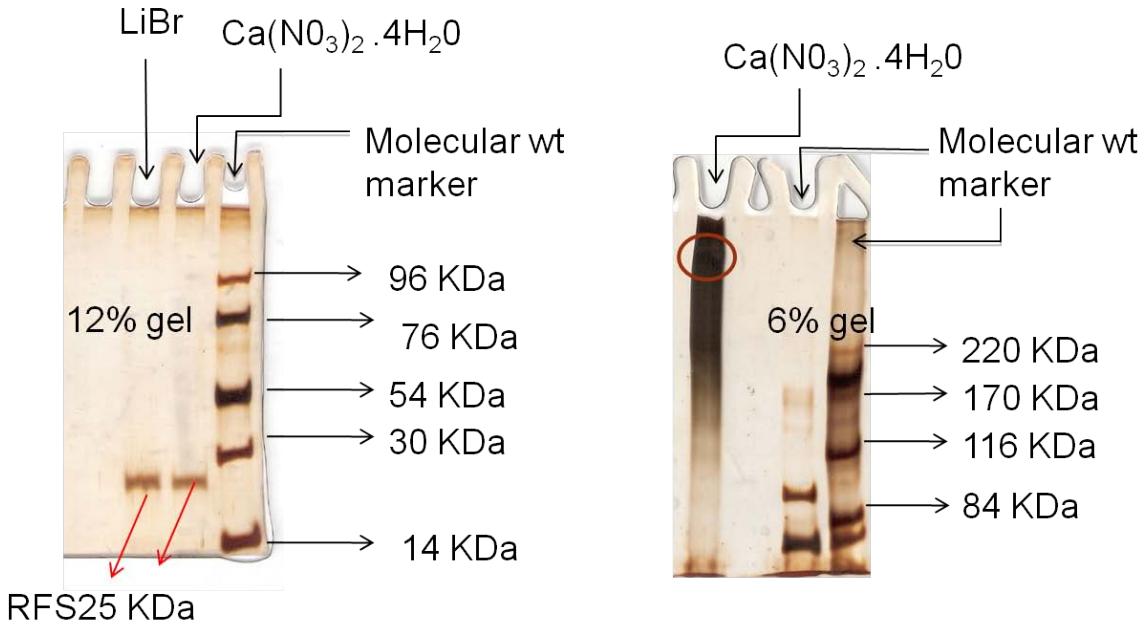

Figure 3.6: SDS page of light and heavy chains of fibroin

3.6.2. Light scattering:

The size and molecular weight of individual fibroin molecules were determined in 4.7M or 2.3M LiBr solutions using static and dynamic light scattering on solutions of concentrations between 0.8 and 7 g/L. At all concentrations a single relaxation mode was observed with a q^2-dependent average relaxation rate that we attribute to diffusion of individual fibroin chains.

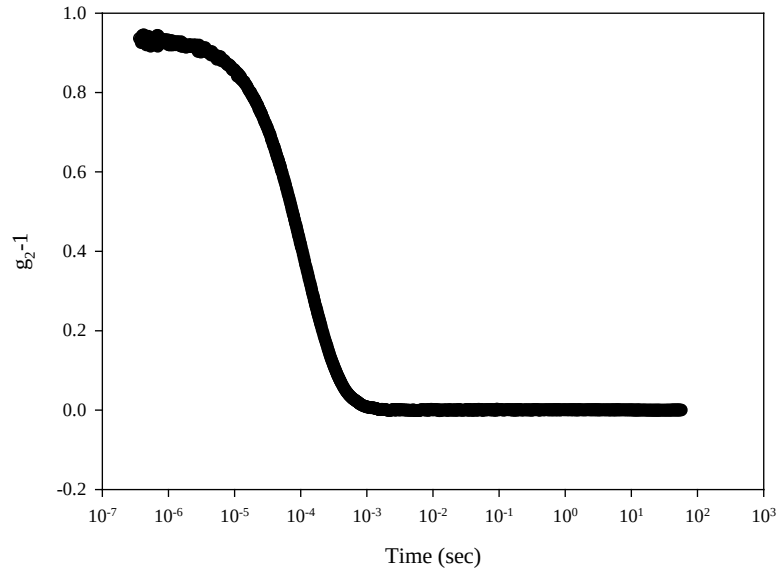

Figure 3.7: Typical auto correlation function.

The diffusion coefficient was only weakly concentration dependent in the range covered in the experiment. The average hydrodynamic radius was calculated using eq.(3.11) taking into account the solvent viscosity 9.6 X 10^{-4} Pa S, yielding R_h=9nm at both LiBr concentrations. This value is in good agreement with the results reported by Hossain et al[115] for equivalent systems dissolved in 6M LiBr. As pointed out by these authors, the molar mass of the RSF in LiBr cannot be determined because of difficulty of measuring the specific refractive index increment ($\frac{dn}{dc}$) in these media.

Static and dynamic light scattering was done on solutions dialysed against 0.1M NaCl and deionized water at pH 7 for which the values of $\frac{dn}{dc}$ (0.18ml.g^{-1}) are available in the literature.[115, 116] In both cases, the relaxation time distributions obtained displayed two diffusive modes of relaxation. The slow mode was attributed to the presence of large aggregates (R_h=50-60nm), whereas the fast mode of relaxation was attributed to individual fibroin molecules (R_h=9 nm). The relative amplitude of the slow mode, and thus the relative scattering intensity of the aggregates, was at most 0.4 in 0.1M NaCl and at most 0.8 in pure water. However, the concentration of the aggregates was negligible. The large relative amplitude of the slow mode results from the fact that the scattering intensity is proportional

to the molar mass of the solute that is orders of magnitude larger for the aggregates than that of the individual fibroin molecules.

The intensity scattered by the fibroin proteins was calculated by multiplying the total scattering intensity with the relative amplitude of the fast mode. After correction the intensity was independent of q. The molar mass of the fibroin proteins was determined by extrapolation to zero concentration and found to be $(3\pm1)\times10^5$ g/mol in pure water (see Figure 3.9). This value is in reasonable agreement with that reported for isolated native fibroin (about 4×10^5 g/mol)[75, 117] and with our gel electrophoresis data discussed earlier. The light scattering data also provide a possible explanation for the observed smear in the SDS-PAGE using 12% polyacrylamide gel. It is likely that the aggregates in the freshly dialyzed RSF appear as the 'high molecular weight' species in the SDS-PAGE. The molecular characterization data for freshly dialyzed RSF presented above suggests that the solutions are intrinsically unstable even at pH near 7. Fibroin molecules were found to aggregate to a small extent even during the dialysis process. This is also in agreement with the observations of Hossain et al who reported that unlike in 6 M LiBr solutions where aggregation of fibroin happened only above a critical concentration of about 0.7 g/L, in water fibroin had a tendency to aggregate even in very dilute solutions.[75]

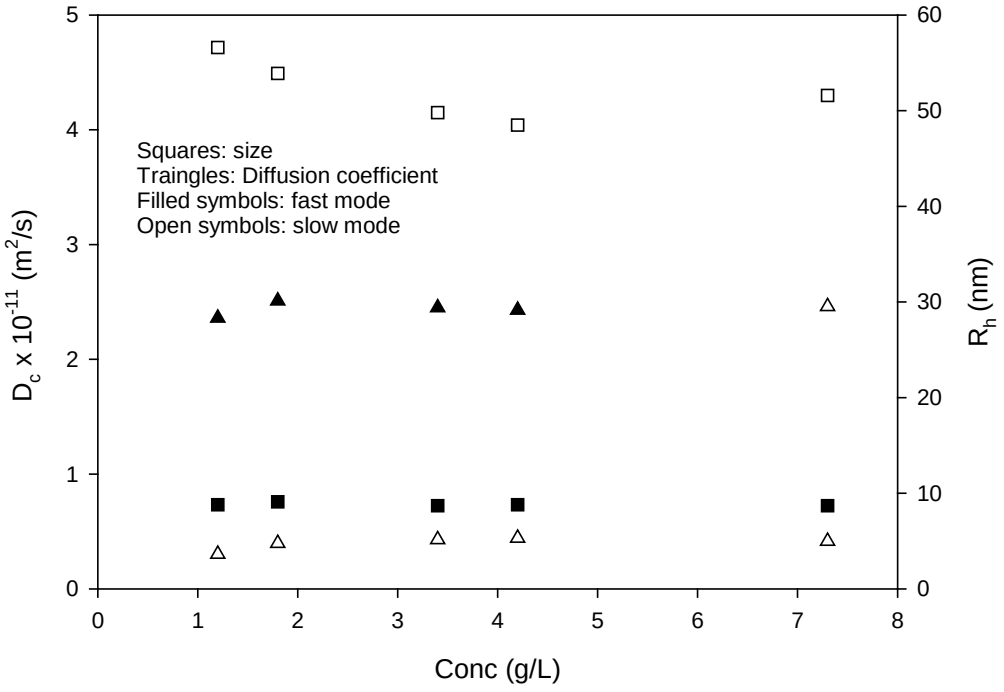

Figure 3.8: DLS of as dialyzed RSF of pH 8.2 at ambient temperature.

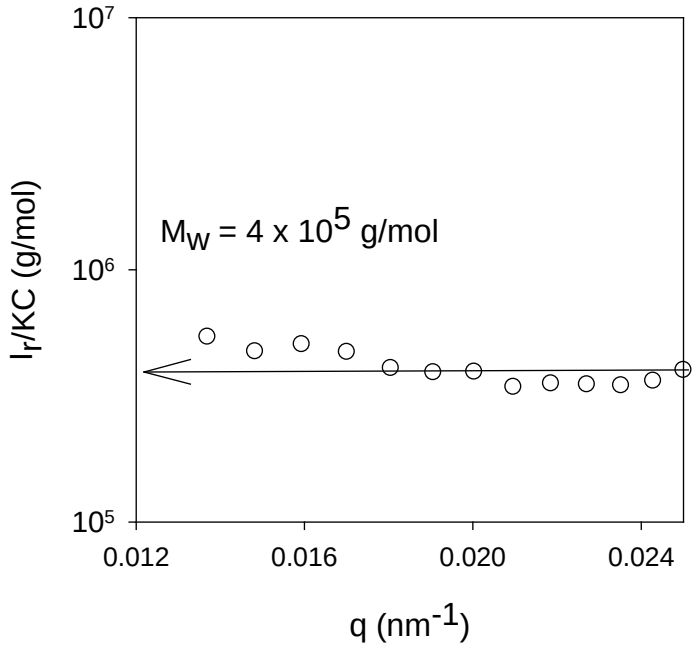

Figure 3.9: Example of SLS data of as-dialyzed RSF of pH 8.2, C=1 g/L.

Finally, note that the C*, i.e. the critical concentration above which chain overlap happens, for the freshly dialyzed RSF solution can be estimated as $C^* \sim \frac{M_w}{N_A\left(\frac{4}{3}\pi R_h^3\right)} \approx 150$ g/L . Thus, the freshly dialyzed RSF solution having a concentration of C ~ 40 g/L is in the dilute regime.

3.6.3 Circular Dichroism:

The conformation of fibroin in freshly dialyzed RSF was studied using CD. The solution of C= 0.5 g/L was prepared and placed in a quartz sample holder of path length 1mm. The spectra was recorded for wavelength region of 190 to 260 nm^{-1}. The as dialyzed RSF solution showed a peak at a wavelength of 204 nm which corresponds to the random coil conformation (Figure 3.10). The sample also showed a shoulder at 217 nm which corresponds to β sheet conformation.

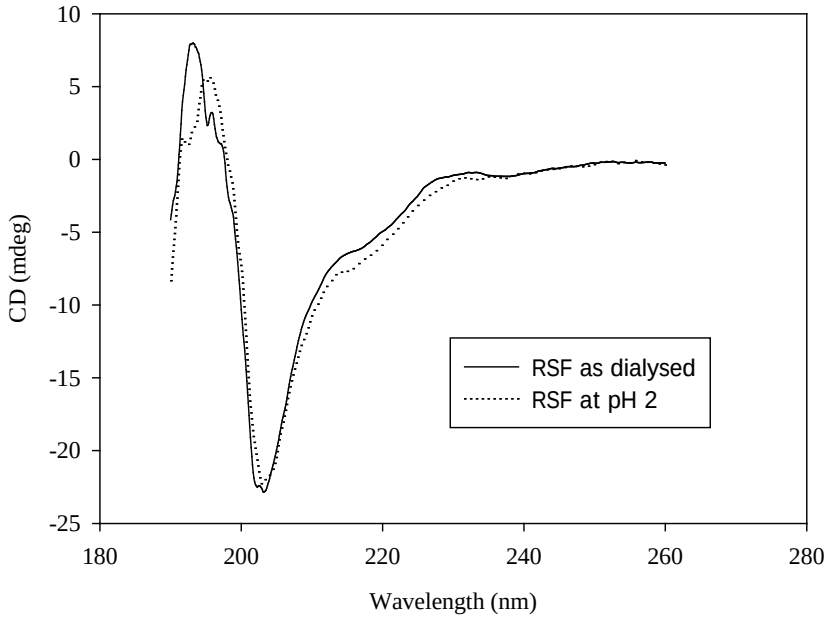

Figure 3.10: CD spectra of RSF as dialysed and RSF after pH adjust to 2.

3.6.4 Confocal Laser Scanning Microscope:

The microstructure of freshly dialyzed RSF diluted to a concentration of C=1 g/L was observed under confocal microscope using the 63x objective and is shown in Figure 3.11(a). The solution of RSF was tagged with rhodamine B of concentration 5 ppm. No visible aggregates can be seen in these images indicating a homogeneous microstructure at length scales above 300 nm.

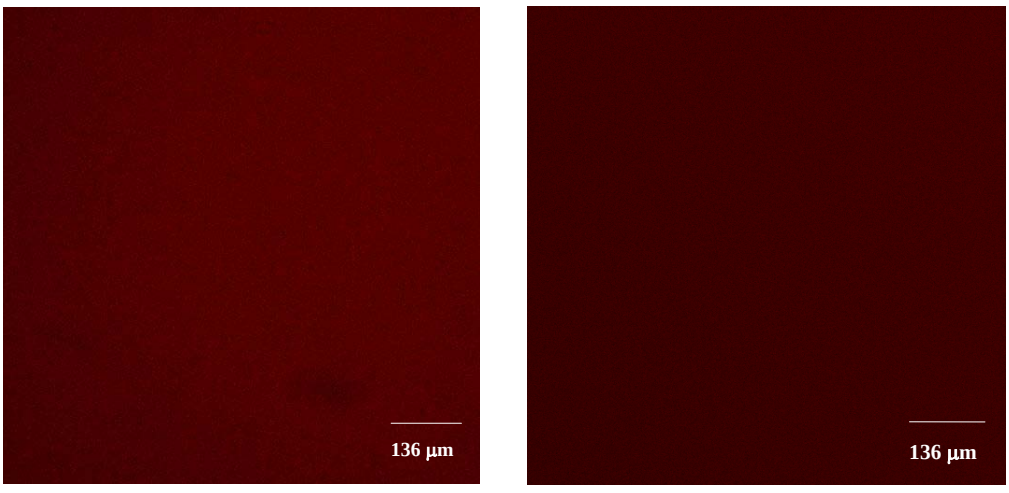

Figure 3.11: CLSM images of as dialysed RSF (left) and RSF at pH 2 (right)

3.7 Preparation of RSF sol:

Samples for sol to gel phase transition studies were prepared using the following procedure. The pH of a portion of the freshly dialysed RSF solution was adjusted to the desired value (between 2.0 and 4.0) by adding 0.1 M HCL solution drop wise under constant stirring. During the pH adjustment a part of the protein precipitated out as the pH approached the overall isoelectric point (pI=3.9) of the fibroin. The precipitate was removed by centrifugation at 15000 RPM for 20 min. The supernatant protein solution thus obtained, hereafter called the 'sol', was transparent and its concentration was determined by UV – visible spectroscopy before using it for further studies. The sol so prepared typically had a concentration of 8-11 g/L. It was further diluted with acidic (HCl) solution of the same pH to the desired fibroin concentration.

3.8 Stability of RSF sol:

The stability of RSF sols of different protein concentrations at various pH and temperatures was investigated by monitoring the samples for a period of 30 days, at the end of which the state of the samples was categorized in four distinctive groups namely opaque gel, translucent/transparent gel, precipitate and sol. Figure 3.12a shows a representative set of samples obtained after keeping sols of different fibroin concentrations and pH 3 at 50^{o}C for 30 days. Going from left to right in this picture the first three samples are opaque gels, the next three are transparent/translucent gels and last three are sols contained small amounts of precipitates. Figures 3.12c show the phase diagram obtained from such observations for all concentrations, pH and temperatures studied in this work, and Figure 3.12b shows a two-dimensional section of this phase diagram. It can be seen from Figure 3.12c that for $C \leq 0.3$ g/L the RSF remains in sol state independent of pH and temperature. For $C \geq 8$ g/L the RSF sol always forms opaque gels irrespective of pH and temperature. In the intermediate concentration regime the sol forms translucent or transparent gels. The tendency to remain in sol state was found to be higher at pH greater than the isoelectric state. It may however be noted that the sol state is metastable at all pH and might gel or form precipitates over a period of time much longer than the 30 days waiting period arbitrarily chosen in this study. In this context Figures 3.12b,c should not be considered as a true equilibrium phase diagram for aqueous regenerated fibroin sols.

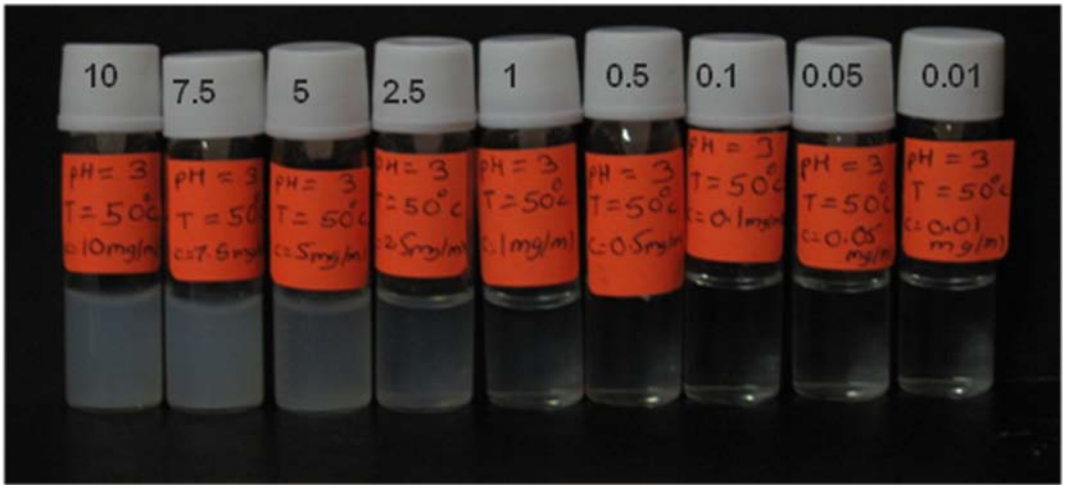

Figure 3.12a: Physical states of RSF of different concentrations upon gelation at pH 3 and 50^{o}C. The number on caps of bottle denotes concentration of RSF in mg/ml present.

Figures 3.10 and 3.11 also show the CD spectrum and CLSM image of RSF sols of pH 2 and C = 0.5 g/L and C = 1 g/L, respectively. The CD data shows that the fibroin in the RSF sol immediately after its preparation has a conformation that is identical to the conformation in the freshly dialyzed solution. The CLSM image shows that the RSF sol has no large scale heterogeneities immediately after its preparation.

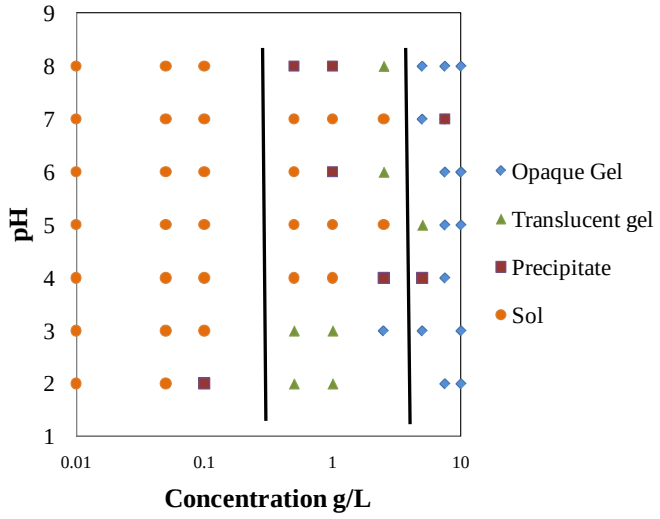

Figure 3.12b: 2DPhase diagram of RSF gel states as a function of pH, temperature and concentration.

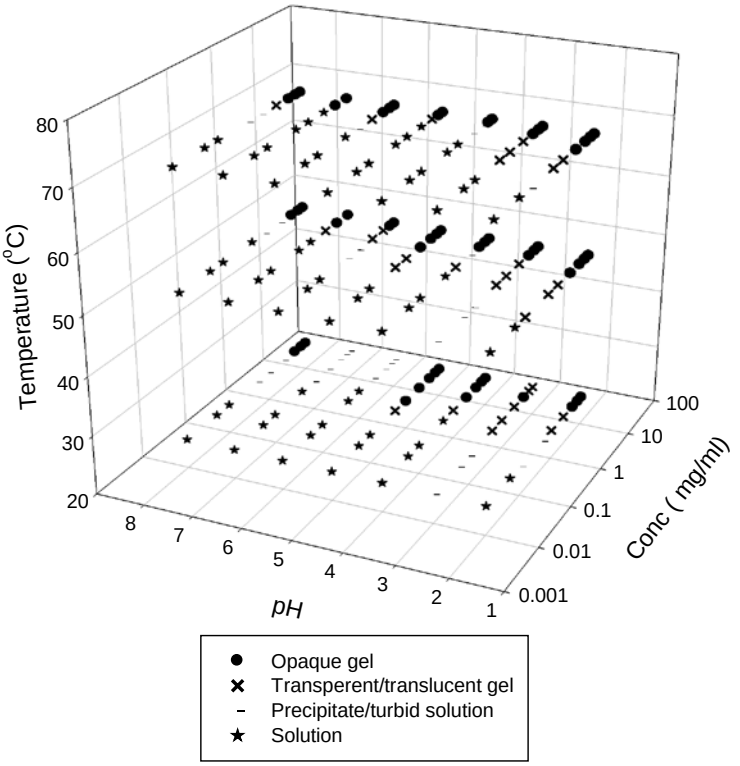

Figure 3.12c: Phase diagram of RSF gel states as a function of pH, temperature and concentration.

3.9 Summary:

Chapter 3 provided a brief background of the various structural characterization techniques and the data analysis methods that were used in this work. Details of experimental protocols followed for each of these techniques were also provided. The methodology adopted for preparing the aqueous RSF solution and results of its preliminary characterization were discussed. It was shown that the aqueous RSF solution has a pH of 8.2 and a fibroin concentration of approximately 40 g/L. It predominantly contains individual fibroin chains of weight average molecular weight 3±1 x 10^5 g/mol and hydrodynamic size 9 nm. The solution also contains a small number of larger aggregates of about 50 nm size. The fibroin is in

random coil conformation in the RSF solution. Zeta potential measurements were also carried out and the measured value between -17 and -22 mV suggested incipient instability. Indeed the RSF solution converted into gels given adequate waiting period. The methodology followed for preparing the RSF sol at pH close to and below the pI of fibroin was discussed. The sol was found to be unstable at pH ≤ pI; the measured zeta potential for a sol of pH 2 was between -4 and -2 mV. The gelation time was found to be less than a day for pH < pI and in excess of several days for pH > pI. A ‘phase diagram’ of the state of the samples was provided. The RSF sol was found to turn into opaque gels at concentration C > 5 g/L irrespective of pH. At concentrations C < 0.5 g/L the RSF remains in sol state at all pH. In the intermediate concentration range the RSF sol converts into weak transparent or translucent gels, and sometimes forms precipitates.

Chapter 4

Microstructure of RSF gel

As described in Chapter 2 previous research on RSF gels have elucidated only a minimal picture of the gel structure. On the other hand, the microstructure of gels made from other types of proteins, especially globular proteins, has been characterized in great detail. Therefore in the present work, an experimental program was undertaken to probe and understand the structure of RSF gels at various length scales using the techniques that have been used for other protein gels. In particular, the structure of the RSF gels was investigated in this work using techniques such as turbiditimeter, rheology, confocal microscopy, light scattering, X-ray scattering and circular dichroism. The effects of the concentration (C=0.5-12 g/L), temperature (T=5-70°C) and pH (2-4) on gel structure were systematically investigated. One of the difficulties encountered in this work was the relatively large variability of some of the gel characteristics between independently prepared samples. The variability demonstrates the sensitivity of silk fibroin to sample manipulation and necessitated measurements on a large number of independently prepared samples in order to extract the general features of the structure of silk fibroin gels.

4.1 Results:

4.1.1 Circular Dichroism:

CD spectrum of a gel prepared from RSF sol of C=1 g/L, pH 2 at 25 ^{o}C is shown in Figure 4.1 along with the spectra of the RSF sol (of pH 2) and freshly dialyzed RSF solution (of pH 8.2). The RSF sol and the freshly dialyzed solution show a predominant peak at a wavelength of 204 nm indicative of a random coil conformation. The two samples also showed a shoulder at 217 nm which corresponds to β sheet conformation. The shoulder suggests the possible existence of a small number of β sheet structures in both the freshly dialyzed RSF solution and the RSF sol. In contrast, the RSF gel shows only one broad peak with a maximum at 217 nm indicative of a large fraction of β sheet conformations. Thus, there is a conformation transition of the fibroin as the RSF sol changes into a gel. This result is in agreement with previous studies.[101] An attempt was made to quantify the fractions of random coil and β sheet conformations in the three samples using different models. However the estimated fractions were found to be highly model dependent, and the model fits were not of acceptable quality in the case of the gels. Hence the fractions of the two conformations in the samples are not reported here.

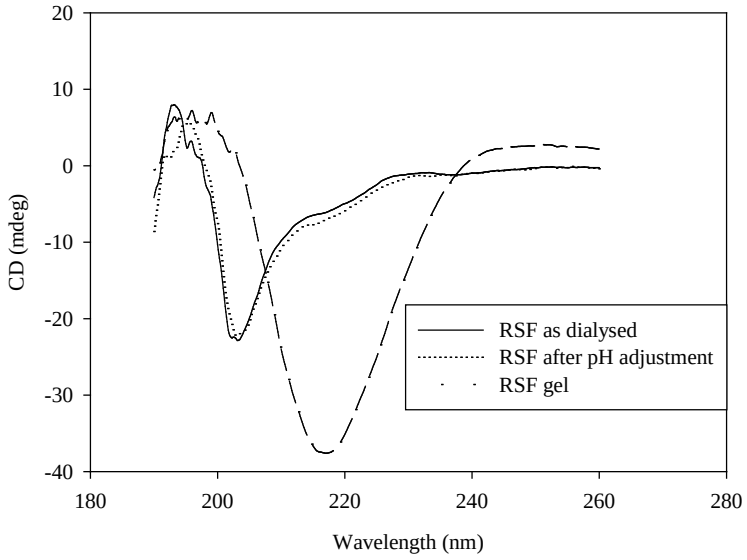

Figure 4.1: CD spectra of freshly dialyzed RSF solution, RSF sol (pH 2, 1 g/L) and gel made from the RSF sol at 25 ^{o}C.

4.1.2 Turbidity measurements:

The turbidity of RSF gel was calculated from the absorbance value recorded with a UV-visible spectrophotometer using eq (3.25). Figure 4.2 shows the concentration dependence of the turbidity of RSF gels measured at a wavelength of 685 nm. Similar concentration dependence was observed at other wavelengths also. The different symbols indicate different temperatures: 70° C (circles), 50° C (squares), 20° C (triangle) and 5^{o} C (Hex). Figure 4.2 shows that within the scatter of the data the turbidity was independent of temperature and pH for any given concentration. The scatter in the data was related to the initial state of the sol as mentioned earlier. The data in Figure 4.2 shows that the increase of the turbidity with concentration is slightly stronger than linear dependence. Matsumoto et al[118-120] reported that the optical density of their RSF gels increased approximately linearly with fibroin concentration in the range 6-72 g/L and was the same at 20 and 37 °C (i.e., nearly independent of temperature). A direct comparison with Matsumoto et al's data is unfortunately not possible, because they did not report the path length of the light. The wavelength dependence of turbidity of gels is shown in Figure 4.3. The data could be fit to a power law $\tau \sim \lambda^{-\alpha}$ with $\alpha \approx 2$.

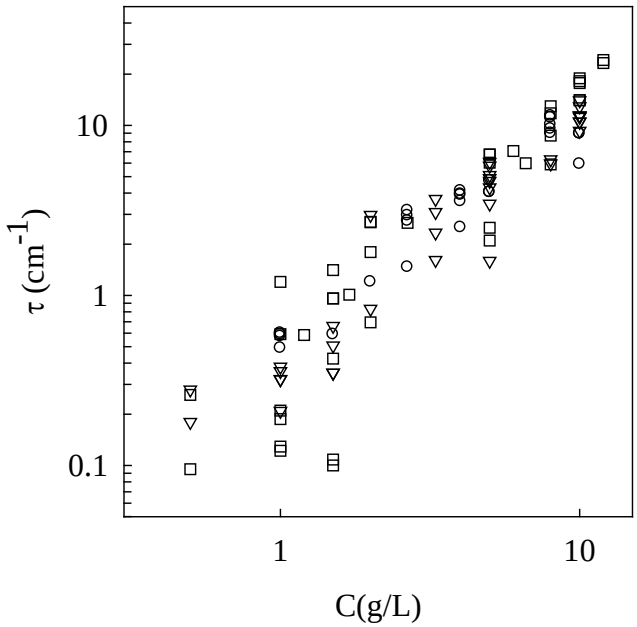

Figure 4.2: Concentration dependence of the turbidity of RSF gels obtained at different temperatures (5, 20, 50, 70°C) and pH (2, 3, 4).

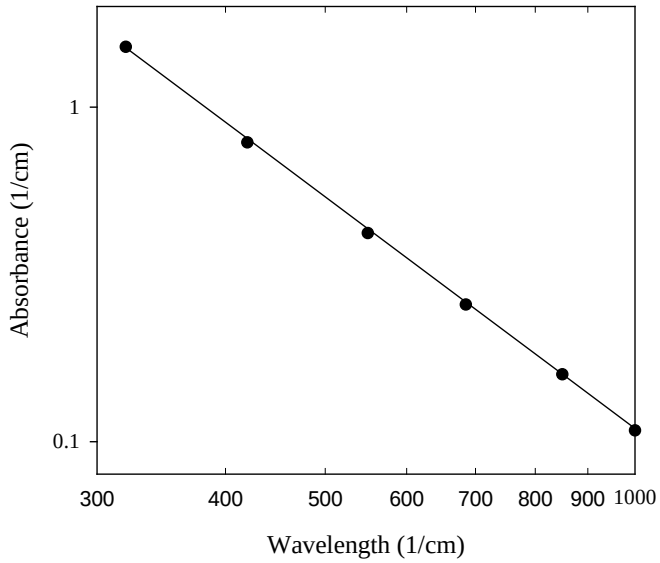

Figure 4.3: Wavelength dependence of transmittance for a RSF of C=10 g/L concentration prepared at pH 2 and temperature 70 ^{o}C. Line through points shows power law fit with exponent of -2.3.

4.1.3. Light scattering:

The structure of the gels on mesoscopic length scales was studied using static light scattering. Gels were prepared from RSF sols of concentrations C=0.5, 1.0 and 1.5 g/L at pH 2, 3 and 4 and at 25 ^{o}C. For these low concentration gels the turbidity was sufficiently small so that multiple scattering can be neglected. The relative scattering intensity I_r / KC of the gels was plotted as a function of the wave vector q and the data is shown in Figure 4.4. For an incident wavelength of 632 nm the optical constant was calculated from the known value of refractive index increment for RSF (*dn/dc* = 0.16 ml/g) to be $K = 2.98\text{x}10^{-11}$ gmol L m^{-1}.[113] The relative scattering intensity showed a power law q-dependence which implies that the microstructure is self similar and characterized by a fractal dimension d_f.[121] For all gels investigated we found that d_f was about 2 as shown in Figure 4.4. For most systems, power law dependence was observed over the whole q-range accessible in the experiments, which means that the fractal structure spanned a length scale range of about 2 μm down to at least 100 nm. In some cases the data deviated from the power law dependence at the smallest q-values indicating that the large size cut off for the self-similar structure of those systems was slightly smaller than 2 μm. The small size cut off for the self-similar structure can be expected to be much less than 100 nm.

The absolute values of I_r / KC at a given q-value varied by about a factor of two around the average, but did not depend systematically on the protein concentration or on the pH. This variation in the I_r / KC is caused either by a variation in the quantity of aggregated material or by a change of the density of the structure on length scales smaller than the low size cut off length scale. Again, the origin of the scatter of data lies in the difficulty in controlling the initial state of the sol as mentioned earlier.

4.1.4. Confocal Laser Scanning Microscopy:

The structure of the gels at length scale larger than that investigated by light scattering was studied in more detail using Confocal Laser Scanning Microscope (CLSM). Typical images of a silk protein gel are shown in Figure 4.5 and all other systems investigated looked similar. The labelling was chosen such that the average fluorescence intensity was the same for all images even though the protein concentration varied. Thus the differences between the images are caused by differences of the gel structure. At these length scales the gels appear to

be formed by agglomeration of micron sized protein aggregates leading to a network with a characteristic pore size that increased with decreasing concentration. Gels formed at pH 3 and 4 or at 25 °C looked similar.

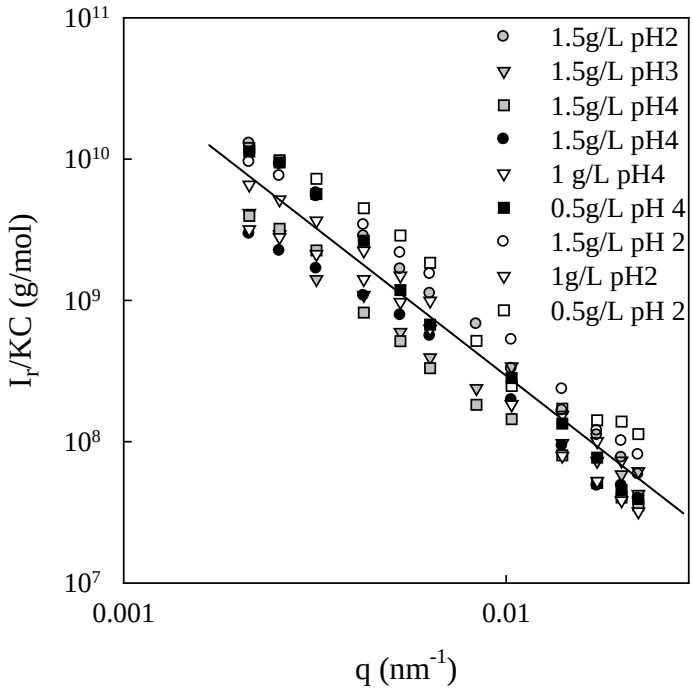

Figure 4.4: Dependence of I_r/KC on the scattering wave vector for RSF gels formed at different conditions indicated in the figure. The solid line has slope -2.1.

Following the work of Ako et al[93] the CLSM images were quantitatively analyzed by calculating the pair correlation function $g(r)$ from the fluorescence signal (A) at coordinates $\vec{i}$ and $\vec{j}$ using the formula given in eq (3.23). For isotropic systems, if the fluorescence signal intensity is proportional to the concentration (A α C), then the pair correlation function $g(r)$ is equal to the concentration pair correlation function given by eq (3.24). To calculate $g(r)$ the pixel positions were chosen randomly within the pixel area in order to ensure that r varies continuously. For small r, A_i and A_j are strongly correlation so that $g(r)$ is a large number whereas for large r, A_i and A_j are no longer correlated so that g(r) becomes unity.

A few examples of g(r) are shown in Figure 4.6. It turns out that all pair correlation functions can be superimposed by horizontal and vertical shift factors on to a master curve

shown in Figure 4.7 that could be well described by a stretched exponential decay with stretched exponent 0.85. This means that $g(r)$ of all systems could be described by:

$$g(r) = B\exp\left[-\left(r/\xi\right)^{0.85}\right]+1 \qquad 4.1$$

where B characterizes the relative amplitude of the concentration fluctuations and ξ the correlation length of the concentration fluctuations. The concentration dependence of B and ξ is shown in Figure 4.8 and 4.9 for pH 2, 3 and 4 at 20 and 50 °C. Again large scatter of the data is observed without a systematic dependence on either T or pH, except perhaps that the values of B at pH 4 appear to be systematically smaller than at pH 2 and pH 3. The amplitude of the concentration fluctuations is independent of the concentration, but the correlation length appears to decrease somewhat with increasing protein concentration. The correlation length indicates the large size cut off for the self-similar structure observed in light scattering. The values of the correlation length shown in Figure 4.8 are of the order 1 – 2 μm, which is in agreement with the inference drawn from the light scattering data presented in Figure 4.4.

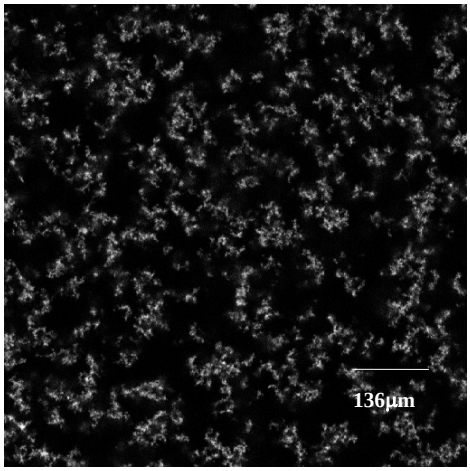

(a)

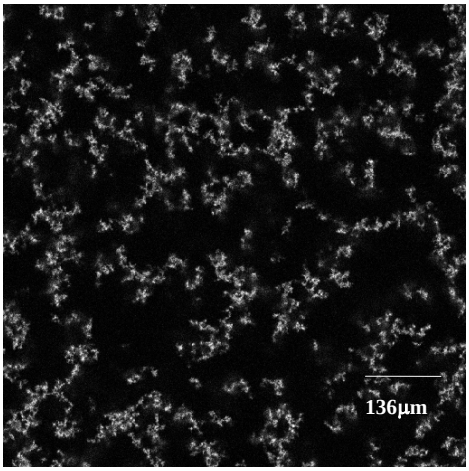

(b)

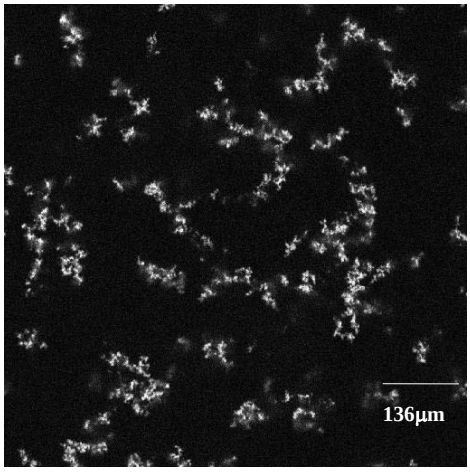

(c)

Figure 4.5: Examples of CSLM images of RSF gels: (a) gel formed at C=0.5g/L, pH 2 and 50°C (ξ=2.4µm), (b) gel formed at C=1.5 g/L, pH 2 and 50°C (ξ=1.6µm), (c) gel formed at C=5g/L, pH 2 and 50°C (ξ=0.9µm). The width of the image represents 160 µm.

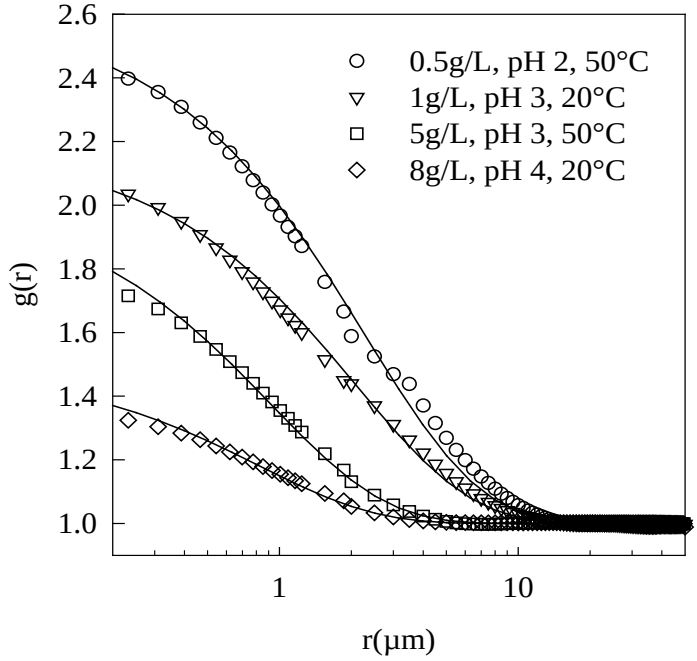

Figure 4.6: Examples of pair correlation functions of gels obtained at different pH, T and C.

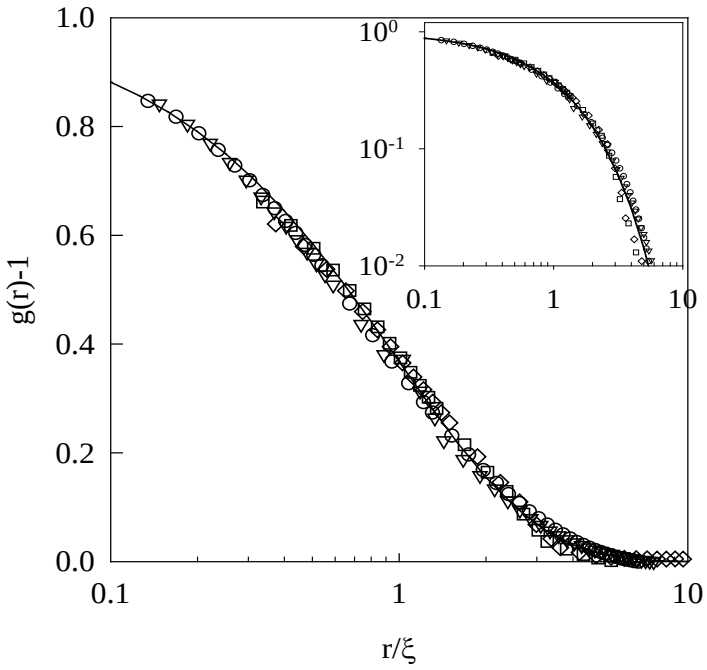

Figure 4.7: Superposition of g(r) obtained at different concentrations at pH 3 at 20° (filled symbols) and 50°C (open symbols). The solid lines represent stretched exponential decays, see text. The inset shows the same data on a log-log plot.

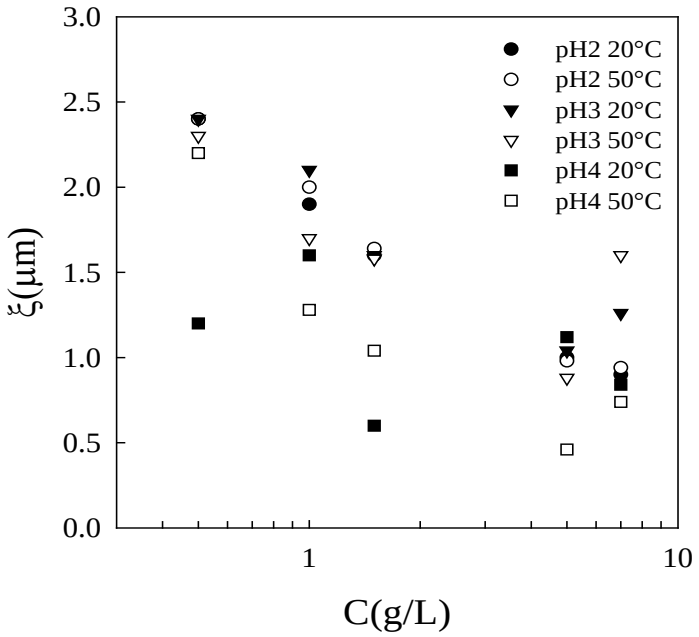

Figure 4.8: Concentration dependence of the correlation length of the concentration fluctuations for gels formed at different pH and T, indicated in the figure.

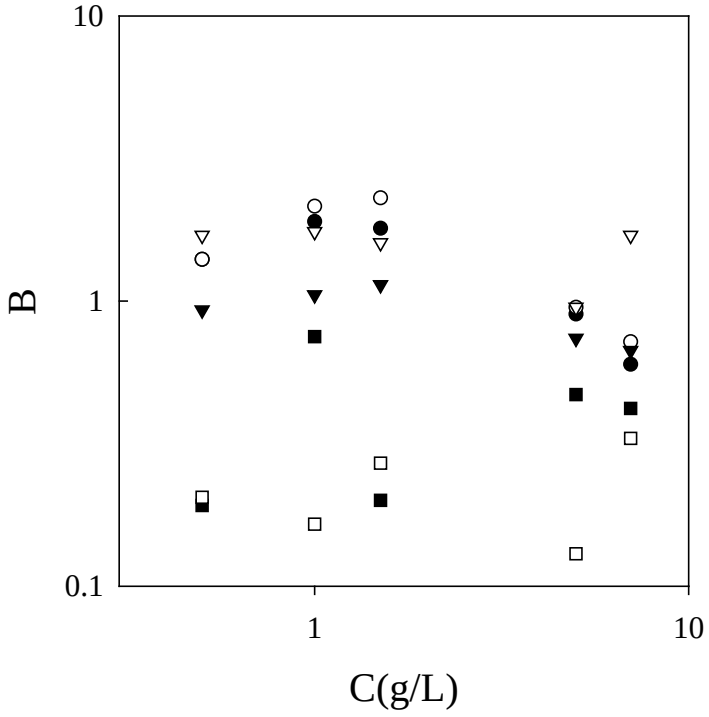

Figure 4.9: Concentration dependence of the amplitude of the concentration fluctuations for gels formed at different pH and T. Symbols as in Figure 4.8.

4.1.5. Small angle x-ray scattering:

While confocal microscopy enabled the observation of gel structure coarser than that observed with light scattering, the finer structure of RSF gels at higher q-values was probed by SAXS. Figure 4.10 shows SAXS data for gels made from RSF sols of two different protein concentrations (C=1 and 5 g/L) and three different pH (2, 3 and 4) at 25 ^{o}C. At low q-values the scattered intensity shows a power law q-dependence with an exponent close to -2 indicating that the self similar structure inferred from light scattering data continues down to smaller length scales. However above q ~ 0.045 – 0.1 Å^{-1}, which corresponds to length scales of about 6 – 15 nm, the scattering intensity shows a power law q-dependence with an exponent of close to -1. This suggests that the fine scale structure below about 6 nm is composed of thin rod-like aggregates (or strands). Random branching of these strands must build the fractal aggregates observed at larger length scales. Thus the lower length cut off of the fractal structure is between 6 and 15 nm. As with the case of light scattering, the SAXS intensity did not show systematic dependence on pH or concentration. High q data suggests variations in the branching density of the strands is likely to cause the variations in scattered intensity.

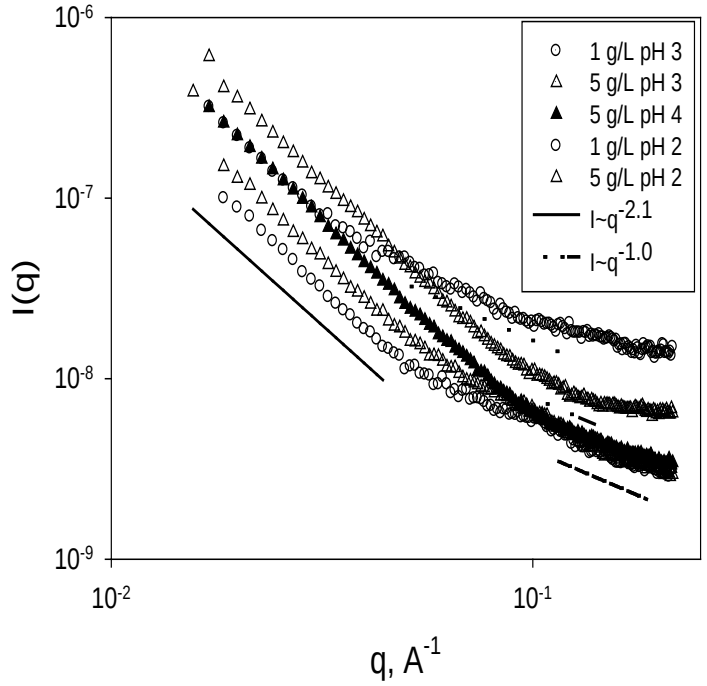

Figure 4.10: I v/s q for protein gels formed at different concentration and pH. Solid and dotted lines have slopes -2.1 and -1, respectively.

4.1.6. Rheology:

The shear rheology of RSF gels was studied in strain sweep and frequency sweep experiments. Figure 4.11(a,b) shows typical data for a gel prepared at 25 ^{o}C from a RSF sol of C=10 g/L and pH 2. The strain sweep ($\gamma_0 = 0.01$ to 100) was done at constant frequency of $\omega = 1$ Hz. A clear distinction between the linear and non-linear regimes is seen. Also, $G' > G''$ as expected. The frequency sweep ($\omega = 0.1$ to 100 rad/sec) experiment was done by imposing a strain of 0.02% and showed that G' is frequency independent for most of frequency regime while G'' shows a weak minimum, which is a typical gel like behaviour. The elastic shear modulus of the gels (G_e) was estimated as the storage modulus G' in a small amplitude oscillatory shear experiment conducted at a frequency $\omega = 1$ Hz and strain $\gamma_0 = 0.2\%$. Even smaller strain amplitudes are required for gels of lower concentrations since they are fragile. All oscillatory measurements were done after long waiting times post gelation to allow for slow evolution (aging), if any, of the mechanical properties of the gel. G_e was measured for gels of several concentrations and was found to increase with increasing concentration as shown in Figure 4.12. The spread in the values of G_e is large at all concentrations, but we did not observe a systematic dependence on the temperature or on the pH. The large scatter of G_e at low concentrations can in part be attributed to the difficulty to study weak RSF gels with shear rheology. However, also at higher protein concentrations for which G_e increased by several orders of magnitude after gelation, the scatter in the values of G_e was important. Thus the main reason of the scatter is not experimental error, but probably the sensitivity of the gel structure to the initial state of the RSF sols, which varies between different preparations.

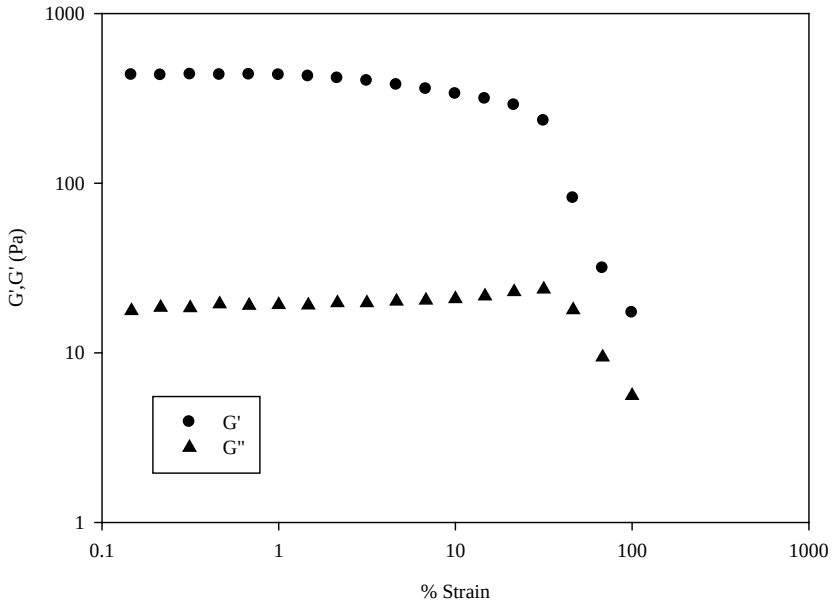

Figure 4.11 a: Strain sweep of RSF gels.

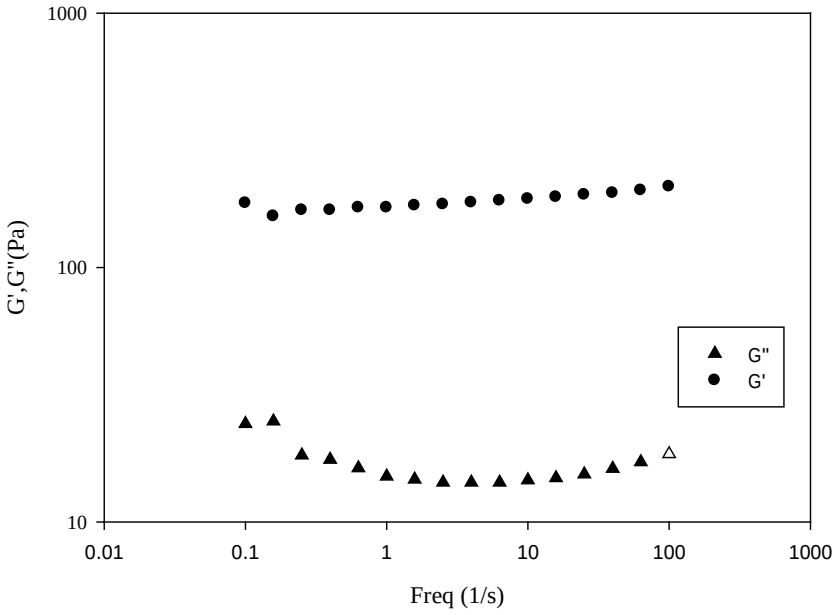

Figure 4.11 b: Frequency sweep of RSF gels.

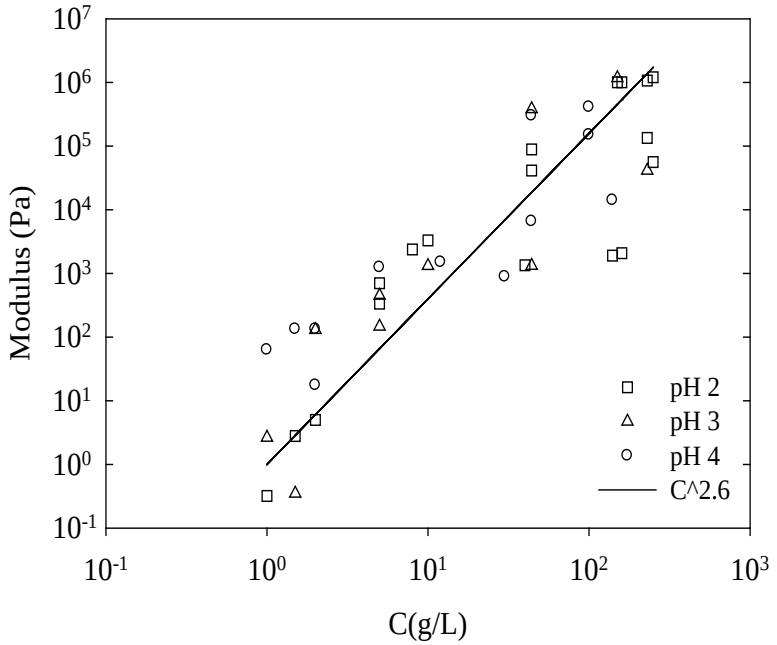

Figure 4.12: Concentration dependence of the storage modulus of silk protein gels obtained at different temperatures and pH. The solid line indicates the 2.6 power law dependence.

The mechanical properties of a few gels were also measured in compression mode using a dynamic mechanical analyzer (DMA). Gels were cast in specially prepared aluminium sample holder cups of 27.5 mm diameter and 5 mm depth. The cup served as the lower plate, while a 25 mm aluminium flat plate was used as the upper plate. The gels were sandwiched between these two surfaces and compression test was carried out by oscillating the upper plate at frequency of 10 Hz and small strain amplitude of 5%. The compression modulus was taken as the storage modulus in compression at high frequency. The variation of compression modulus with fibroin concentration is shown in Figure 4.13.

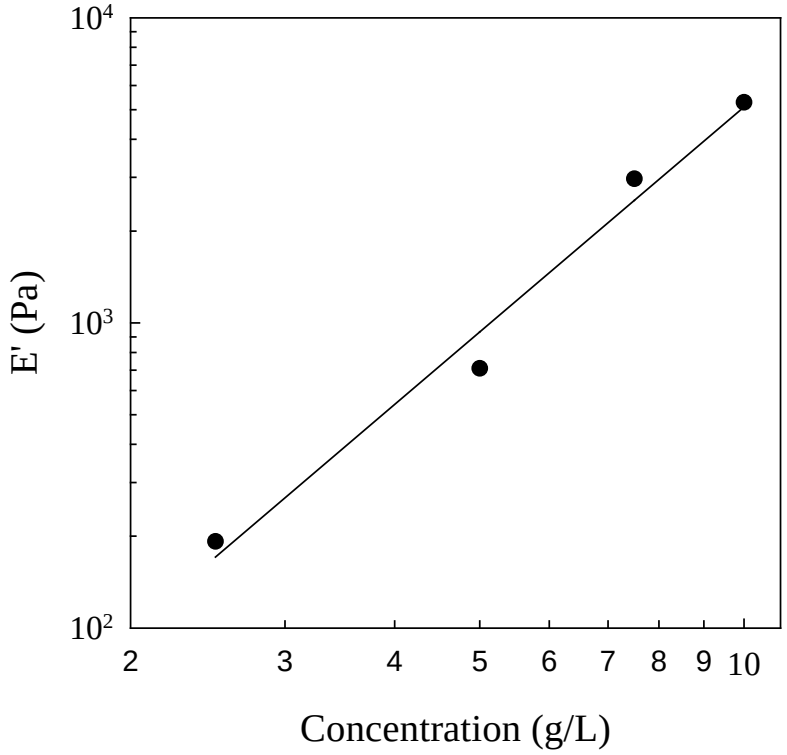

Figure 4.13: Concentration dependence of compression modulus of RSF gels of pH 2 prepared at 25 ^{o}C. The line indicates a power law fit of exponent 2.5.

4.2 Discussions:

The structure of RSF gels was probed at different length scales using a variety of techniques. At the molecular conformation level the gels contained a significant amount of β sheets, in agreement with the results of the previous studies. However the data presented above shows that there is a hierarchy of structures at mesoscopic length scales in the RSF gels that were hitherto not investigated.

Static light scattering experiments showed that the RSF gels have a self similar structure of fractal dimension $d_f = 2$. Of course, the structure can only be self similar over a limited range of length scales. Small angle x-ray scattering experiments showed that the proteins assemble into fine strand-like structures of 6 – 15 nm length. These are the basic building blocks of the fractal structure; they randomly branch to form the self similar aggregates of larger size. Thus the lower size cut off the fractal structure is approximately 10 nm. The low structural density of the RSF gels explains why they can form even at very low

protein concentrations and also why they easily break under stress at low concentrations. The fractal structure exists till an aggregate size of about 1 μm (large size cut off), which is detected as the correlation length of concentration fluctuations in confocal microscopy. At still higher length scales the protein aggregates of about one micron size agglomerate to form a three dimensional percolating porous structure which can bear some stress. The size of the pores decreases with increasing protein concentration. A schematic of the gel structure is shown in Figure 4.14.

As indicated previously, the turbidity of RSF gels showed slightly greater than linear concentration dependence. Since the correlation length and therefore the apparent molar mass of aggregates decreased weakly with increasing concentration, it would be expected from eq. (3.26) that the turbidity would increase slightly weaker than linear with increasing protein concentrations. This apparent deviation from theoretical expectation is due to the following reason. As the size of the concentration fluctuations becomes larger than about a micron, which is the case for the lower fibroin concentrations, scattering happens at very small angles ($< 3^o$) and is detected as transmitted light in the spectrophotometer. This causes an underestimation of turbidity. However as the protein concentration increases the correlation length decreases, or in other words the length scale of the concentration fluctuations is attenuated. This reduces the underestimation of turbidity, and hence results in a greater than linear dependence of turbidity on protein concentration.

The turbidity of RSF gels also showed a wavelength dependence given approximately by $\tau \sim \lambda^{-2}$. The value of the power law index can be explained on the basis of eq (3.26) in which the optical constant has a wavelength dependence of $K' \sim \lambda^{-4}$ while the structure factor has a wave vector dependence given by $S(q) \sim q^{-2}$ because of the self-similar structure of the gel. Since $q \sim 1/\lambda$, eq (3.26) shows why the turbidity should have the scaling of $\tau \sim \lambda^{-2}$ which is seen in the data.

The turbidity, light scattering intensity and x-ray scattering intensity of the gels was found to be consistently independent of the temperature and the pH within the scatter of the data. This is also consistent with the confocal microscopy data and the shear modulus data indicating that the structure of the gels was independent of these parameters.

Shih et al [92] suggested that fractal aggregates have load bearing backbone chains that percolate the structure, and have a fractal dimension that can be calculated from the formula given in equation (2.1). Typically the fractal dimension of the backbone can be expected to be approximately 1.0. Unfortunately, the concentration dependence of shear modulus suggested in Figure 4.12 provides an unphysical value for the fractal dimension of the backbone. This could be because of the poor fit to the experimental data caused by the large amount of scatter.

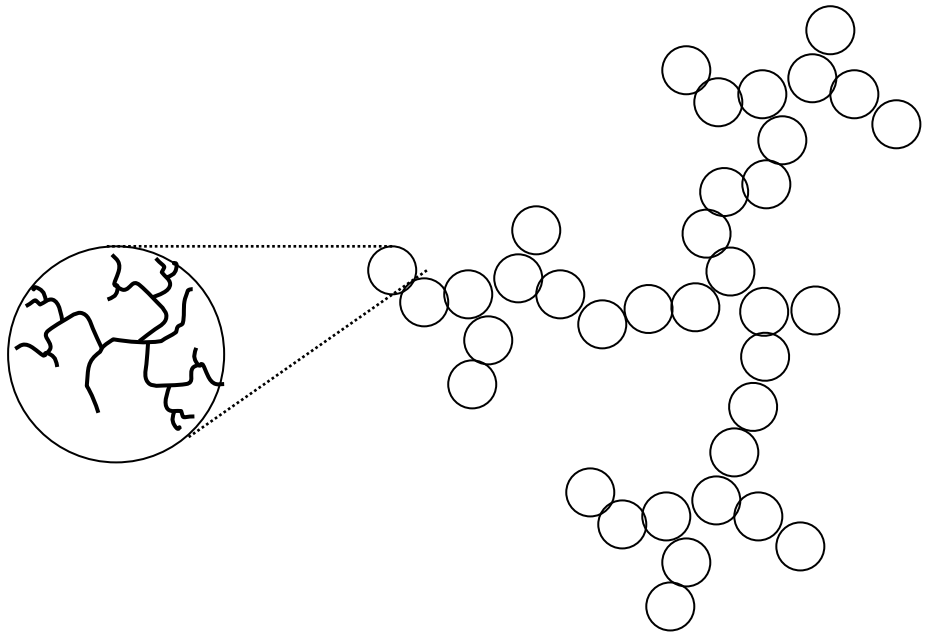

Figure 4.14: Schematic drawing of low density silk protein gels. Randomly branched protein chains with form aggregates with a radius close to one micron, that connect into a system spanning network.

4.3 Summary:

RSF hydrogels have a hierarchy of microstructures which have fractal nature within a lower cut off limit (approximately 10 nm) and higher cut off limit (approximately 1 μm). At a molecular level the proteins take on β-sheet conformation. The fractal structure provides the gels with a three dimensional architecture of connected porosity, which could be of use to applications such as scaffolds for tissue engineering.

Chapter 5

Gelation of Regenerated Silk Fibroin

In the previous chapter the structure of RSF gels was discussed in detail. This chapter presents experimental data on the time evolution of the viscoelastic properties and mircostructure of RSF during its sol to gel transition. The effect of the pH (2-4), concentration (0.5-10 g/L) and temperature (5-70 °C) on gelation kinetics was systematically investigated. Once again, the structure development was tracked from molecular to macroscopic length scales using different techniques to develop a comprehensive understanding of the gelation process. As mentioned in the previous chapter there was a relatively large variability of some of the parameters characterizing gelation of RSF between independently prepared samples. The variability demonstrates the sensitivity of silk fibroin to sample manipulation and necessitated measurements on a large number of independently prepared samples in order to extract the general features of silk fibroin gelation. The implications of the present experimental results for the aggregation and gelation mechanism of RSF sols will be discussed.

5.1 Results:

5.1.1. Rheology:

Gelation was tracked by performing isothermal creep experiments repetitively after a fixed interval of waiting period as described in section 3.4.1. The creep time for each test was kept much smaller than the waiting time interval between tests to ensure that there is no substantial change in the rheology of the sample during any test. Figure 5.1 shows the creep response of a 0.5 g/L RSF sol of pH 2 at temperature 25 ^{o}C during gelation. The ‘zero hour’ data shown in the figure was collected immediately upon loading the sample in the cup and bob fixture. Further creep tests were performed after three hour intervals between consecutive tests.

Figure 5.1a also shows creep data for the freshly dialyzed RSF solution of C=0.5 g/L, pH 8.2. The creep compliance of this solution is clearly seen to be dominated by its viscous character. From the long time slope of the compliance data the viscosity of this freely flowing solution was calculated to be approximately 9 cP. In contrast, the sol of pH 2 at zero hour showed a significantly lower compliance and also showed damped oscillations of the compliance, i.e. creep ringing. This is indicative of a weak gel-like nature of the sol even at zero time. Thus, the lowering of pH of the freshly dialyzed RSF seems to change its rheological response from being dominantly viscous at pH 8.2 to distinctly elastic at pH 2. In

a separate experiment a creep test was first performed on the sol of pH 2 followed immediately by addition of a calculated amount of NaOH to raise its pH to 8, which is the same as that of the freshly dialysed solution. A second creep test was then performed on the sample. Figure 5.2 shows the results of these test sequences. It can be seen that after changing the pH from 2 to 8 the sol showed predominantly viscous response almost comparable to the response of the freshly dialyzed RSF solution. This shows that the viscoelastic behaviour of the RSF sol is initially reversible with respect to pH changes.

The data in Figure 5.1a shows that with time the creep compliance of the RSF sol of pH 2 progressively reduced while creep ringing became increasingly predominant in amplitude and frequency. Data for 12 h and 15 h showed a distinct jump in the frequency of ringing, which suggests a rapid increase in the elasticity of the sample in this time interval. From the creep ringing data it is possible to calculate elasticity of the sample using Struick's formula[109](see equation (3.21a). The elastic modulus for the 0.5 g/L plotted in Figure 5.3 can be seen to increase rapidly between 12 h and 15 h.

The lines going through each of the data sets in Figure 5.1a (which is shown more clearly in Figure 5.1b for the case of 18 h) represent calculations of the Jeffery's model given by equations (3.13-3.14). For creep data above 3 h only a single Jeffery mode was required to fit the data, whereas below this time at least two modes were required. The data for zero time could not be satisfactorily modeled by even a two-mode fit. Increasing the number of modes might have provided better fit to the data albeit at the cost of requiring large number of fitting parameters. A single mode Jeffery model has three material parameters, η_1, η_2 and G_J, in addition to a fourth rheometer related parameter I/b that are required to be determined in order to fit the creep data. Consequently an *n*-mode Jeffery model would require 3*n*+1 model parameters. In view of the difficulties associated with determination of the values of a large number of fitting parameters unambiguously, we have restricted to a maximum of two modes in our model fitting exercise. The determination of model parameters in the case of a single mode fitting procedure was done as follows. The value of G_J was determined from $G_J \approx 1/J(t_{ring})$, where $J(t_{ring})$ is the compliance at the end of the oscillations. η_2 was determined from the slope of the plot of long time creep compliance versus time. The value of I/b was obtained by fitting the very short time data to the equation $J(t) \approx \frac{b}{2I}t^2$. This

leaves only one parameter viz, η_1 for fitting the model to the data. Data fitting was done by visually comparing the model calculations and experimental data.

The value of I/b was taken as 0.5 N.s^2/m^2 and the values of the material parameters are shown in Figure 5.4 in the form of the two time constants namely the relaxation time $\tau_1 = \frac{\eta_1 + \eta_2}{G_J}$ and the retardation time $\tau_2 = \frac{\eta_1}{G_J}$. The values of the two viscosities were found to be such that $\eta_2 >> \eta_1$ for all times starting from zero time. Thus η_1 represents a microscopic viscosity in the sample, while η_2 represents the macroscopic viscosity of the sample. In chapter 4, it was demonstrated that the RSF gel has a self similar microstructure formed by aggregation of colloidal protein particles. In view of this structure the viscosity η_2 most likely represents the resistance to flow of the percolating structure of the gel while η_1 might be a local viscosity experienced by the colloidal protein aggregates in the structure. Figure 5.4 shows time evolution of the two time constants during gelation. Creep data starting from 3 h after zero time was used since it can be reasonably well described by a single mode Jeffery model. The model predictions show that while the relaxation time decreases slightly during the gelation process, the retardation time changes significantly between 12 h and 15 h. This happens because both η_2 and G_J increase during gelation whereas η_1 remains essentially constant. This suggests that the percolating structure builds up during gelation by increasing the number of cluster-cluster bonds, while the microscopic self-similar structure remains unchanged. Decrease in the retardation time with time has been reported for other systems such as aging soft colloidal glasses (e.g., laponite suspensions). [108] There again, the decrease is caused by the greater build up of elastic modulus compared to the microscopic viscosity η_1 of the samples.

The creep data for 7.5 g/L RSF sol of pH 2 is shown in Figure A-1 in the Appendix as evidence that it is qualitatively similar to the data for the 0.5 g/L RSF sol. The data for intermediate concentrations C= 1.0 g/L and 1.5 g/L (not presented) also showed similar trends. The value of creep compliance decreased with increasing fibroin concentration of the sample. For all concentrations the creep compliance at zero time showed a weak gel structure. The data at initial times could be modeled only by assuming more than one mode in the Jeffery model. After about 3 h from zero time the ringing data could be modeled nearly quantitatively using a single mode Jeffery model. In the course of gelation the ringing

became increasingly predominant, and for all concentrations a jump in ringing frequency was observed between 9 h and 15 h after zero time. This suggests that the time at which rapid gelation occurs (t_g) is weakly dependent on the fibroin concentration of the RSF sol. For all concentrations the relaxation time decreased slightly with gelation time whereas the retardation time changed to a greater extent near the t_g.

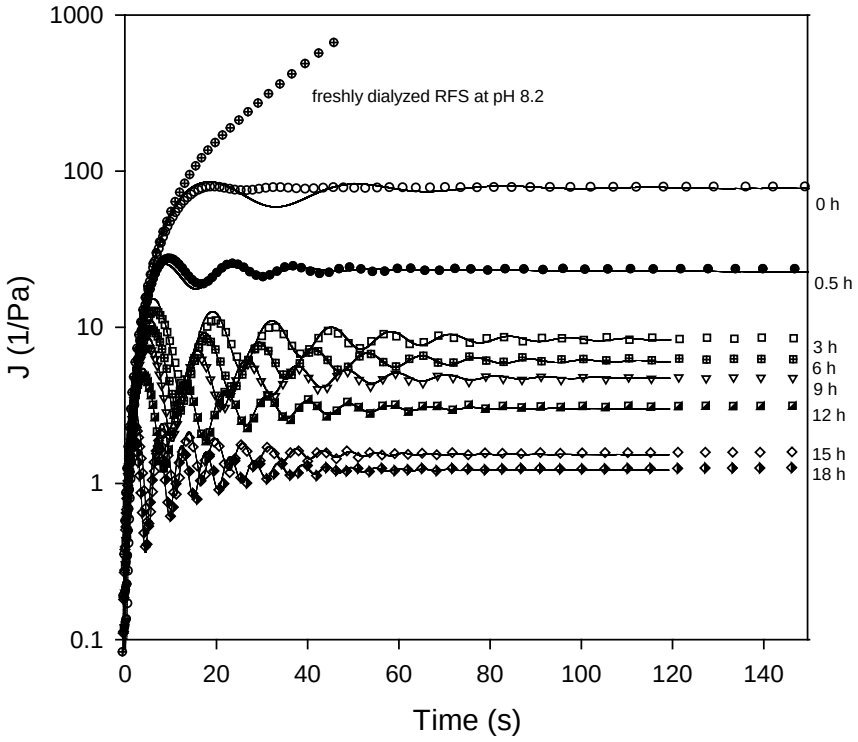

Figure 5.1a: Time evolution of the creep behavior of 0.5 g/L RSF sol of pH 2 at 25 ^{o}C

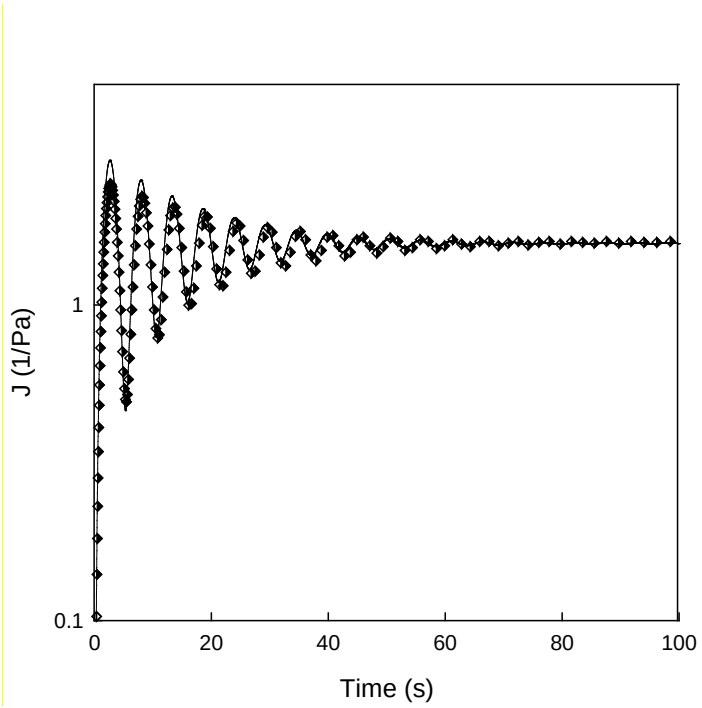

Figure 5.1b: Creep after waiting period of 18h presented to bring out more clearly the comparison between experimental data and model.

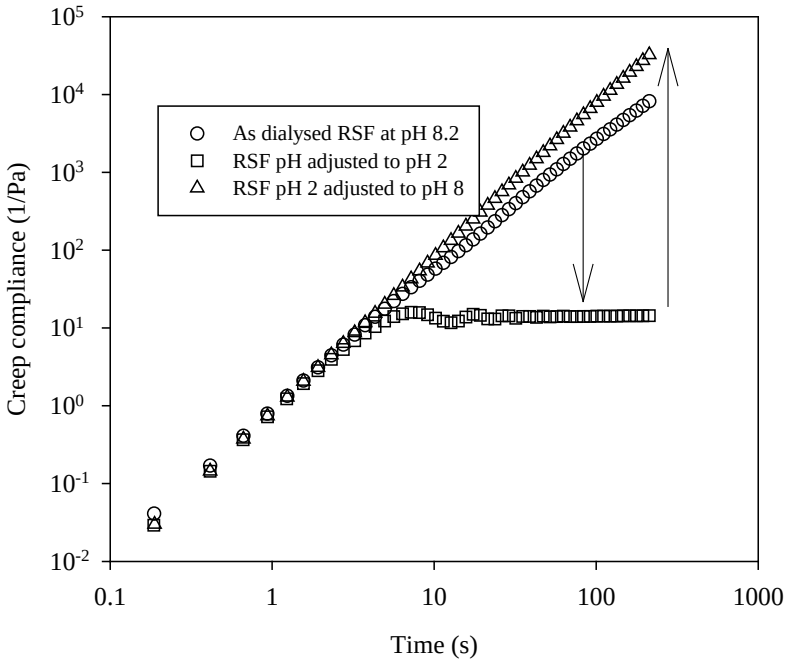

Figure 5.2: Creep behaviour of RSF sol of C=1 g/L, pH 2 compared with the creep behaviour of a freshly dialyzed RSF solution of the same concentration at pH 8, and the creep behaviour of the RSF sol after its pH was readjusted to pH 8 by adding NaOH.

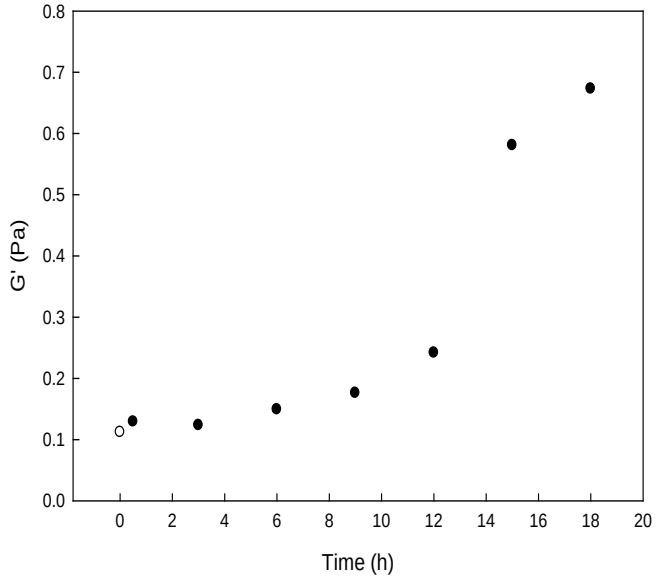

Figure 5.3: Evolution of storage modulus calculated from the Struick formula [eq 3.22].

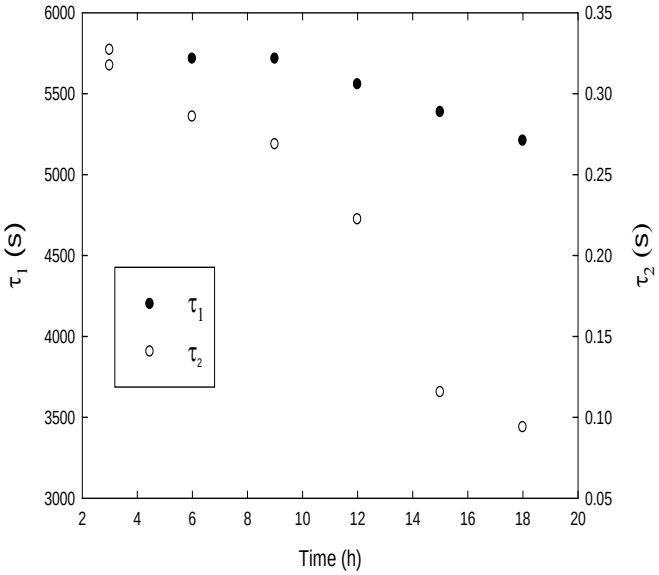

Figure 5.4: Relaxation and retardation times estimated by fitting single mode Jeffery model to the creep data shown in Figure 5.1a.

A few isothermal dynamic frequency sweep experiments were also done to probe the sol to gel transition of fibroin sols. The moduli $G'(\omega), G''(\omega)$ were tracked by conducting

tests after every three hours. Storage modulus data for a RSF sol of C=5 g/L, pH 2 at 25 ^{o}C is shown in Figure 5.5. Even at 0 h the sample showed frequency independent G', which is a typical gel like response. At this stage the sample flows upon tilting the vial indicating that it might be a weak gel. The small value of G' supports this inference. Also, the weak gel-like response is in agreement with the creep data presented earlier. The low frequency complex viscosity values calculated from this data matched fairly well with the η_2 values from the creep data. It was however noted that different geometries (cup and bob vs. cone and plate) gave values of G' which differed from each other sometimes by as much as a factor of 10. It is not clear whether this is caused by an interfacial effect given that fibroin is an amphiphilic polymer. However, for every sample the storage modulus consistently increased with time gradually till 9 h after which there was a rapid rise over the next three hours. After about 15 h no further rise in G' was observed till 21 h indicating little aging.

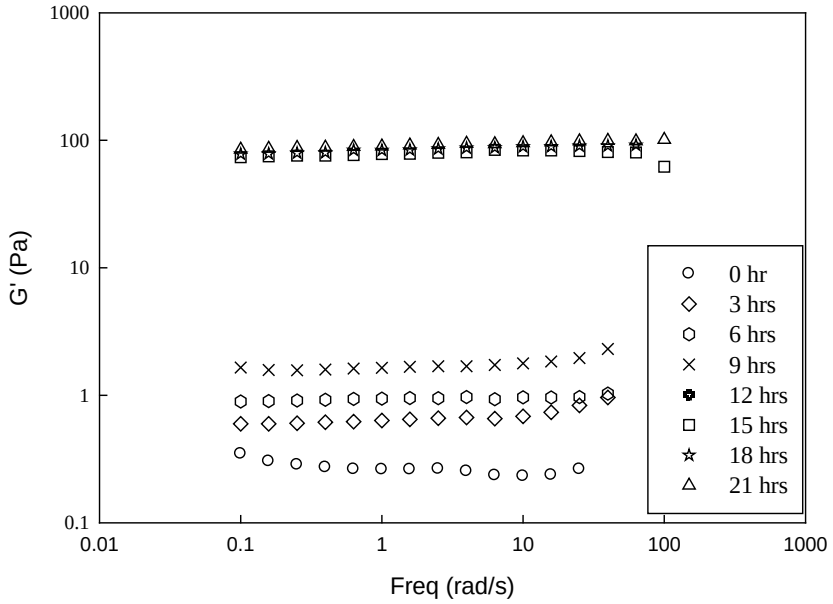

Figure 5.5: Time evolution of the storage modulus of a RSF sol (C=5 g/L, pH 2) during gelation at 25 ^{o}C.

5.1.2 Turbidity:

The RSF sols of various pH and concentrations changed from being transparent to turbid during gelation. This change was probed continuously using UV-visible spectrophotometer at different wavelengths as shown in Figure 5.6. For all wavelengths the

turbidity increased relatively slowly at first and then abruptly at a certain time which was wavelength dependent. The sudden increase of the turbidity of RSF sol has been reported before and was found to be correlated to the formation of a gel.[37] Notice, however, that there is not necessarily a casual relationship between the two phenomena since heated globular proteins may also form transparent gels or turbid solutions.[122] Gelation implies the formation of a percolating or cross-linked network, while the increased turbidity implies the appearance of heterogeneity on length scales comparable to the wavelength of visual light.

The increase in turbidity before the abrupt rise is shown in a magnified view in Figure 5.8. The rise was faster for shorter wavelengths than for longer wavelengths indicating that smaller aggregates grow before the larger aggregates. The increase in turbidity can be fit to exponential functions for all wavelengths as shown by the lines through the data.

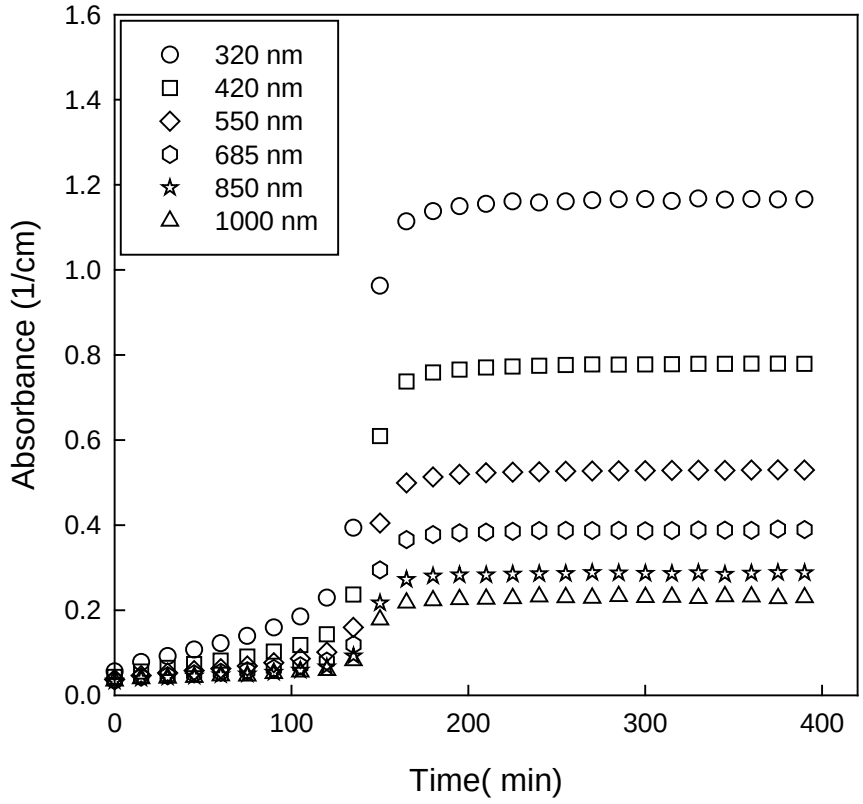

Figure 5.6: Absorbance at diiferent wavelengths as function of time for a RSF sol of C=10 g/L, pH 2 during gelation at 70 ^{o}C.

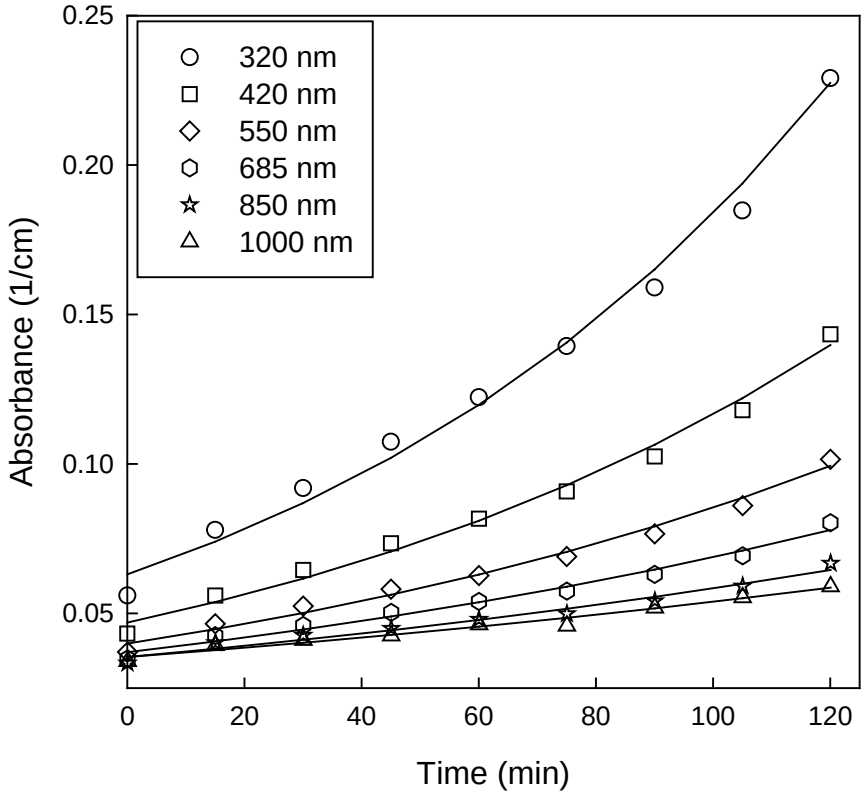

Figure 5.7: Same data as in Figure 5.6 magnified in the range 0 to 160 min showing turbidity rise before the abrupt change.

Several experiments were performed in which the turbidity of RSF sols was monitored in a UV-spectrophotometer and simultaneously isothermal dynamic time sweep experiments were also performed on the same sol to probe the sol to gel transition. Data for a RSF sol of C=8g/L, pH 2 is shown in Figure 5.8 during its gelation at 50 °C. The increase of the storage and loss moduli at 1Hz are compared with the increase of the turbidity at λ= 685nm. At the start of the experiment (‘zero’ time) G' was larger than G" indicating a weak gel-like nature of the sample, which is in agreement with the creep and frequency sweep data presented earlier. With time the moduli increased slowly initially and then abruptly after which no further slow restructuring occurred. The increase in moduli was also accompanied with an increase in the turbidity at approximately the same time followed by stagnation of turbidity at longer times. The tubidity data indicates that already before the moduli increased abruptly large aggregates are formed leading to an increase in turbidity although the sol may still flow. But since the aggregate growth rate was exponential this situation lasted only a short time so that in practice the steep rise of the turbidity was almost always accompanied

with a steep increase in the moduli. It may be noted, however, that it is possible to form transparent protein gels for which there is no such correlation.[122] This is the case when aggregates strongly repel each other and highly ordered gels are formed.

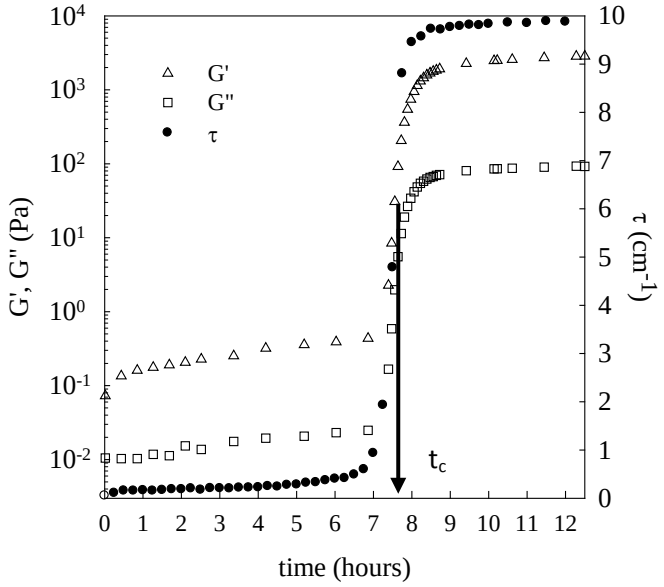

Figure 5.8: Evolution of the storage and loss shear moduli and the turbidity with time during gelation of a RSF sol of C= 8 g/L, pH 2 at 50°C.

A characteristic gel time (t_c) was defined arbitrarily as the time needed to reach half of the final values of the storage modulus or the turbidity. Since the increase of both G' and τ is steep, the gel times are not sensitive to the exact definition of t_c. Measurements at different C, T and pH showed that in all cases the time at which the turbidity increased abruptly was close to that where G' increased if the same solution was used in both measurements. However, when different preparations were used a large spread of the values of t_c was found. This spread may be related to a variation of the initial state of the sols after pH adjustment.

Figure 5.9 shows a plot of t_c as a function of C for three different temperatures (20, 50 and 70°C) and three values of the pH (2, 3 and 4). For a given temperature the spread of t_c around the average value was about a factor of two. t_c appears to be independent of the concentration in the low concentration range covered here (C<10 g/L). Matsumoto et al[120] also found only weak concentration dependence at lower concentrations (6-12 g/L), but at higher concentrations they observed a decrease of the gel time with increasing protein

concentration. The concentration independence of gelation time indicates that the rate limiting step for gelation must involve individual fibroin chains.

No systematic dependence of the gel time on the pH was observed between 2 and 4, but further increase of the pH above 4 led to a strong increase of t_c in accordance with observations reported previously in the literature. For example, a RSF sol of C=1 g/L, pH 6 took more than three weeks to gel at ambient temperature. As mentioned in chapter 2, the isoelectric point of a fibroin molecule is close to pH 4.[49] Thus the strong increase of the gel time above pH 4 is correlated to the ionisation of carboxyl groups which increases electrostatic repulsion between the proteins.[120]

In spite of the relatively large scatter of the data a systematic decrease of t_c with increasing temperature was found as has been reported before in the literature.[120, 123] The average value decreased from about 17 h at 20°C to about 5 h at 70°C. A few measurements were done at 5°C showing even longer gelation times. The temperature dependence of the gelation time for silk protein solutions is weak compared to the very strong dependence for heat induced gelation of globular proteins.[118, 119] In the latter case the compact ordered structure needs to be unfolded, which is a cooperative process characterized by a high activation energy.

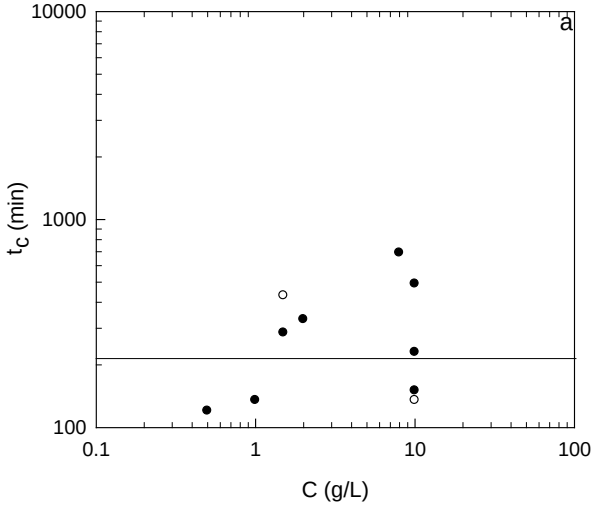

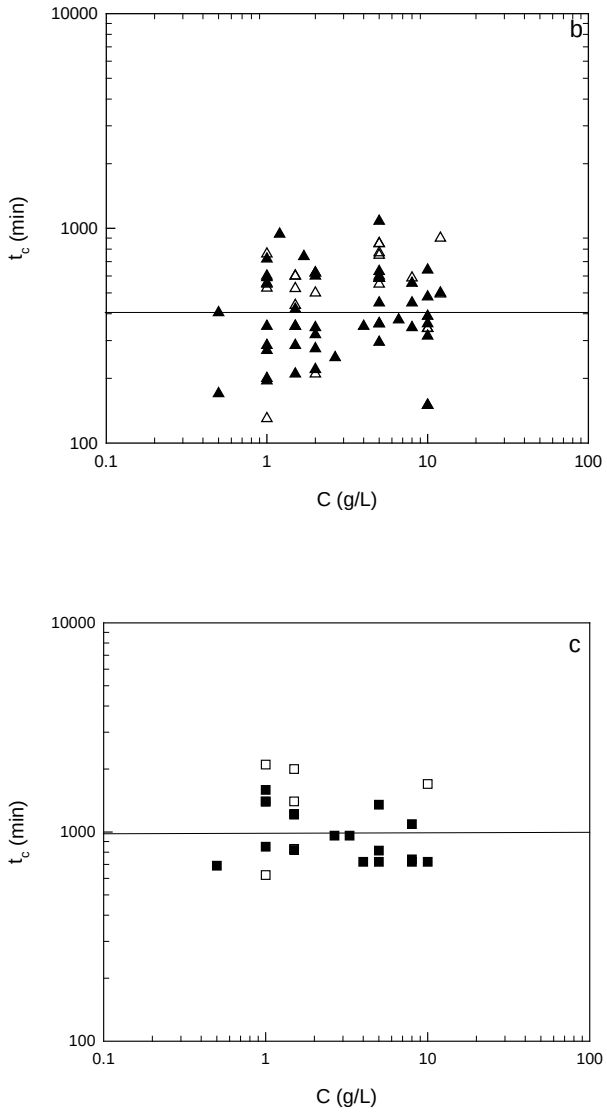

Figure 5.9: Concentration dependence of the characteristic time where the turbidity (closed symbols) and the shear moduli (open symbols) of silk protein solutions increased strongly. Figure a, b, c for 20°C (squares), 50°C (triangles) and 70° (circles). The solid lines represent the average values at that temperature. For clarity, the same symbols are used for data obtained at different pH (2, 3 and 4), as no systematic effect of the pH was found.

5.1.3 Light scattering:

Static light scattering experiments were performed to track the sol to gel transition of three RSF sols of pH 2 and C=0.5, 1.0 and 1.5 g/L. At these concentrations the sols were dilute enough to avoid multiple scattering. Data was collected over the angular range of 15 – 115 degree with a waiting time of 3 h between successive experiments. Dynamic light

scattering data of the sol showed two modes, a fast mode and a slow mode, indicative of at least two different sizes of particles present in the sol. The amplitudes of these two modes were calculated using equation (3.10) and were found to be a maximum of 0.4 for the slow mode. The slow mode nearly disappeared after the first 6 h of gelation, after which only the fast mode was seen in DLS data. The static scattered intensity of only the fast mode was obtained by multiplying the measured total time-averaged scattering intensity with the amplitude of the fast mode. The relative scattered intensity of the fast mode is plotted versus the wave vector in Figure 5.10 for the RSF sol of C=1.0 g/L, pH 2 as a function of time during the gelation process. The relative scattered intensity was normalized by the product of protein concentration (C) and optical constant (K) so that the Y-axis represents the product $M(w)S(q)$ of the sol at any given time.

It can be seen from Figure 5.10 that the relative scattered intensity I_r / KC was nearly q-independent between 0 and 9 h. During this time span the intensity increased gradually with time, but after 12 h the scattered intensity increased rapidly and showed increasing q-dependency. A strong q-dependence of the scattered intensity indicates the development of heterogeneous structures. After 18h, I_r / KC no longer evolved with time and a power law q-dependence was observed with an exponent of about -2. A power law q-dependence implies that the structure is self similar and characterized by a fractal dimension (d_f) that is equal to the power law exponent.[78] This was discussed in detail in chapter 4. The rapid increase of the scattering intensity is of course the origin of the rapid increase of the turbidity discussed earlier. In the same time duration where the rapid rise in scattering intensity was observed the rheological parameters namely, the frequency of creep ringing and the dynamic moduli of the sample also increased rapidly for this sample. Similar scattering data was obtained for the C = 0.5 g/L and 1.5 g/L RSF sols. They are shown in Figures A-2 and A-3 in the Appendix.

The apparent molar mass (M_w) of aggregates at various times between 0 and 12 h was obtained from the q-independent relative scattered intensity data shown in Figure 5.10. In the low q region ($q \rightarrow 0$) the structure factor is unity, hence the Y-intercept of the data is equal to the molar mass. The weight average apparent molar mass increased from about 10^6 g/gmol at 0 h to about 3×10^7 g/gmol at 12 h. The corresponding average hydrodynamic radius (R_h) of the aggregates at various times were calculated from the dynamic light scattering data

as follows. The relaxation time of the fast mode $\left\langle \tau_{LS,fast}^{-1} \right\rangle$, obtained using equation (3.10), was plotted versus q^2 for various times between 0 h and 15 h and is shown in Figure 5.12. A straight line equation passing through the origin provided an excellent fit ($R^2 > 0.99$) to each of the $\left\langle \tau_{LS,fast}^{-1} \right\rangle$ versus q^2 data up to 12 h indicating diffusive behaviour of the aggregates. For the data collected at 15 h after zero time and above, the error in fitting a straight line to the $\left\langle \tau_{LS,fast}^{-1} \right\rangle$ versus q^2 data was higher ($R^2 < 0.75$) so that eq (3.10) may be considered to be inapplicable. The diffusion coefficients of aggregates at various times between 0 and 12 h were calculated from the slopes of the straight line fits shown in Figure 5.11. The corresponding hydrodynamic radii of the aggregates were then calculated using the Stokes-Einstein relation, eq (3.11), assuming that intermolecular interactions can be neglected. This seems like a reasonable assumption for such dilute sols. Indeed no significant concentration dependence on the values of I_r / KC was seen between C=0.5 and C=1.5g/L. Reliable estimates of the hydrodynamic radius may be obtained by diluting the sol at each time during gelation and measuring their scattering in the dynamic mode. The assumption here is that dilution process would not alter the structure of the aggregates. Alternatively the hydrodynamic radii of aggregates can be estimated from the non-diluted sols. To do this we need to make assumptions about the value of viscosity appearing in eq (3.11). If the viscosity of the medium containing the aggregates is assumed to be the microscopic viscosity η_1=0.2 Pa s obtained from fitting the creep ringing data to a single mode Jeffery model then the hydrodynamic radius of aggregates in the sol is estimated to be about 0.1 nm at 0 h and 0.4 nm at 12 h. This value of viscosity is considerably larger than the viscosity of water, and would therefore imply a concentrated suspension of aggregates. Consequently, the calculation of R_h using eq (3.11) would be incorrect. If on the other hand the viscosity in eq (3.11) is considered to be that of water, thereby implying a dilute suspension of the aggregates, then their hydrodynamic radius is estimated to be about 20 nm at 0 h and 80 nm at 12 h, which seem more reasonable numbers.

Figure 5.12 shows that M_w and R_h of the aggregates increased approximately exponentially with time. For self similar aggregates the size and the molar mass are related through the fractal dimension: $M_w \sim R_h^{d_f}$, that should, of course, be the same as the one

describing the structure factor. The inset of figure 5.13 shows that the dependence is indeed compatible with a power law with d_f =2

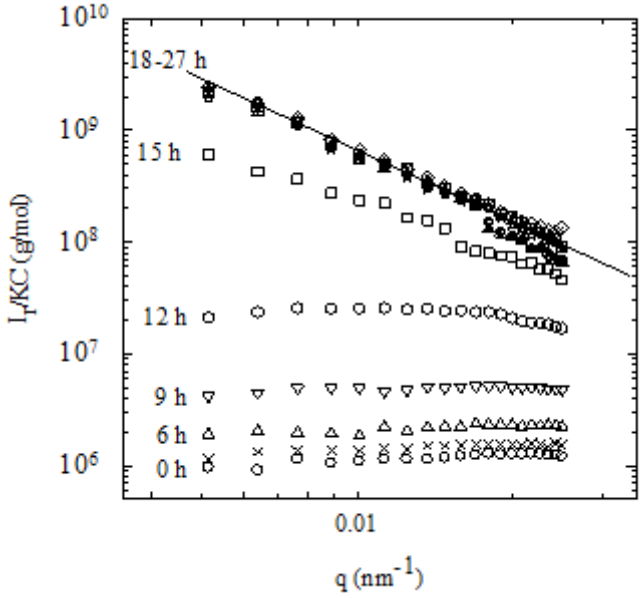

Figure 5.10: Results of scattering experiments on a RSF sol during gelation (C = 1.0 g/L, pH 2, 25°C). q-dependence of I_r/KC after different waiting times. The line through the data after long waiting times has slope -2.1.

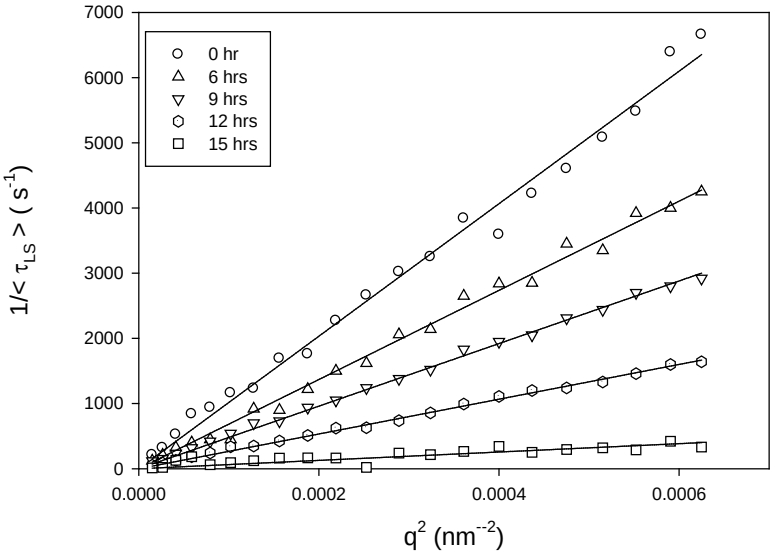

Figure 5.11: Relaxation time versus q^2 for RSF sol of pH 2 at 25°C as a function of time.

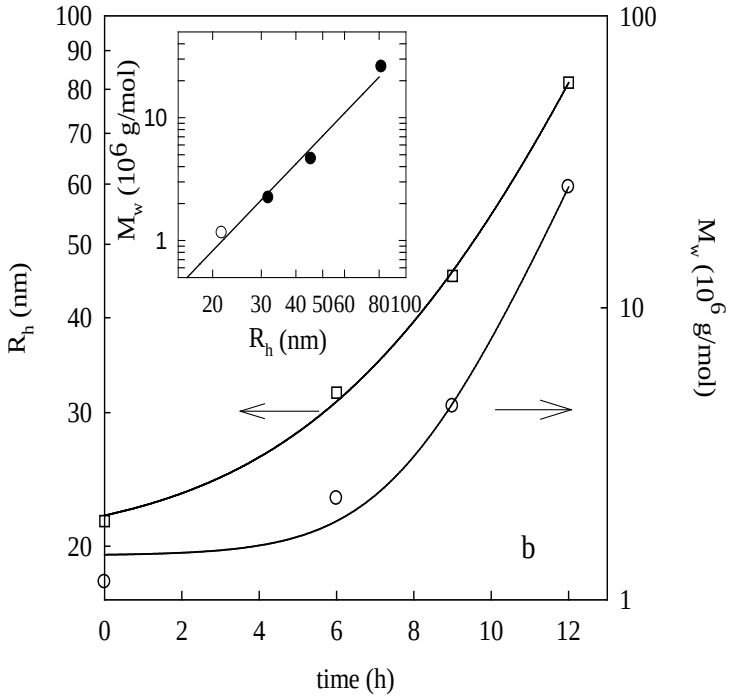

Figure 5.12: Semi-logarithmic representation of the time dependence of the hydrodynamic radius and the molar mass. The solid lines represent an exponential increase. The inset of figure shows the power law dependence between M_w and R_h. The solid line of the inset has slope 2.1.

5.1.4 Small angle x-ray scattering:

The gelation of sol of C= 1 g/L, pH 2 at 25 ^{o}C was also probed using SAXS. The scattering intensity was collected at three hour intervals after the first data set (viz, the 'zero-time' data), which was collected immediately upon loading the sample. The scattering intensity from the sample was obtained by correcting for background as per procedure given in Chapter 3 (see equations 3.30-3.31).

The corrected intensity was normalized by the GC intensity and plotted against q as shown in Figure 5.13. The $I(q)-q$ data shows two power law regimes: in the high q region the scattering intensities for all times overlap on each other and has an exponent of nearly -1, whereas in the low q region the scattering intensity increases with time, albeit only slightly, and the power law exponent is about -2. As discussed in chapter 4, the SAXS data for the RSF gel showed two power law regimes of exponents -2 and -1 respectively, in the low q

and high q regions indicating that the self-similar structure of the gel continues down to about 10 nm below which thin strand-like aggregates exist. The 36 h data in Figure 5.13 is in fact the data after complete gelation. What is interesting to observe in Figure 5.14 is that even at 0 h the scattering intensity shows similar q-dependence as that shown by the gel. Thus the RSF sol (0 h sample) also has a fractal structure with $d_f = 2$ at low q and fine strand-like structures at high q. During gelation of the sol the high q microstructure does not change further with time but the larger fractal structure (low q) evolves in agreement with the light scattering data presented earlier.

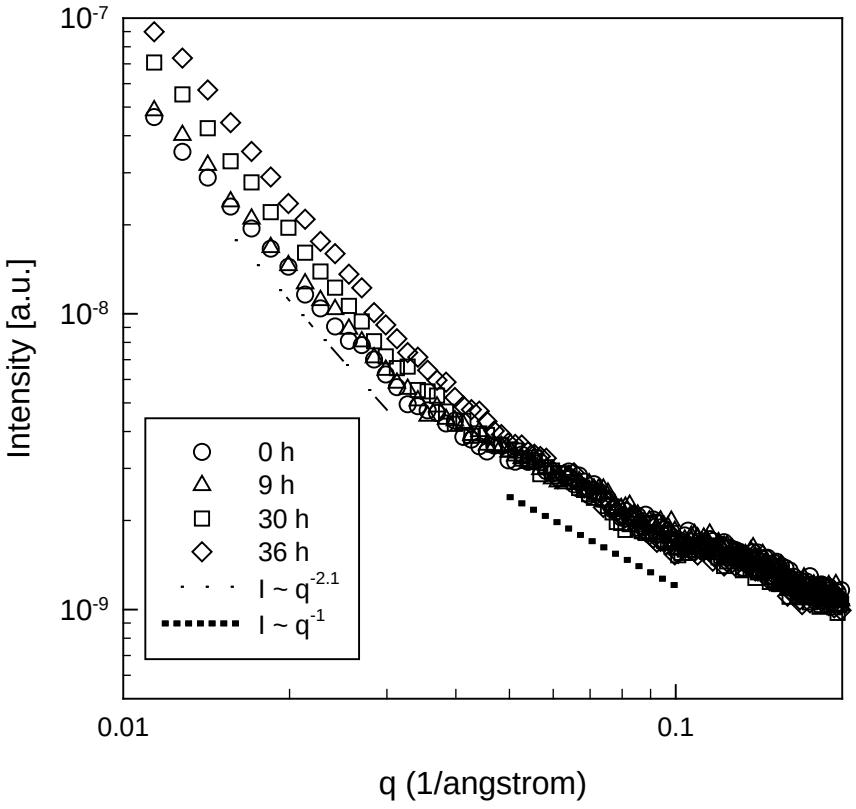

Figure 5.13: Time evolution of SAXS intensity during gelation of a RSF sol of C= 1 g/L, pH 2 at 25 ^{o}C.

5.1.5. Circular Dichroism:

Circular dichroism spectra were obtained every one hour during gelation at 25^{o}C of a sol of C=0.5 g/L, pH 2. These data are shown in Figure 5.14 together with data for a freshly dialyzed RSF solution at the same concentration and pH 7. The peak at about 204 nm is

caused by amino acids in the random coil conformation, while the peak at about 217 nm is due the β-sheet conformation. It is clear from Figure 5.14 that the gelation process is accompanied by transition of the protein conformation from a predominantly random coil state in the sol to a predominantly β-sheet state in the gel. It is also evident that upon reducing the pH of the freshly dialyzed RSF solution from pH 7 to pH 2 there is almost no change in the protein conformation. Thus, the conformation change happens not during reduction of the pH but during the subsequent gelation process. The time dependence of the peak amplitude at 217 nm is plotted in Figure 5.15. With time the β-sheet content increased exponentially until about 15 h and then stagnated rapidly. The observed increase of β-sheet structures upon gelation confirms earlier work reported in the literature.[86] Exponential growth rate data such as the ones shown in Figures 5.15 can also be fit to kinetic models that describe the random coil to β sheet transition as a first order reaction.[124]

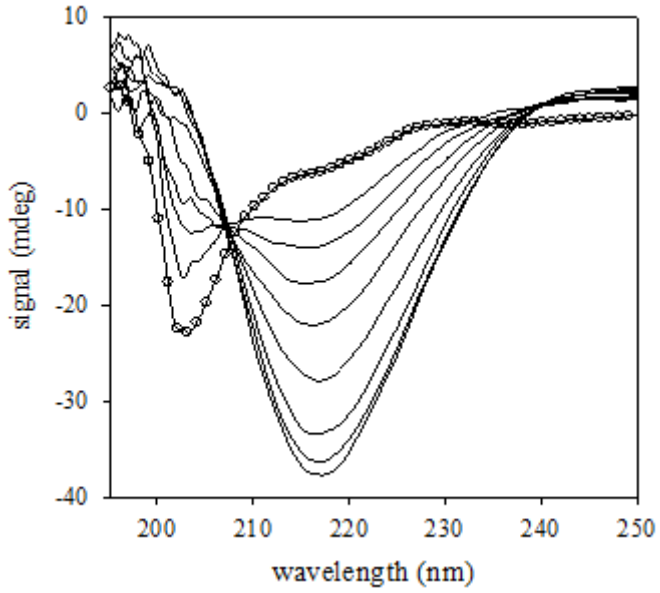

Figure 5.14: Wave length dependence of the circular dichroism of a RSF sol at C=0.5 g/L during gelation at pH 2 and T=25^{o}C at different times after pH adjustment. The initial dependence before and after adjusting the pH is indicated with open circles. The other wavelength dependences that are shown were obtained between 9 and 16h with one hour interval.

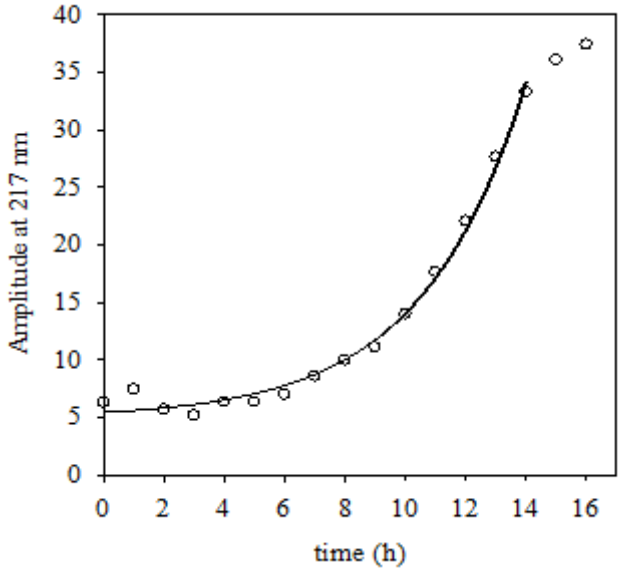

Figure 5.15: The amplitude of peak at 217 nm plotted as a function of waiting time. The solid line represents a fit to an exponential increase through the data up to t=14h.

In principle, the fractions of various protein conformations can be quantified from the CD data by fitting it to different models. One such fit to the Reed model [125] is shown in Figure 5.17. The model predicts increase in beta sheet fraction and a corresponding decrease in the random coil conformation as gelation proceeds. However, it was observed that such quantifications are highly model-dependent, and hence not very reliable. CD data for C=5 g/L was observed to be similar qualitatively to the data shown in Figure 5.14. The data is shown in Figure A-4(a) in the appendix. The corresponding growth of peak intensity and Reed model predictions are shown in Figures A-4(b) and A-4(c).

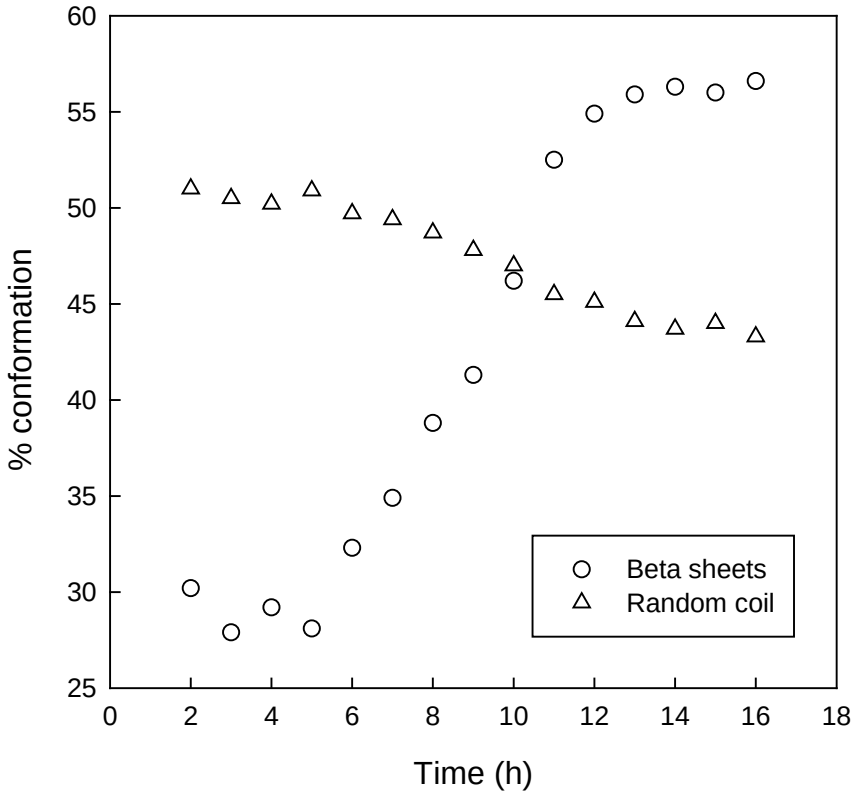

Figure 5.16: Predicted protein conformation changes during gelation as per Reed model.

5.2 Discussion:

Gelation of RSF sols was studied at relatively low protein concentrations, because reducing the pH at higher protein concentrations led to extensive precipitation. In addition, dilute solutions are easier to characterize and investigate using scattering techniques. Light scattering experiments showed that the freshly prepared relatively dilute RSF solutions contained mainly individual proteins and a small amount of aggregates. The zeta potential of this solution was measured to be between -17 and -22 mV, indicating incipient instability of the solution. Upon reduction of the pH to below the pI of fibroin, the zeta potential of the RSF sol was measured to be in the range -4 to -2 mV indicating its highly unstable nature. The sols formed more or less turbid gels after a certain waiting time t_c. Relatively large quantitative differences in t_c were observed between measurements on independently prepared RSF solutions. This shows that the detailed features of the aggregation process are sensitive to the perturbation of the proteins induced by the setting of the pH. The effect was

especially pronounced at lower protein concentrations. Nevertheless, clear general features of the gelation process could be distinguished.

With time the average size and molar mass of the aggregates grew exponentially until a system spanning network was formed. During growth the aggregates retained their self similar microstructure which was characterized by a fractal dimension of about two. This strongly suggests a random aggregation process of the proteins. Both the exponential aggregation rate and the value of the fractal dimension are consistent with a reaction limited cluster aggregation (RLCA) process.[96] It is interesting to note that such self similar structures have also been observed for gels formed by very different types of proteins such and β-lg([78]), caseinate[79] and myosin.[126] The actual bonding mechanism is, of course, likely to be different for different proteins, but at length scales larger than a few particle diameters the structure is determined by the random association process and local details no longer matter. Light scattering showed that the elementary unit of the fractal aggregates was less than about 15nm. Small angle x-ray scattering showed that the aggregates are made from randomly branched thin strands of length less than 15 nm. Other techniques such as cryo transmission electron microscopy can also be used to elucidate the local structure of fractal protein aggregates.[89]

The aggregation and gelation rate of proteins depends sensitively on the type of proteins and often also on the external conditions such as pH, ionic strength and temperature.[85] Remarkably the aggregation rate of silk fibroin proteins is only very weakly dependent on the temperature and is independent of the concentration at least for C<10g/L and of the pH in range between 2 and 4. This means that the activation energy for binding is weak and that the rate limiting aggregation step at low concentrations involves single proteins. Indeed circular dichroism results show that immediately upon reduction of the pH the fibroin chains in RSF sols have a predominantly random coil conformation. The lack of secondary structure in fibroin suggests that unlike other proteins such as β-lg, for which a thermally activated denaturing process is required before gelation can proceed, no such thermal activation is necessary for RSF sols. Hence the gelation of RSF sol shows only weak temperature dependence. Furthermore, light scattering and circular dichroism data showed that both the size of the aggregates and the fraction of β-sheets increased together in an exponential manner up to the gel point and then stopped evolving. Microcalorimetry data on a few samples (Figure 6.7a and b, chapter 6) also showed an exponential rise in the heat

liberated during gelation, presumably due to the formation of β-sheets. There is obviously a correlation between the two phenomena, but it is not clear if β-sheet formation drives aggregation or if aggregation drives β-sheet formation. However the concentration independence of gelation process suggests the former possibility.

The initial structure of the RSF sol is a result of the pH reduction step, and is likely to decide the subsequent gelation process. Although the RSF sol flows rather easily initially, creep and oscillatory shear measurements described above indicate that it has a weak gel structure. However rheological measurements on the initial RSF sol using different measuring geometries were not very reproducible, which raised the possibility that the origin of the gel-like character might be caused by some interfacial phenomenon. Silk fibroin is an amphiphilic molecule because of the presence of blocky hydrophobic and hydrophilic amino acid sequences. It is therefore possible that the fibroin can assemble at liquid-air interfaces in the measuring geometries forming elastic films, which then contribute to the observed rheological behaviour.

However, two preliminary experiments provided seemingly contrary evidences. The first was a micro-rheology experiment in which Stober silica particles of about 400 nm were suspended in a rhodamine B labelled RSF sol of C=5 g/L, pH 2 by keeping the sample in an ultrasonic bath for about 2 min. The silica concentration was about C_p=1 g/L. The sol was then placed on a glass slide having a concave cavity, covered with a cover slip and hermetically sealed. It was then observed under a confocal microscope at a z plane that was sufficiently away (~ 100 μm) from the sol-glass boundary. Well dispersed fluorescing silica particles were observed under the microscope along with some larger aggregates. The fluorescence of silica particles suggests that either the labelled fibroin or free rhodamine, if any, from the solution had adsorbed on the particles. More interestingly, the particles appeared to be almost immobile. In contrast silica particles dispersed in a freshly dialysed RSF solution of pH 8.2 and same concentration exhibited random Brownian motions as expected. The relatively high immobility of the silica particles in the RSF sol could be a result of the existence of a gel-like structure.

The second experiment namely, SAXS, clearly showed a fractal structure of $d_f = 2$ in the initial RSF sol. Interestingly however, DLS experiments showed liquid-like behaviour of the sol. Figure 5.17 shows the autocorrelation function measured at the scattering angle of 90^o

for a RSF sol of C=1 g/L, pH 2 undergoing gelation at 25^{o}C. A single nearly exponential decorrelation event is seen for the RSF sol at all times throughout the gelation process. The decorrelation time scale increases relatively slowly till 12 h and then rapidly until 18 h, in agreement with the rapid rise of the scattering intensity observed for this sample in static light scattering and the rapid increase of modulus seen in rheology. The single decorrelation event suggests good mobility of the scattering particles. Taking all these observations together suggests that the RSF sol consists of mobile aggregated protein particles (as observed by DLS) of fractal microstructure (as observed by light scattering and SAXS), which assemble to form a weak gel at longer length scales (as observed by macro-rheology and micro-rheology). Furthermore, circular dichroism data showed that initially the RSF sol does not have a large fraction of β sheet structures. This means that the gel-like character of the sol arises from purely weak and possibly hydrophobic associations of protein chains. The reversible rheological nature of the RSF sol, as evidenced by the creep experiment sequence discussed in Figure 5.2, supports this hypothesis.

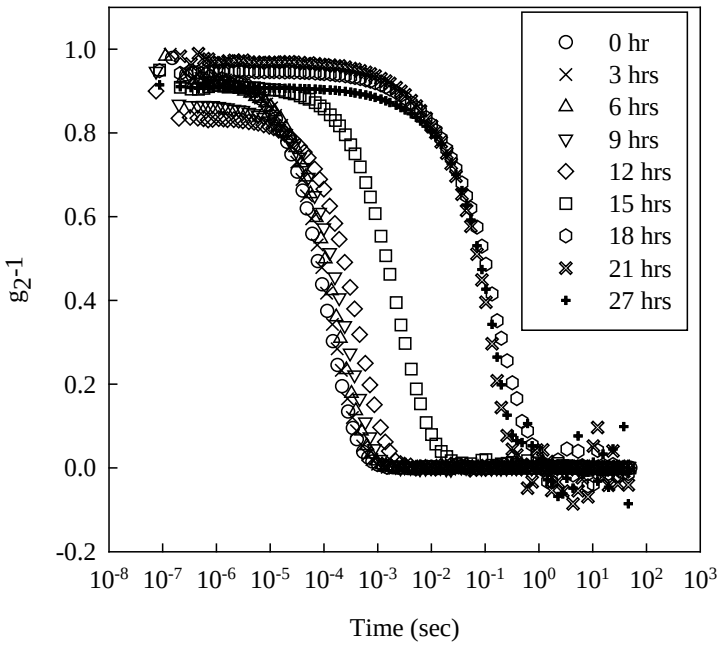

Figure 5.17: Time evolution of autocorrelation function calculated from DLS experiments at 90^{o} scattering angle.

5.3 Summary:

Based on all the evidences presented here the gelation process can be described as follows. At the concentrations studied in this work (C << C*; note that C* ≈ 150 g/L) the freshly dialyzed solution of pH 8 comprises mostly individual fibroin chains and a few larger aggregates. Upon reducing the pH and centrifuging out the precipitate, an unstable RSF sol is obtained which gels with time. The initial state of the sol consists of protein aggregates of average size 20 nm and average molar mass of ~ 10^6 g/gmol. Since light scattering is always heavily biased by scattering from larger aggregates it is likely that the RSF sol consists of many individual fibroin chains together with a distribution of few large aggregates. The aggregates are fractal objects. The RSF sol has a weak gel-like structure arising possibly from the association of aggregates at longer length scales. The fibroin chains in the sol are predominantly in a random coil conformation. Their association is driven by two factors: a decrease in intermolecular electrostatic repulsion due to protonation of carboxyl groups on the fibroin molecules at pH lower than the isoelectric point, and a simultaneous increase in intermolecular attractions caused perhaps by hydrophobic interactions. It is interesting to note that the volume fraction of the small aggregates, as calculated from their mass, size and protein concentration, is about 0.002. That such a dilute suspension of aggregates is able to form a percolating network is perhaps suggestive of an open structure.

With time the fine scale structure, i.e., the interior structure of aggregates, remains unchanged where as the size and mass of the aggregates themselves increase exponentially. The simultaneous exponential increase of β sheet structures lead to the possibility that gelation is driven by β sheet formation. The fractal dimension of 2 suggests random aggregation of the protein by the RLCA process. At a certain time, defined as the gel time in this work, the aggregates percolate to form a sample spanning network causing an abrupt increase in the shear modulus.

Chapter 6

Gelation at high pH

6.1 Introduction:

Experimental results presented in chapter 5 on gelation of RSF sols were limited to a pH range below the pI (4.0) of fibroin. The data showed that gelation time was weakly dependent on the pH, concentration of protein in sol and temperature. The main reason for limiting the pH range to below pI was the fact that it took a long time (on the order of 15 – 60 days) for the gelation of a fresh dialyzed RSF solution of about C=40 g/L at pH > pI. The higher the pH the longer it took for gelation, making it practically impossible to perform the detailed studies on microstructure evolution during gelation. These preliminary observations on pH dependence of gelation time were in agreement with the previous studies of Matsumoto et al [101]; see Figure 6.1. Studies on low pH gels, however, have limited utility for at least one of the intended applications namely, as scaffolds for tissue engineering. The desirable pH range for this application is about 7.2 - 7.4. At this pH a fresh dialyzed RSF solution of C ~ 40 g/L would take around 10 to 20 days to change into a gel.

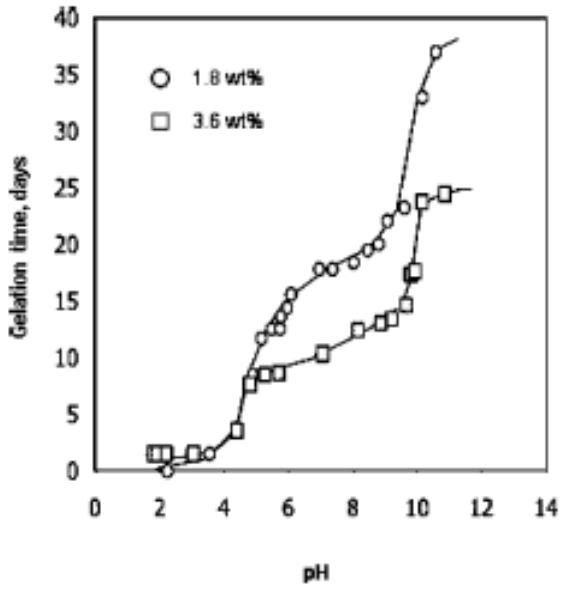

Figure 6.1: RSF gelation time study at various pH (Matsumoto A. et al, [101]

If the gelation rate at higher pH were to be accelerated it would enable undertaking detailed mechanistic studies on gelation. It would also provide for preparing RSF gels more rapidly for tissue engineering purposes. In this work a new strategy was explored to accelerate the gelation of RSF solutions at pH > pI. The central idea was based on the understanding of gelation mechanism acquired from the result presented in chapters 4 and 5, which showed

that gelation of RSF at pH < pI is most likely driven by the conformation transition of the fibroin from a random coil state to β sheet structures. It is quite possible that the beets sheet of fibroin acts as nuclei which drives gelation to form aggregates, which then further grow in size and mass by the reaction limited cluster aggregation (RLCA) process to form the RSF gel. This suggests that if the RSF solution at higher pH can be seeded with the right nuclei then it might trigger rapid gelation of the solution.

In this context two different strategies were explored. In the first method RSF solutions various pH (5-8) were seeded with Stober silica nanoparticles as external nucleating agent. In the second method the 'self-seeding' technique was adopted. Here RSF sols were prepared at pH < pI and allowed to gel for various times after which the pH of the solution was adjusted using an alkali to the desired pH (5-8). The gelation was allowed to proceed at the high pH and gelation times were recorded. Both strategies are analogous to the standard heterogeneous and homogeneous nucleation processes that are commonly used in crystallization.

6.2. Silica assisted gelation:

6.2.1. Experimental

Measurements of gelation time of RSF solutions in the presence of silica nanoparticles were done by sample vial tilting method. The protein concentration of RSF solutions was varied from 1g/L to 5 g/L by diluting a freshly dialyzed RSF solution with aqueous solutions of the required pH. Stober silica nanoparticles of sizes 40, 150 and 400nm were used to study gelation. The particles were kindly supplied in dry powder form by the Materials Chemistry group at the National Chemical Laboratory. Predetermined quantities of nanosilica powder were added to about 5 ml of RSF solutions to achieve particle concentration C_p = 1 - 25 g/L. Mixing was done by first sonicating the solution for a few seconds. This resulted into aggregation of the silica on the surface of the solution. The aggregates were immersed in the solution with the tip of a micropipette and then sonicated for a further 2 min. This resulted in break up of the agglomerate and dispersion of the silica particles. Solutions containing silica loading of up to 5 g/L were translucent. Above this C_p the solutions were turbid. The state of the sample was checked roughly every 3 hours. Gelation time was recorded as the approximate time when the solution did not flow upon tilting the vials to about 45-60 deg. Some gels were also prepared in a specially made

aluminium cups for measurements of the compression modulus a RSA III dynamic mechanical analyzer. Finally, the conformation of fibroin was recorded using circular dichorism (CD).

6.2.2. Results and Discussion:

The freshly dialyzed RSF solution of C~ 30g/L and pH 8.2 required more than 30 days to gel. Upon mixing the silica nanoparticles with the RSF solution an immediate observation was that the dispersion of the particles was excellent. Stober silica particles can form stable suspension in water provided they are charge stabilized. However if they are isolated as a powder by precipitation from aqueous solutions, they cannot be easily redispersed in water. The silica particles used in this work were in the form of a dry powder which remained in a largely agglomerated state when mixed with water. However in the RSF solution they could be redispersed with relative ease. This suggests some amount of stabilization of the nanopaticles in the RSF solution presumably by the fibroin.

Upon aging the samples under isothermal conditions the solutions gelled with time. The gelation time of RSF solutions containing silica nanoparticles varied from 6 days to 3 hours depending on the concentration of silica nanoparticles and the temperature. This gelation time is considerably shorter than the time required for the RSF solution to gel at the same pH in the absence of nanosilica particles. The gelation times of RSF solutions containing silica nanoparticles of different sizes and amounts are shown in Tables 6.1 and 6.2. The gelation time appears to be independent of the particle size except for the smallest particle size for which it takes a slightly longer time to gel. The gelation time seems to depend on the temperature and protein concentration, and is relatively independent of silica loading.

It is well known that dilute aqueous suspensions of charged nanoparticles can form soft glasses or gels. For example, aqueous suspensions of laponite are known to form a Wigner glass due to charge repulsions at high pH [127] and a gel comprising a house-of-cards structure at low pH.[128] Theoretically the RSF-silica suspension could also form similar gels due to essentially the interparticle interactions of silica that is perhaps mediated by the fibroin. The other possibility is that the silica particles enable nucleation of β sheet structures which further drives the gelation process. CD measurements were carried out on gels formed by mixing silica nanoparticles of 400nm diameter in RSF solutions. The data was compared

with CD spectra of the freshly dialyzed RSF solution and of a gel formed by gelation of the freshly dialyzed RSF solution in the absence of silica nanoparticles. The CD spectra are shown in Figure 6.2. While the fibroin in a freshly dialyzed RSF solution shows a predominant peak at 204 nm corresponding to the random coil conformation, the three gels show dominant peaks at 217 nm corresponding to the β sheet conformation. It is clear that gels formed by the addition of silica nanoparticles contain significant fractions of β sheet structures. Admittedly this evidence by itself does not rule out the possibility of gel formation by protein mediated interactions between silica particles. However the combined observations of redispersion and stabilization of silica particles by fibroin, and the formation of β sheet structures, can be explained by the mechanism illustrated schematically in Figure 6.3. On mixing silica nanoparticles with RSF solutions the fibroin chains from the solution adsorb on the particle surfaces. Adsorption of chains constrains their translational mobility and increases their surface concentration, which enhances their conformation transition to β sheet structures. Once formed, the β sheet structures facilitate gelation of the remaining protein chains in the RSF sol.

The compression modulus of RSF gels with and without silica particles are shown Figure 6.4. The data shows substantial increase in the modulus of the gel indicating that silica particles reinforce RSF gel. The compression modulus of RSF gels of same protein concentrations but containing different loadings of silica nanoparticles is shown in Figure 6.5. The modulus is independent of silica loading, indicating probably that the silica nanoparticles by themselves do not associate to form a percolating structure in the gel. This may be expected because even at the maximum loading of silica nanoparticles (C_p = 25 g/L) the volume fraction occupied by the particles is $\phi_p = C_p/\rho_p = 0.0125$, ρ_p=2 g/cc being the density of silica. At such low volume fractions silica may not form a percolating network unless they experience long range interactions through the adsorbed protein.

Table 6.1: Gelation time of RSF solutions of two different protein concentrations C = 1 and 5 g/L containing an equal concentration of silica nanoparticles C_p = 1 and 5 g/L. Gelation was carried out at three different temperatures.

Sr. No	Temperature [^oC]	Protein Conc [C; g/L]	Gelation time for RSF sols containing different sizes of silica nano particles at concentration C_p =C		
			40 nm	150 nm	400 nm
1)	25	1	6 days	5 days	5 days
2)	50	1	12 hrs	10 hrs	10 hrs
3)	70	1	12 hrs	10 hrs	10 hrs
4)	25	5	2 days	2 days	2 days
5)	50	5	4 hrs	3 hrs	3 hrs
6)	70	5	4 hrs	3 hrs	3 hrs

Table 6.2: Effect of increasing silica particles concentration on gelation time of RSF solutions.

Sr. No	Temperature [^oC]	Protein Conc. [g/L]	Gelation time for RSF sols containing different silica nanoparticle concentrations (C_p)				
			25 g/L	12.5 g/L	6.25 g/L	3.12 g/L	1.81 g/L
1)	25	5	14 hrs	20 hrs	20 hrs	24 hrs	30 hrs

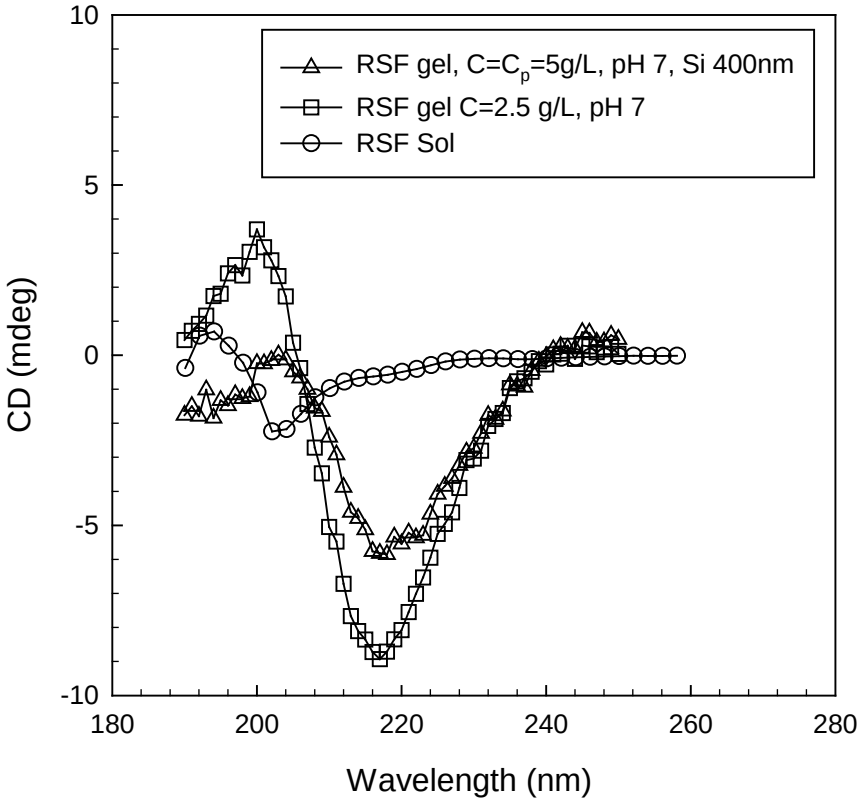

Figure 6.2: Circular dichorism study on RSF sol and gel of various silica nanoparticle at pH 7 and 25^{o}C.

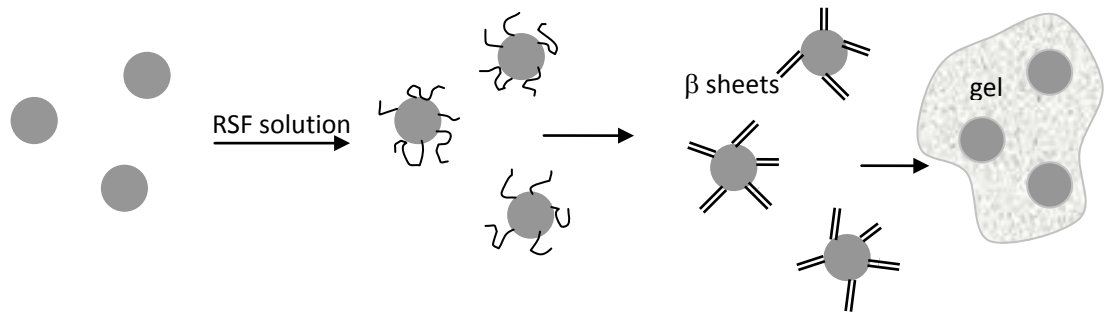

Figure 6.3: Schematic of gelation mechanism of RSF solutions in the presence of silica nanoparticles.

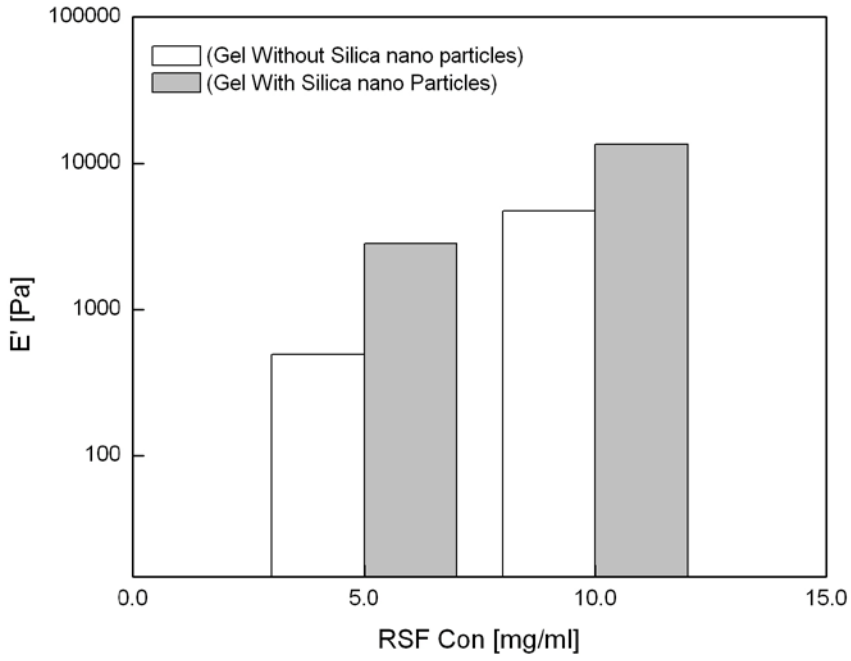

Figure 6.4: Compression modulus of RSF gels with and without nanoparticles.

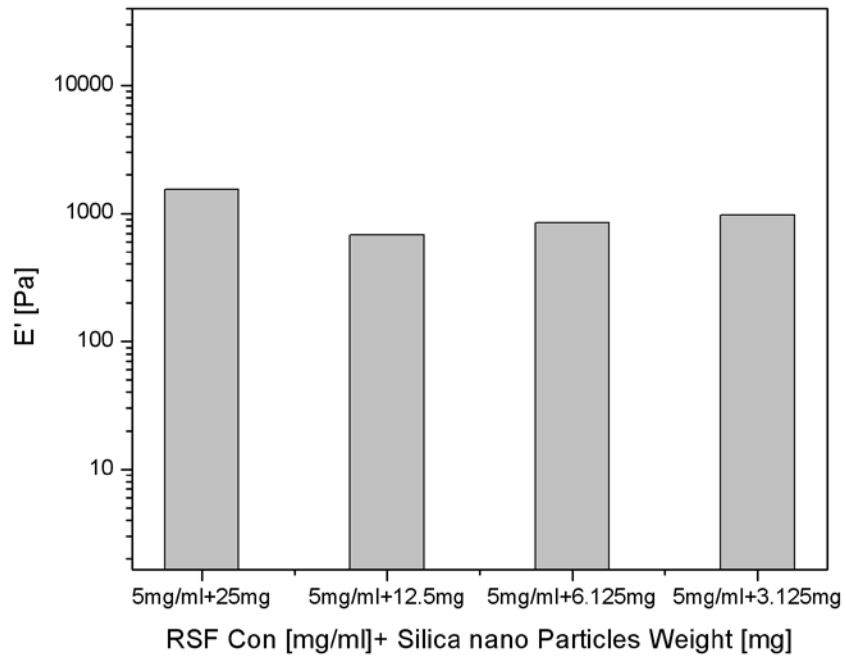

Figure 6.5: Compression modulus of 5 g/L RSF gels prepared in the presence of different concentrations of silica nanoparticles.

6.3. Self seeding:

In this technique the time evolution of β sheets in RSF sols of pH < pI is used to accelerate the gelation at pH > pI. Here, the irreversibly formed β sheets in the sol are used as the 'seeds' to initiate gelation. An analogous concept in crystallization is that of self-nucleation, in which the nuclei are the tiny partially molten crystallites of the same material. Self nucleation is the most efficient among the heterogeneous crystallization processes because of the minimum surface energy barrier and the high degree of epitaxy provided by the nuclei.

6.3.1. Experimental:

RSF sol of C = 1 g/L, pH 2 was prepared and 5 ml of the same was taken each in nine sample vials. 27 μl of 3M NaOH was added to sample vial no. 1 to increase its pH to 8.7 which is equal to the pH of the freshly dialyzed RSF solution. We will refer to this sample as one having zero 'seeding' time. The sol samples in the other eight vials were maintained at low pH for different 'seeding' times between 0 and 24 h as mentioned in Table 3 after which 27 μl of 3M NaOH was added to each of them to adjust their pH to about 8.7. Gelation was allowed to proceed at 25 ^{o}C.

6.3.2. Results:

The data in the above Table shows that gelation time at pH 8.7 reduced considerably upon allowing partial gelation to occur at pH 2 and that the gelation time decreased with increase in seeding time. The lowest gelation time in the self seeding experiment was slightly lower than the silica assisted nucleation at the same temperature.

Table 6.3: Results of self nucleation experiments.

Sample no	Seeding time (hrs)	State of sample vial at seeding time	Gelation time* after addition of 3 M NaOH	Gelation time for sol at pH 2 (h)
1	0	Flow upon tilting	30 days	27
2	3	Flow upon tilting	2 days	24
3	6	Flow upon tilting	2 days	24
4	9	Flow upon tilting	18 h	24
5	12	Flow upon tilting	18 h	24
6	15	Flow upon tilting	18 h	24
7	18	Translucent, flow	20 h	24
8	21	Turbid, flow	21 h	24
9	24	Gel	gel	24

*Sample does not flow upon tilting the vial.

Chapter 7

Conclusions and Future work

7.1 Conclusions

Although silk has been popular as a textile fibre since antiquity because of its lustre, feel and comfort, there is a growing interest in developing other value added applications of silk because of its excellent thermomechanical properties and biocompatibility. The discovery of high specific strength and toughness of silk fibers had led to a surge of recent research in understanding the microscopic origins of such properties. In addition to its excellent mechanical properties, the realization that silk fibroin can be degradable in a slow and controlled way, that it has a favourable immune response, and that it can be converted into an aqueous solution has led to the development of several types of biomaterials based on silk fibroin. Thus regenerated silk fibroin has been used to make non-woven electrospun mats, porous sponges, films and hydrogels. These materials have potential use as scaffolds for tissue engineering and as drug delivery vehicles.

This work presented in this thesis was concerned with studies on regenerated silk fibroin (RSF) hydrogels. In general, hydrogels are attractive materials to make scaffolds because they provide an environment that resembles the extra cellular matrix in terms of hydrophilicity, porosity and mechanical properties. The preparation of RSF hydrogels and their utility as scaffolds for growing cells has been reported. A few reports that describe the influence of state variables such as temperature, pH and concentration on gelation time were summarized in the literature survey presented in chapter 2. It has been proposed that these hydrogels have a microporous structure. Based on such studies earlier researchers have proposed a mechanism of gelation that is based on the modulation of protein-protein interactions by the pH of the RSF solution. However, other than the irreversible formation of β-sheets during gelation these studies have not probed the microstructure of RSF gels in great detail. Interestingly, the microstructures of many globular proteins such as β-lactoglobulin and of protein aggregates such as casein have been extensively studied at various length scales. Similar investigations have not been done on gels formed by fibrous proteins such as silk fibroin.

This gap in the understanding of RSF hydrogels led to the formulation of the main aims of the research presented in this thesis, which were described in chapter 1. To recap the main goal was to probe the microstructure of RSF gels at various length scales using a set of characterization tools. Such a study is pertinent for the successful application of RSF gels in

tissue engineering. This is because of the fact that the microstructure of hydrogels is ultimately responsible for providing the requisite aqueous environment, topology and the mechanical properties that are important to the cells growing inside. Another important aim of the present research was to understand the mechanism of gelation, i.e. to provide a clear picture of how the microstructure evolves during gelation. Understanding these details can enable control of the microstructure. As an interesting aside, the natural silk spinning process in Bombyx mori silkworm also involves a step in which the silk dope undergoes partial gelation upon reduction of pH inside the spinning duct. As explained in chapter 2 the extent of gelation is critical to the success of spinning. Therefore understanding the gelation of RSF might also shed more light on the complex transformations that happen during the natural silk spinning process.

In chapters 4 and 5 of this thesis the main results of this thesis with regards the microstructure of RSF gels and the gelation mechanism, respectively, were presented. A limited range of pH 2 – 4 (i.e., pH < pI of fibroin) was chosen for gelation studies in this work because the gelation times, which were less than one day, were suitable for in situ measurements. Note that when the pH of fresh dialyzed RSF solution was reduced from about 8 to less than the pI of fibroin a part of the protein precipitated out, and this limited the maximum concentration of the RSF sol that could be studied to about 10 g/L. The protein in the sol was of the same molecular weight as that in the fresh dialyzed solution thus confirming that there is no fractionation of the protein during precipitation. A wide range of temperature (5 – 70 ^{o}C) was probed in this study. The key results were summarized at the end of each chapter, and some of them are reiterated here in the context of their utility for the intended application of scaffolds in tissue engineering.

It was shown in chapter 4 that in addition to the presence of β-sheet structures the RSF hydrogels have a hierarchy of microstructure that was hitherto not known. In particular the RSF gels have a self similar microstructure of fractal dimension 2 over the length scale range of approximately 10 nm to 1 μm. Below 10 nm the fibroin aggregates to form fine strands, which then randomly branch to form the larger scale fractal structure. Above 1 μm larger protein clusters aggregate to form a porous percolating structure of high shear and compressive moduli. Although not studied in this work, the macroporosity of RSF can be further engineered by the use of porogens, gas expansion and freeze drying. Such a structure consisting of micro and macro porosity could be of considerable interest from tissue

engineering perspective. This is because the structure presents a cascade of length scales from few tens nanometers to few tens of microns which cells can recognize and use for their growth. It is widely believed that while cells can sense porosity of the order of tens of microns, the cell membranes can also sense roughness of the order of tens of nanometers to navigate. The three dimensional fractal structure of connected porosity could therefore present interesting opportunities that can be exploited by cells for growth. Such a structure enables easy vascularisation and thereby ensures supply of nutrients to the growing cells. Moreover, the RSF gels studied in this work have in excess of 99 wt% water content and display mechanical properties that resemble those of the extra cellular matrix. Thus RSF gels should be able to provide the right aqueous environment and the mechanical stresses for cells to grow and proliferate.

Interestingly, the fractal dimension of the RSF gels is no different than that of globular proteins. Thus, the details of the microstructure of protein gels are not sensitive to whether the proteins are fibrous or globular. However, the gelation process itself is sensitive to the type of protein. Globular proteins are stabilized by secondary structures, which have to be destroyed before gelation can begin. The denaturation of globular proteins being a thermally activated process, the overall gelation of such proteins becomes strongly temperature dependent. In contrast, RSF exists in a random coil state in the fresh dialyzed aqueous solution. The absence of any secondary structure therefore does not demand a thermal activation step prior to gelation. Hence the gelation of RSF sol is only weakly dependent on temperature. Chapter 5 presented results on the gelation process from which the kinetics and the mechanism of gelation were inferred. At a molecular level the reduction in pH causes protonation of the predominant carboxyl groups, which decreases electrostatic chain repulsion and increases inter-chain attraction through hydrophobic interactions. This causes protein aggregation leading to gelation. However, more details about the structural evolution have emerged from the studies presented in chapter 5.

It was observed that upon reduction of pH to less than pI the apparently free flowing RSF sol had in fact weak gel like characteristics. Although no aggregates were seen in this sol over the length scales of 200 nm – 1 μm by light scattering, smaller aggregates and presence of strand-like structures were suggested by SAXS studies. Also, the sol did not have any significant amount of β-sheet content. Thus the small amount of initial protein aggregation in the sol was caused only by weak reversible intermolecular attraction. From

this initial state, which is formed in the pH reduction step, further aggregation of proteins took place with time to eventually form the gel. It was shown that the aggregation happens by the reaction-limited cluster aggregation process, which is possibly driven at the molecular scale by the formation of β-sheets. The β sheet content grew exponentially during gelation and simultaneously the size and mass of the aggregates grew exponentially with time, retaining their fractal nature during the growth, until the structures percolated to form a non-flowing gel. It was found that gelation happened even for RSF sols that contained only 0.05 wt% of protein. The formation of an open percolating fractal structure shows why even such low protein content is sufficient to form a gel.

Based on the detailed understanding of gelation mechanism, a novel method was used to accelerate the gelation of RSF at pH higher than the pI of fibroin. At pH > 5, where it normally takes of the order of several days for gelation, a 'seeding' protocol was proposed to accelerate gelation. It was shown in chapter 6 that two types of seeding experiments can be done, one in which external nuclei could be added to the RSF sol and the other in which the irreversibly formed β-sheets at low pH could themselves be used as seeds for gelation at high pH. The gel formed by both techniques finally contained substantial amount of β sheets. The external seeding was achieved in this work by using silica nanoparticles. It was proposed that proteins were first adsorbed on the particles and underwent conformation transition on the surface to form β sheets, which were responsible for the rapid gelation of the rest of the solution. Addition of an external inorganic component to the RSF gel also has the possibility of bringing other interesting properties to the gel. In chapter 6 it was shown that silica increases the mechanical strength of the gel. It is equally possible to add other biocompatible particles such as hydroxyapityte or β-trichlorophosphate to RSF to create gels that could be useful for engineering stronger tissues with biomineralization ability. It is also possible to partially modify the surfaces of such particles with growth factors to help cell growth.

In summary, the work presented in this thesis has enabled a detailed understanding of the structure of RSF gels and its gelation mechanism for the case of pH < pI, which were the main aims of the study. The work has also demonstrated a novel methodology for accelerating gelation at pH > pI.

7.2 Recommendations for future work:

7.2.1 Gelation at pH < pI:

Although chapters 4 and 5 present a detailed study on the structure of RSF gels and the gelation process itself, there are still several issues which remain incompletely understood. Some of these are pointed out below, and possible experimental approaches to study them are also suggested.

a. The evolution of structure at mesoscale was studied in this work using light scattering and SAXS. An example of a combination of these results is shown in Figure 7.1. While the light scattering data showed significant growth in scattering intensity during the gelation process, the SAXS intensity did not grow very much with time implying that fibroin agglomeration during gelation happens at intermediate larger length scales. This transition might be better captured using ultra-SAXS, a facility that was not available for the present study.

b. Circular dichroism was used in the present work to study conformation transition of fibroin from its initial random coil state to beta-sheet state. Although quantification of the increase in beta sheet structures was done using the Reed model, the growth rates are highly model dependent. Two other techniques could be used to study the conformation transition: FTIR and Microcalorimetry. The former has been used by Matsumoto et al in their work. [101] During the course of this work the microcalorimetry technique can tried on a few samples. Figure 7.2 (a) shows an example of heat released during gelation of a RSF sol of C = 10 g/L, pH 2 using a Calorimetric Sciences Corporation (CSC).instrument 2 ml sol was injected into the sample holder and heat flow was monitored as a function of time during isothermal gelation at 25 ^{o}C. From this data the fractional heat released during gelation can be calculated and the same is presented in Figure 7.2 (b). The data can be fit with an exponential growth curve (solid line), which is in agreement with the exponential growth trends observed for other parameters such as the peak height of CD peak at 217 nm, turbidity increase, and the increase in M_w and R_h of aggregates. The heat released during gelation could be due to an enthalpy of demixing of protein from the solution or due to the formation of β sheet structures. The exothermic heat associated with the random coil to β sheet

structures has been reported for native silk fibroin by Magoshi et al. [129] Detailed microcalorimetry studies could provide more information about the molecular level events happening during gelation.

c. The initial structure of the RSF sol is still not clearly understood. Detailed macro-rheology studies presented in this work and the preliminary micro-rheology studies discussed briefly in this work point to the possibility of a weak-gel state of the sol at large length scales. Dynamic light scattering studies on the other hand do not show a distinct gel-like character of the sol, but in fact shows mobile particles and fractal agglomerates. SAXS studies also show a fractal structure. Reconciliation of the rheology data with structural data needs to be done by more detailed studies on micro-rheology, interfacial rheology and cryo-TEM and. The two rheological techniques will possibly help in identifying whether the observed gel-like rheological behavior of the sol is an interfacial or a bulk phenomenon. Cryo-TEM, will possibly detect the microstructure of the sol directly, and might compliment the LS and SAXS data.

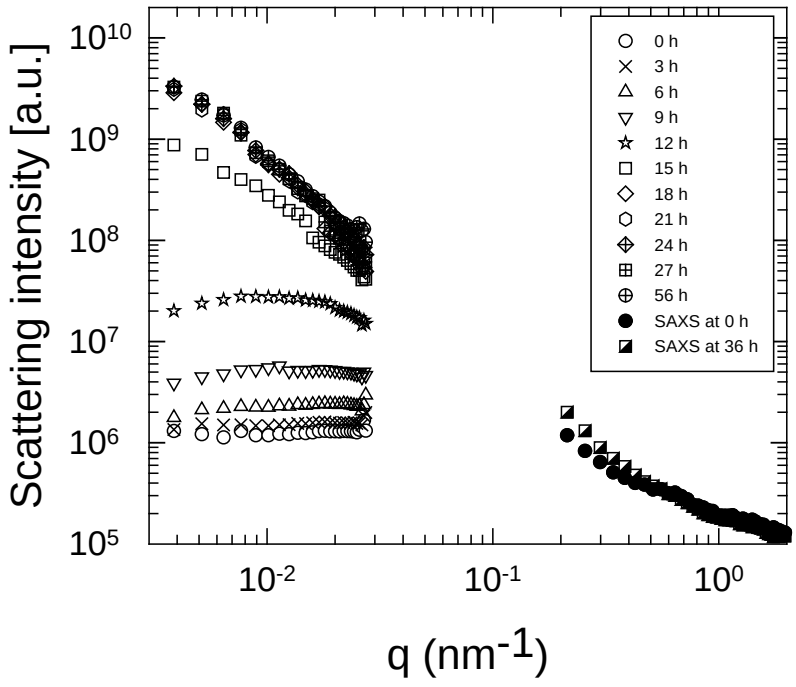

Figure 7.1: Combination of light scattering and SAXS data for RSF sol of C = 1 g/L, pH 2 during its gelation at 25 ^{o}C.

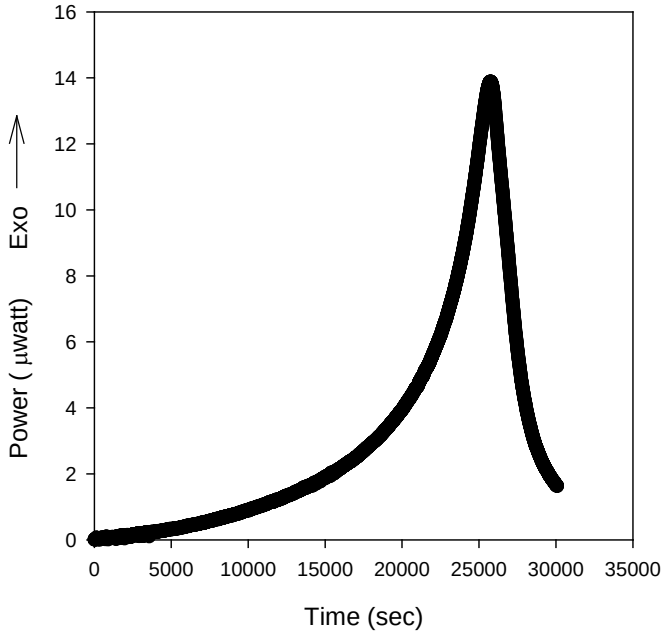

Figure 7.2 a : Micro-calorimetry data for RSF sol of C = 1 g/L, pH 2 during its gelation at 25 ^{o}C.

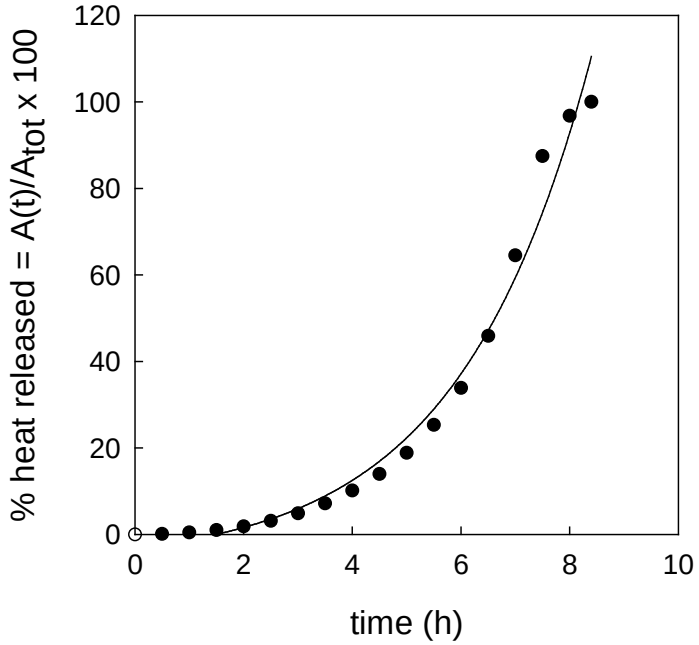

Figure 7.2 b: Fractional heat evolution as a function of time during gelation. Data is the same as in (a).

7.2.2 Accelerated gelation at pH > pI:

Silica assisted gelation of fibroin is an interesting phenomenon that has been reported here for the first time. There have been a few recent reports on silica-fibroin composite gels however, these researches have focused on the increase in the mechanical properties of the gels rather than on the nucleation effects. The possible mechanism for silica assisted nucleation of RSF was shown in Figure 6.3. This involves several rate processes namely, adsorption of fibroin on the silica nanoparticles, conformation change of the adsorbed protein, and gelation of the solution. The last step most likely involves changes at various length scales as probed in chapter 5. Of course, the conformation change of fibroin and its gelation must happen in the bulk solution as well in parallel to the changes happening on the silica particles, but presumably at lower rates. The following experiments could be used to check the proposed hypothesis:

1. Adsorption studies of fibroin on silica nanoparticles: An excellent equipment to study this rate process is a quartz crystal microbalance (QCM), which can measure the mass deposited per unit area by measuring the change in the frequency of a quartz crystal resonator.[130] Since frequency changes can be detected very accurately, the QCM can measure mass densities as low as 1 $\mu g/cm^2$. QCM has been used to study adsorption kinetics of protein on surfaces.[131]

2. Conformation transition of protein on silica: Adsorption of human carbonic anhydrase I (HCAI) on silica nanoparticles and the conformation transition of the protein on the surface has been studied by Lundqvist et al.[132] They have used several techniques including CD, IR and NMR study the conformational changes of proteins on silica. Similar techniques could be used to study the absorption and subsequent conformation change of fibroin on nanosilica.

3. Gelation: Tables 6.1-6.2 show only preliminary trends about the effect of temperature, protein concentration, silica concentration and silica particle size on gelation time. These effects will have to be studied in details in order to gain mechanistic insights into the gelation process. Various techniques used in this work as described in chapters 3-5 can be used to study the gelation process in greater detail.

4. Self-seeding experiments: All the techniques described in chapters 3-5 can be used directly to monitor the gelation process of RSF solutions.

Finally, other types of inorganic particles could be used to prepare RSF composite gels. Useful candidate particles could be hydroxyapetite and β-trichlorophosphate, which are biocompatible and could assist biominerilization of stronger tissues.

Appendix

This Appendix provides additional experimental results which show that the important trends presented in chapters 4 and 5 were also observed for other concentrations of RSF and were thus generic. Figure A-1 shows the evolution of creep compliance during gelation of a RSF sol of concentration C = 7.5 g/L, pH 2 at 25 ^{o}C. The data shows creep ringing, whose frequency increases with time, accompanied simultaneously with a decrease in the creep compliance. Both observations suggest an increase in the modulus of the sample, with a more rapid increase observed between 9 and 12 h. Figures A-2 and A-3 show light scattering data for RSF sols of C = 0.5 and 1.5 g/L respectively. As in the case of the C= 1.0 g/L sol, the scattering intensity increased with time and showed no *q*-dependence initially suggesting a homogeneous structure. After 12 h for the 0.5 g/L sol and 9 h for the 1.5 g/L sol the scattering intensities increased suddenly and showed *q*-dependence suggesting formation of heterogeneous structures. The $I(q)$ showed a power law dependence on q with an exponent of 2.1 for both concentrations suggesting RLCA mechanism of gelation. This was also supported by exponential increase in the size and mass of aggregates (not shown here). Figure A-5 shows CD spectra of RSF sol of 5 g/L at various times during gelation. A special cell of very small path length had to be used for this high concentration sample. The data for the initial state of the RSF sol shows an asymmetric peak with a maximum at about 207 nm. The peak maximum shifts to 218 nm during gelation accompanied with in increase in intensity. This indicates the formation of β-sheets during gelation.

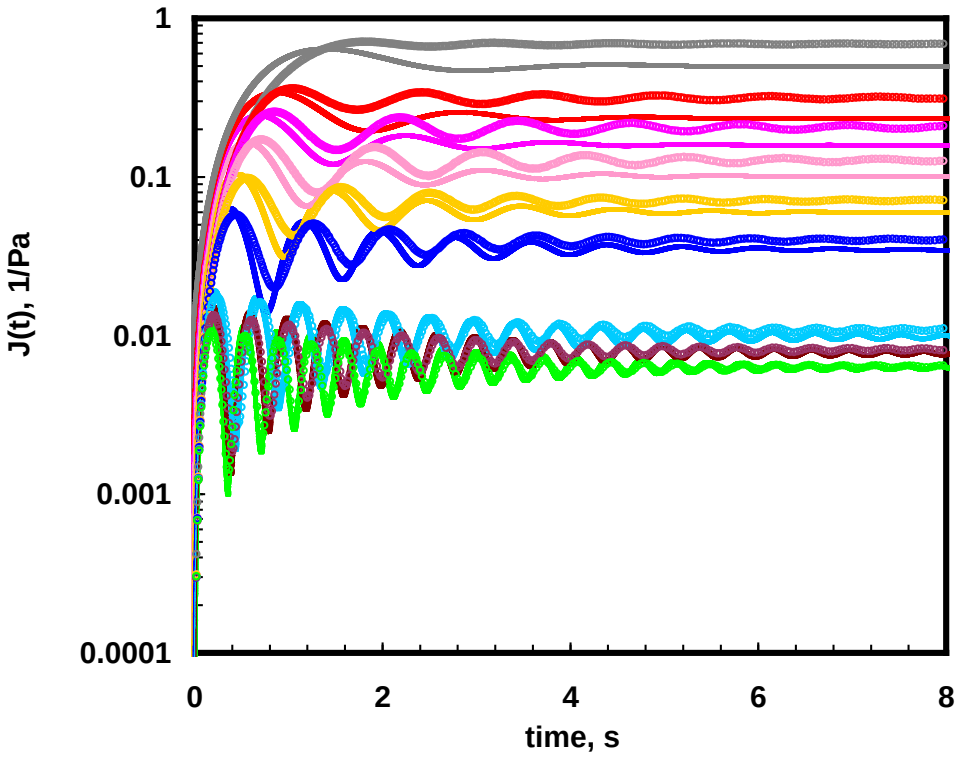

Figure A-1: Time evolution of the creep behavior of 7.5 g/L RSF sol of pH 2 at 25 ^{o}C

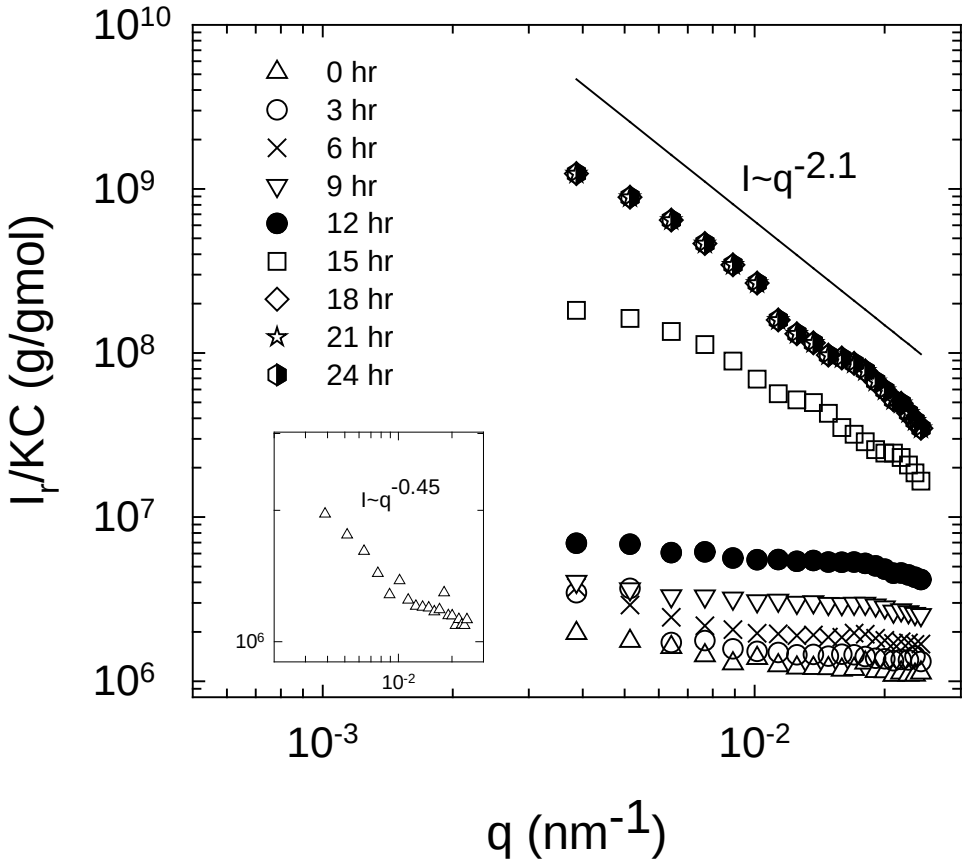

Figure A-2: Light scattering data during gelation of a RSF sol of C=0.5 g/L, pH 2, T=25 ^{o}C. The total scattering intensity (comprising scattering from fast plus slow modes) is shown here as an example. Between 0 h and 6 h a measurable q – dependence was seen at small values of q suggesting perhaps the existence of a larger length scale structure in the sol. This feature was not seen very clearly for the C= 1 g/L and C=1.5 g/L samples. On multiplying the total scattering intensity with the amplitude of the fast mode the scattering intensity became nearly q – independent.

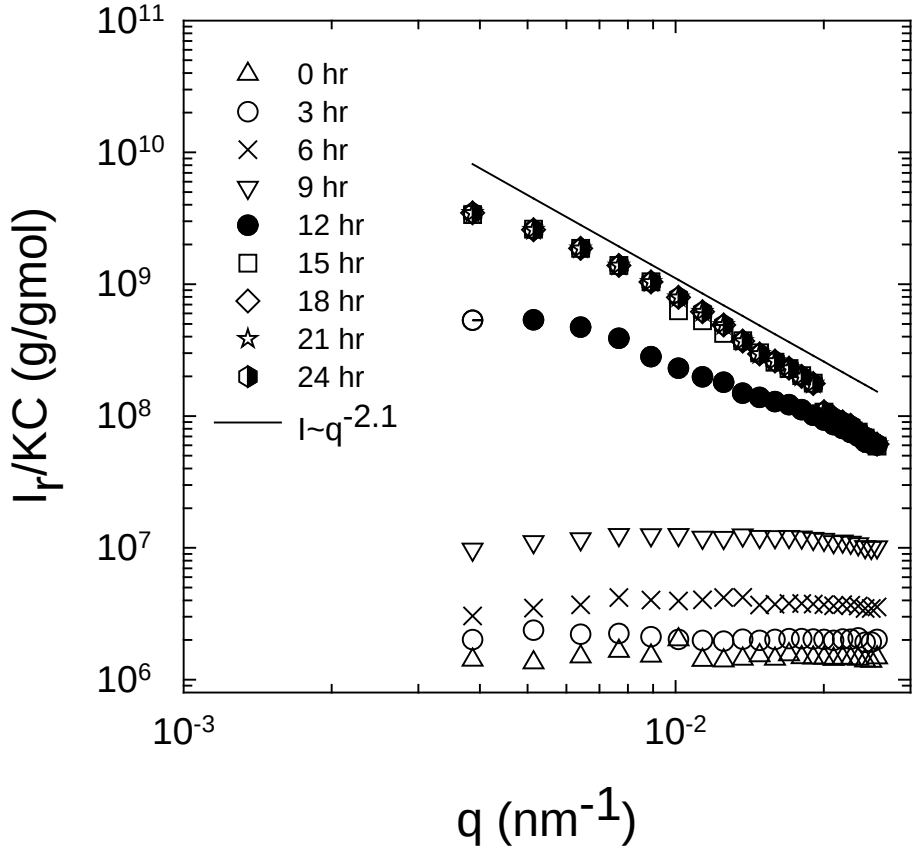

Figure A-3: Light scattering data during gelation of a RSF sol of C=1.5 g/L, pH 2, T=25 ^{o}C

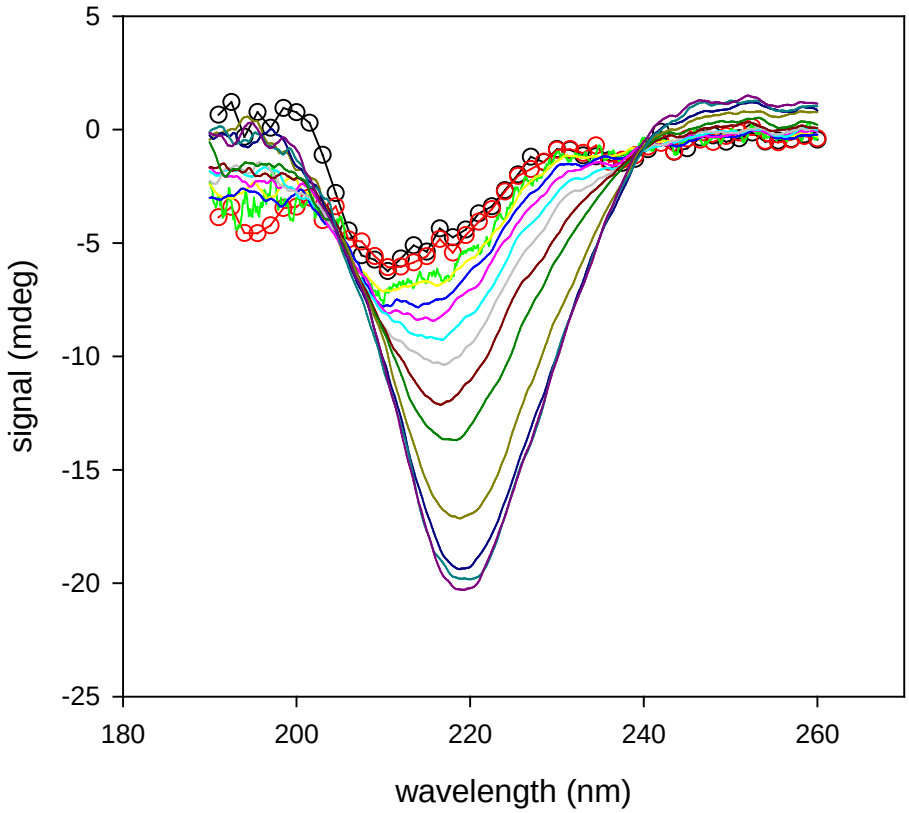

Figure A-4 a: CD spectra of RSF sol of C = 5g/L, pH 2 during gelation at 25 ^{o}C. Spectra indicated with circles are for the freshly dialyzed RSF solution of same concentration and pH 8.2 (black circles) and for RSF at 0 h (red circles). The rest of the spectra are taken every 1 h during gelation. This experiment was performed using a quartz cell of 0.01 mm path length. Smaller path length is required because of the higher concentration of the RSF.

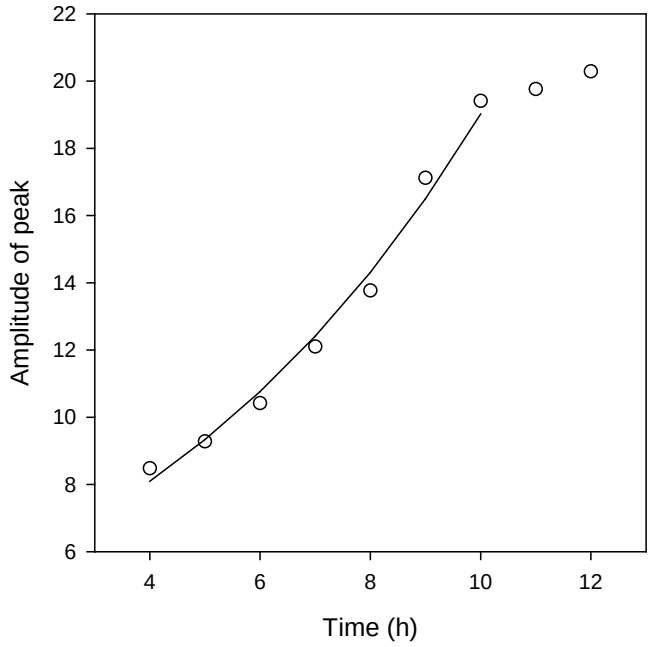

Figure A-4 b: Growth of amplitude of the major peak seen in (a). The line is an exponential fit to the data. The peak wavelength increased by about 4 nm from 4 h to 12 h during gelation.

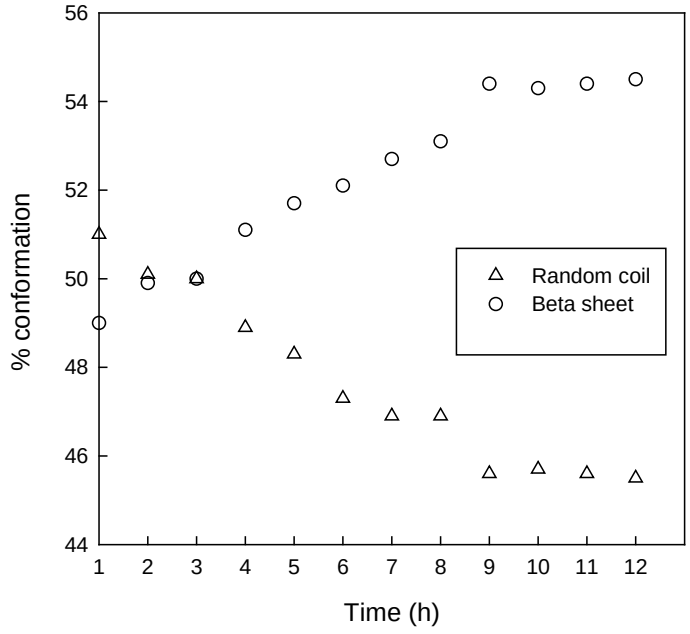

Figure A-4 c: Predicted protein conformation changes during gelation as per Reed model for data shown in (a)

References

1. Vepari, C., and D. L. Kaplan, *Silk as a biomaterial.* Progress in Polymer Science (Oxford), 2007. **32**(8-9): p. 991-1007.
2. Goldsmith, M., and J. R. Shi, *Molecular Map for the Silkworm*, in *Silk Polymers*. 1993, American Chemical Society: Washington, DC. p. 45-58.
3. Sen, K., and M. K. Babu, *Studies on Indian Silk. II. Structure-Property Correlations.* Journal of Applied Polymer Science, 2004. **92**(2): p. 1098-1115.
4. Shao, Z., and F. Vollrath, *Surprising strength of silkworm silk.* Nature, 2002. **418**(6899): p. 741.
5. Devision, F.A.A.O.o.U.N.E.A.S.D.T.S. [cited; Available from: http://www.fao.org/es/ess/top/commodity.html?lang=en&item=1185&year=2005
6. Vollrath, F., and D. P. Knight, *Liquid crystalline spinning of spider silk.* Nature, 2001. **410**(6828): p. 541-548.
7. Gosline, J. M., P. A. Guerette,, C. S. Ortlepp, and K. N. Savage,, *The mechanical design of spider silks: from fibroin sequence to mechanical function.* J Exp Biol, 1999. **202**(23): p. 3295-3303.
8. PÃ©rez-Rigueiro, J., C. Viney, , J. Llorca, and M. Elices, *Mechanical properties of single-brin silkworm silk.* Journal of Applied Polymer Science, 2000. **75**(10): p. 1270-1277.
9. Cunniff, P. M., S. A. Fossey, M. A. Auerbach, J. W. Song, D. L. Kaplan, W. W Adams, R. K. Eby, D. Mahoney, D. L. Vezie, *Mechanical and thermal properties of dragline silk from the spider Nephila clavipes.* Polymers for Advanced Technologies, 1994. **5**(8): p. 401-410.
10. Bunning, T. J., H. Jiang, W. W. Adams, R. L. Crane., B. Farmer, and D. Kaplan, *Applications of Silk*, in *Silk Polymers*. 1993, American Chemical Society: Washington, DC. p. 353-358.
11. Liivak, O., A. Blye, N. Shah, and L. W. Jelinski, *A microfabricated wet-spinning apparatus to spin fibers of silk proteins. Structure-property correlations.* Macromolecules, 1998. **31**(9): p. 2947-2951.

12. Zhou, G., Z. Shao, D. P. Knight, J. Yan, and X. Chen, *Silk fibers extruded artificially from aqueous solutions of regenerated bombyx mori silk fibroin are tougher than their natural counterparts.* Advanced Materials, 2009. **21**(3): p. 366-370.
13. Ha, S. W., Y. H. Park, and S. M. Hudson, *Dissolution of bombyx mori silk fibroin in the calcium nitrate tetrahydrate-methanol system and aspects of wet spinning of fibroin solution.* Biomacromolecules, 2003. **4**(3): p. 488-496.
14. Minoura, N., S. I. Aiba, M. Higuchi, Y. Gotoh, M. Tsukada, and Y. Imai, *Attachment and growth of fibroblast cells on silk fibroin.* Biochemical and Biophysical Research Communications, 1995. **208**(2): p. 511-516.
15. Rossitch Jr, E., D. E. Bullard., and W. J. Oakes, *Delayed foreign-body reaction to silk sutures in pediatric neurosurgical patients.* Child's Nervous System, 1987. **3**(6): p. 375-378.
16. Salthouse, T. N., B. F. Matlaga, and M. H. Wykoff, *Comparative tissue response to six suture materials in rabbit cornea, sclera, and ocular muscle.* American Journal of Ophthalmology, 1977. **84**(2): p. 224-233.
17. Wound closure manual. The suture: specific suturing materials. Non-absorbable sutures.
18. Soong, H. K., and K. R. Kenyon, *Adverse reactions to virgin silk sutures in cataract surgery.* Ophthalmology, 1984. **91**(5): p. 479-483.
19. Engler, A. J., S. Sen, H. L. Sweeney, and D. E. Discher, *Matrix Elasticity Directs Stem Cell Lineage Specification.* Cell, 2006. **126**(4): p. 677-689.
20. Altman, G. H., R. L. Horan, H. H, Lu, J. Moreau, I. Martin, J. C. Richmond, and D. L. Kaplan, *Silk matrix for tissue engineered anterior cruciate ligaments.* Biomaterials, 2002. **23**(20): p. 4131-4141.
21. Ghosh, S., S. T. Parker, X. Wang, D. L. Kaplan, and J. A. Lewis, *Direct-Write Assembly of Microperiodic Silk Fibroin Scaffolds for Tissue Engineering Applications.* Advanced Functional Materials, 2008. **18**(13): p. 1883-1889.
22. Meinel, L., S. Hofmann, V. Karageorgiou, L. Zichner, R. Langer, D. Kaplan, G. Vunjak-Novakovic, *Engineering cartilage-like tissue using human mesenchymal stem cells and silk protein scaffolds.* Biotechnology and Bioengineering, 2004. **88**(3): p. 379-391.
23. Marolt, D., A. Augst, L. E. Freed, C. Vepari, R. Fajardo, N. Patel, M. Gray, M. Farley, D. Kaplan, D. and G. Vunjak-Novakovic, *Bone and cartilage tissue constructs*

grown using human bone marrow stromal cells, silk scaffolds and rotating bioreactors. Biomaterials, 2006. **27**(36): p. 6138-6149.

4. Aoki, H., N. Tomita, Y. Morita, K. Hattori, Y. Harada, M. Sonobe, and Y. Tamada, *Culture of chondrocytes in fibroin-hydrogel sponge.* Bio-Medical Materials and Engineering, 2003. **13**(4): p. 309-316.

25. Altman, G. H., R. L. Horan, H. H. Lu, J. Moreau, I. Martin, J. C. Richmond, and D. L. Kaplan, *Silk matrix for tissue engineered anterior cruciate ligaments.* Biomaterials, 2002. **23**(20): p. 4131-4141.

26. Dal Pra, I., G. Freddi, J. Minic, A. Chiarini, and U. Armato, *De novo engineering of reticular connective tissue in vivo by silk fibroin nonwoven materials.* Biomaterials, 2005. **26**(14): p. 1987-1999.

27. Li, C., C. Vepari, H. J. Jin, H. J. Kim, and D. L. Kaplan, D. L. , *Electrospun silk-BMP-2 scaffolds for bone tissue engineering.* Biomaterials, 2006. **27**(16): p. 3115-3124.

28. Motta, A., C. Migliaresi, F. Faccioni, P. Torricelli, M. Fini, and R. Giardino, *Fibroin hydrogels for biomedical applications: Preparation, characterization and in vitro cell culture studies.* Journal of Biomaterials Science, Polymer Edition, 2004. **15**(7): p. 851-864.

29. Sofia, S., M. B. McCarthy, G. Gronowicz, and D. L. Kaplan, *Functionalized silk-based biomaterials for bone formation.* Journal of Biomedical Materials Research, 2001. **54**(1): p. 139-148.

30. Kino, R., T. Ikoma, A. Monkawa, S. Yunoki, M. Munekata, J. Tanaka, and T. Asakura, *Deposition of bone-like apatite on modified silk fibroin films from simulated body fluid.* Journal of Applied Polymer Science, 2006. **99**(5): p. 2822-2830.

31. Meinel, L., V. Karageorgiou, R. Fajardo, B. Snyder, V. Shinde-Patil, L. Zichner, D. Kaplan, R. Langer, and G. Vunjak-Novakovic, *Bone tissue engineering using human mesenchymal stem cells: Effects of scaffold material and medium flow.* Annals of Biomedical Engineering, 2004. **32**(1): p. 112-122.

32. Kim, H.J., U. J. Kim, G. Vunjak-Novakovic, B. H. Min, and D. L. Kaplan, *Influence of macroporous protein scaffolds on bone tissue engineering from bone marrow stem cells.* Biomaterials, 2005. **26**(21): p. 4442-4452.

33. Vepari, C. and D. Kaplan, *Silk as a biomaterial.* Progress in Polymer Science. **32**(8-9): p. 991-1007.

34. Kim, H. J., U. J. Kim, G. Vunjak-Novakovic, B. H. Min, and D. L. Kaplan, *Influence of macroporous protein scaffolds on bone tissue engineering from bone marrow stem cells.* Biomaterials, 2005. **26**(21): p. 4442-4452.

35. Wang, Y. Z., H. J. Kim, G. Vunjak-Novakovic, and D. L. Kaplan, *Stem cell-based tissue engineering with silk biomaterials.* Biomaterials, 2006. **27**(36): p. 6064-6082.

36. Matsumoto, A., J. Chen, A. L. Collette, U-J Kim, G. H. Altman, P. Cebe, and D. L. Kaplan, *Mechanisms of Silk Fibroin Sol Gel Transitions.* The Journal of Physical Chemistry B, 2006. **110**(43): p. 21630-21638.

37. Kim, U.-J., J. Park, C. Li, H-J Jin, R. Valluzzi, D. Kaplan, *Structure and Properties of Silk Hydrogels.* Biomacromolecules, 2004. **5**(3): p. 786-792.

38. Shao, Z. and F. Vollrath *Materials: Surprising strength of silkworm silk.* Nature, 2002. **418**(6899): p. 741-741.

39. Sashina, E. S., A. M. Bochek, N. P. Novoselov, D. A. Kirichenko, *Structure and solubility of natural silk fibroin.* Russian Journal of Applied Chemistry, 2006. **79**(6): p. 869-876.

40. Tashiro, Y., E. Otsuki, and T. Shimadzu, *Sedimentation analyses of native silk fibroin in urea and guanidineÂ·HCl.* BBA - Protein Structure, 1972. **257**(2): p. 198-209.

41. Tanaka, K., N. Kajiyama, K. Ishikura, S. Waga, A. Kikuchi, K. Ohtomo, T. Takagi, and S. Mizuno, *Determination of the site of disulfide linkage between heavy and light chains of silk fibroin produced by Bombyx mori.* Biochimica et Biophysica Acta - Protein Structure and Molecular Enzymology, 1999. **1432**(1): p. 92-103.

42. Tanaka, K., S. Inoue, and S. Mizuno, *Hydrophobic interaction of P25, containing Asn-linked oligosaccharide chains, with the H-L complex of silk fibroin produced by Bombyx mori.* Insect Biochemistry and Molecular Biology, 1999. **29**(3): p. 269-276.

43. Inoue, S., K. Tanaka, F. Arisaka, S. Kimura, K. Ohtomo, and S. Mizuno, *Silk fibroin of Bombyx mori is secreted, assembling a high molecular mass elementary unit consisting of H-chain, L-chain, and P25, with a 6:6:1 molar ratio.* Journal of Biological Chemistry, 2000. **275**(51): p. 40517-40528.

44. Zhou, C.-Z., F. Confalonieri, N. Medina, Y. Zivanovic, C. Esnault, T. Yang, M. Jacquet, J. Janin, M. Duguet, R. Perasso, and Z-G Li, *Fine organisation of Bombyx Mori fibroin heavy chain gene.* Nucleic Acid Research 2000. **28**(12): p. 2413-2419.

45. Asakura, T., R. Sugino, J. Yao, H. Takashima, and R. Kishore, *Comparative structure analysis of tyrosine and valine residues in unprocessed silk fibroin (silk I)*

and in the processed silk fiber (silk II) from Bombyx mori using solid-state 13C,15N, and 2H NMR. Biochemistry, 2002. **41**(13): p. 4415-4424.

46. Jin, H. J., and D. L. Kaplan, *Mechanism of silk processing in insects and spiders.* Nature, 2003. **424**(6952): p. 1057-1061.
47. Asakura, T., R. Sugino, J. Yao, H. Takashima, and R. Kishore, *Comparative structure analysis of tyrosine and valine residues in unprocessed silk fibroin (silk I) and in the processed silk fiber (silk II) from Bombyx mori using solid-state 13C,15N, and 2H NMR.* Biochemistry, 2002. **41**(13): p. 4415-4424.
48. Foo, C. W. P., E. Bini, J. Hensman, J. Hensman, S. Y. Xu, R.V. Lewis, and D. L. Kaplan, *Role of pH and charge on silk protein assembly in insects and spiders.* Applied Physics A: Materials Science and Processing, 2006. **82**(2): p. 223-233.
49. Ayub, Z. H., M. Arai, and K. Hirabayashi, *Mechanism of the gelation of fibroin solution.* Biosci. Biotech. Biochem., 1993. **57**(11): p. 1910-1912.
50. Ha, S. W., A. E. Tonelli, and S. M. Hudson, *Structural study of Irregular amino acid sequences in the heavy chain of Bombyx mori silk fibroin.* Biomacromolecules, 2005. **6**(5): p. 2563-2569.
51. Ochi, A., K. S. Hossain, J. Magoshi, and N. Nemoto, *Rheology and dynamic light scattering of silk fibroin solution extracted from the middle division of Bombyx mori silkworm.* Biomacromolecules, 2002. **3**(6): p. 1187-1196.
52. Sprague, K.U., *The Bombyx mon silk proteins: Characterization of large polypeptides.* Biochemistry, 1975. **14**(5): p. 925-931.
53. Wu, J. H., Z. Wang, and S. Y. Xu, *Preparation and characterization of sericin powder extracted from silk industry wastewater.* Food Chemistry, 2007. **103**(4): p. 1255-1262.
54. Gamo, T., T. Inokuchi, and H. Laufer, *Polypeptides of fibroin and sericin secreted from the different sections of the silk gland in Bombyx mori.* Insect Biochemistry, 1977. **7**(3): p. 285-295.
55. Willcox, P.J., S. P. Gido, W. Muller, and D. L. Kaplan, *Evidence of a cholesteric liquid crystalline phase in natural silk spinning processes.* Macromolecules, 1996. **29**(15): p. 5106-5110.
56. Magoshi, J., Y. Magoshi, and S. Nakamura, *Physical properties and structure of silk: 10. The mechnism of fiber formation from liquid silk of silkworm Bombayx Mori.* Polymer communications Guildford, 1985. **26**(10): p. 309-311.

57. Nagarkar, S., R. Ojha, J. Mankad, P. Patil, V. Soni and A. Lele, *Measuring the elongation viscosity of lyocell using a semi-hyperbolic die.* Rheologica Acta, 2006. **45**(3): p. 260-267.
58. Subramanian, G., V. Ranade, S. Nagarkar, and A. Lele, *Matched asymptotic solution for flow in a semi-hyperbolic die.* Chemical Engineering Science, 2005. **60**(11): p. 3107-3110.
59. Asakura, T., K. Umemura, Y. Nakazawa, H. Hirose, J. Higham, and D. Knight, *Some observations on the structure and function of the spinning apparatus in the silkworm Bombyx mori.* Biomacromolecules, 2007. **8**(1): p. 175-181.
60. Kataoka, K., Sen'i Gakkaishi, 1978. **34**: p. 80-88.
61. Yamane, T., K. Umemura, Y. Nakazawa, and T. Asakura, *Molecular dynamics simulation of conformational change of poly(Ala-Gly) from silk I to silk II in relation to fiber formation mechanism of Bombyx mori silk fibroin.* Macromolecules, 2003. **36**(18): p. 6766-6772.
62. Breslauer, D. N., L. P. Lee and S. J. Muller, *Simulation of Flow in the Silk Gland.* Biomacromolecules, 2008. **10**(1): p. 49-57.
63. Iizuka E., *Silk Thread: Mechanism of spinning and its mechanical properties.* Journal of Applied Polymer Science Applied Polymer Symposia, 1985. **41**: p. 173-185.
64. Liivak, O., A. Blye, N. Shah, and L. W. Jelinski, *A microfabricated wet-spinning apparatus to spin fibers of silk proteins. Structure-property correlations.* Macromolecules, 1998. **31**(9): p. 2947-2951.
65. Ha, S. W., A. E. Tonelli, and S. M. Hudson, *Structural studies of Bombyx mori silk fibroin during regeneration from solutions and wet fiber spinning.* Biomacromolecules, 2005. **6**(3): p. 1722-1731.
66. Marsh, R.E., R. B. Corey, and L. Pauling, *An investigation of the structure of silk fibroin.* BBA - Biochimica et Biophysica Acta, 1955. **16**(C): p. 1-34.
67. Valluzzi, R. and S. P. Gido, *The crystal structure of bombyx mori silk fibroin at the air-water interface.* Biopolymers - Nucleic Acid Sciences Section, 1997. **42**(6): p. 705-717.
68. Wilson, D., R. Valluzzi, and D. Kaplan, *Conformational transitions model silk peptides.* Biophysical Journal, 2000. **78**(5): p. 2690-2701.
69. Shen, Y., M. A. Johnson, and D. C. Martin, *Microstructural characterization of Bombyx mori silk fibers.* Macromolecules, 1998. **31**(25): p. 8857-8864.

70. Valluzzi, R. and H. J. Jin, *X-ray evidence for a "super"-secondary structure in silk fibers.* Biomacromolecules, 2004. **5**(3): p. 696-703.

71. Lotz, B. and F. C. Cesari *The chemical structure and the crystalline structures of Bombyx mori silk fibroin.* Biochimie, 1979. **61**(2): p. 205-214.

72. Altman, G. H., F. Diaz, C. Jakuba, T. Calabro, T., R. L. Horan, J. Chen, and H. Lu, J. Richmond, and D. L. Kaplan, *Silk-based biomaterials.* Biomaterials, 2003. **24**(3): p. 401-416.

73. Chen, X., D. P. Knight, Z. Shao, and F. Vollrath, *Regenerated Bombyx silk solutions studied with rheometry and FTIR.* Polymer, 2001. **42**(25): p. 9969-9974.

74. Ohgo, K., Z. Chenhua, K. Mitsuhiro, and A. Tetsuo, *Preparation of non-woven nanofibers of Bombyx mori silk, Samia cynthia ricini silk and recombinant hybrid silk with electrospinning method.* Polymer, 2003. **44**(3): p. 841-846.

75. Hossain, K. S., E. Ohyama, A. Ochi, J. Magoshi, and N. Nemoto, *Dilute-solution properties of regenerated silk fibroin.* Journal of Physical Chemistry B, 2003. **107**(32): p. 8066-8073.

76. Iridag, Y. and M. Kazanci, *Preparation and characterization of Bombyx mori silk fibroin and wool keratin.* Journal of Applied Polymer Science, 2006. **100**(5): p. 4260-4264.

77. Tsukada, M., Y. Gotoh, M. Nagura, N. Minoura, N. Kasai, and G. Freddi, *Structural changes of silk fibroin membranes induced by immersion in methanol aqueous solutions.* Journal of Polymer Science, Part B: Polymer Physics, 1994. **32**(5): p. 961-968.

78. Gimel, J. C., D. Durand, and T. Nicolai, *Structure and distribution of aggregates formed after heat-induced denaturation of globular proteins.* Macromolecules, 1994. **27**(2): p. 583-589.

79. Bremer, L. G. B., B. H. Bijsterbosch, R. Schrijvers, T. van Vliet, and P. Walstra, *On the fractal nature of the structure of acid casein gels.* Colloids and Surfaces, 1990. **51**(C): p. 159-170.

80. Kato, A., H. R. Ibrahim, H. Watanabe, K. Honma, and K. Kobayashi, *Structural and gelling properties of dry-heating egg white proteins.* Journal of Agricultural and Food Chemistry, 1990. **38**(1): p. 32-37.

81. Green, R. J., I. Hopkinson, and R. A. L. Jones, *Unfolding and intermolecular association in globular proteins adsorbed at interfaces.* Langmuir, 1999. **15**(15): p. 5102-5110.

82. Mine, Y., *Laser Light Scattering Study on the Heat-Induced Ovalbumin Aggregates Related to Its Gelling Property.* Journal of Agricultural and Food Chemistry, 1996. **44**(8): p. 2086-2090.

83. Saleh, A. M., A. T. Florence, T. L. Whateley, and L. K. Khordagui, *The effect of hydrotropic agents on the heat coagulation of bovine serum albumin.* Journal of Pharmacy and Pharmacology, 1989. **41**(5): p. 298-301.

84. Dominique D. and T. Nicolai, *Handbook of food science technology vol 2.*

85. Clark, A. H., G. M. Kavanagh, and S. B. Ross-Murphy, *Globular protein gelation - Theory and experiment.* Food Hydrocolloids, 2001. **15**(4-6): p. 383-400.

86. Le Bon, C., T. Nicolai, and D. Durand, *Kinetics of aggregation and gelation of globular proteins after heat-induced denaturation.* Macromolecules, 1999. **32**(19): p. 6120-6127.

87. Pouzot, M., T. Nicolai, D. Durand, and L. Benyahia, *Structure factor and elasticity of a heat-set globular protein gel.* Macromolecules, 2004. **37**(2): p. 614-620.

88. Langton, M. and A. M. Hermansson, *Fine-stranded and particulate gels of Î²-lactoglobulin and whey protein at varying pH.* Food Hydrocolloids, 1992. **5**(6): p. 523-539.

89. Durand, D., C. Gimel, and T. Nicolai, *Aggregation, gelation and phase separation of heat denatured globular proteins.* Physica A: Statistical Mechanics and its Applications, 2002. **304**(1-2): p. 253-265.

90. Verheul, M. and S. P. F. M. Roefs, *Structure of particulate whey protein gels: effect of NaCl concentration, pH, heating temperature, and protein composition.* Journal of Agricultural and Food Chemistry, 1998. **46**: p. 4909-4916.

91. Renard D., A. Axelos, and J. Lefebvre, *In Food Macromolecules and Colloids.* Dickenson, E., D. Lorient, Eds. ed. 1995: Royal Society of Chemistry, Cambridge. 390.

92. Shish. W. H., K. I. Seong. L. Jun, A. A. Iihan, *Scaling behaviour of elastic properties of colloidal gels.* Physcial Review A, 1990. **42**(8): p. 4772-4780.

93. Ako, K., D. Durand, T. Nicolai, L. Becu, *Quantitative analysis of confocal laser scanning microscopy images of heat-set globular protein gels.* Food Hydrocolloids, 2009. **23**(4): p. 1111-1119.

94. Ould Eleya, M. M., S. Ko, and S. Gunasekaran, *Scaling and fractal analysis of viscoelastic properties of heat-induced protein gels.* Food Hydrocolloids, 2004. **18**(2): p. 315-323.

95. Nicolai, T., C. Urban and Schurtenberger, P., *Light scattering study of turbid heat-set globular protein gels using cross-correlation dynamic light scattering.* Journal of Colloid and Interface Science, 2001. **240**(2): p. 419-424.

96. Ikeda, S., E. A. Foegeding, and T. Hagiwara, *Rheological study on the fractal nature of the protein gel structure.* Langmuir, 1999. **15**(25): p. 8584-8589.

97. Hagiwara, T., H. Kumagai, H., and K. Nakamura, *Fractal Analysis of Aggregates Formed by Heating Dilute BSA Solutions Using Light Scattering Methods.* Bioscience, Biotechnology and Biochemistry, 1996. **60**(11): p. 1757-1763.

98. Dietler, G., C. Aubert, D. S. Cannell, and P. Wiltzius, *Gelation of colloidal silica.* Physical Review Letters, 1986. **57**(24): p. 3117-3120.

99. Weitz, D. A., J. S. Huang, M. Y. Lin, and J. Sung, *Limits of the fractal dimension for irreversible kinetic aggregation of gold colloids.* Physical Review Letters, 1985. **54**(13): p. 1416-1419.

100. Nazarov, R., H. J. Jin, and D. L. Kaplan, *Porous 3-D scaffolds from regenerated silk fibroin.* Biomacromolecules, 2004. **5**(3): p. 718-726.

101. Matsumoto A., J. Chen, A. Collette, U-J Kim, G. H, Altman, P. Cebe, and D. Kaplan, *Mechanisms of silk fibroin sol-gel transitions.* Journal of Physical Chemistry B, 2006. **110**(43): p. 21630-21638.

102. Pecora, R., *Dynamics of light scattering: Application of photon correlation spectroscopy*. 1985: Springer.

103. Brown, W., *Light Scattering. Principles and Developments*. 1996, Oxford: Clarendon Press.

104. [cited; Available from: http://www.malvern.co.uk/common/downloads/campaign/MRK656-01.pdf)

105. Berne, B. J. and P. Pecora, *Dynamic Light Scattering with Applications to Chemistry, Biology and Physics*. 1976, New York: Wiley.

106. Stepanek, P., in *Dynamic Light Scattering*, W. Brown, Editor. 1993, Oxford University Press: Oxford.

107. Baravian, C. and D. Quemada, *Using instrumental inertia in controlled stress rheometry.* Rheologica Acta, 1998. **37**(3): p. 223-233.

108. Joshi, Y. M., G. Reddy, K. Ranjith, A. Kulkarni, N. Kumar, and R. Chhabra, *Rheological behaviour of aqueous suspensions of laponite: new insights into the ageing phenomena.* Proceedings of the Royal Society A: Mathematical, Physical and Engineering Science, 2008. **464**(2090): p. 469-489.

109. Ewoldt R., H. and G. H. McKinley, Rheology Bulletin, 2007: p. 7.

110. Kelly, S. M. and N. C. Price, Current protein and peptide science, 2000. **1**: p. 349-384.

111. Linder, P.a.Z.T., *Neutrons, X-Rays and Light scattering method applied to soft condensed matter*. North-Holland Delta Series. 2002.

112. Valluzzi, R., S. J. He, S. P. Gido and D. L. Kaplan, *Bombyx mori silk fibroin liquid crystallinity and crystallization at aqueous fibroin–organic solvent interfaces.* International Journal of Biological Macromolecules, 1999. **24**: p. 227-236.

113. Iizuka, E. and J- T Yang, *The disordered and Î²-conformations of silk fibroin in solution.* Biochemistry, 1968. **7**(6): p. 2218-2228.

114. Horan, R. L., K. Antle, A. L. Collette, Y. Wang, J. Huang, J. E. Moreau, V. Volloch, and D. L. Kaplan, and G. H. Altman, *In vitro degradation of silk fibroin.* Biomaterials, 2005. **26**(17): p. 3385-3393.

115. Hossain, K. S., E. Ohyama, A. Ochi, J. Magoshi, and N. Nemoto, *Dilute-Solution Properties of Regenerated Silk Fibroin.* J. Phys. Chem. B, 2003. **107**: p. 8066-8073.

116. Tashiro, Y. and E. Otsuki, *Studies on the Posterior silk gland of the silkworm Bombix Mori IV. Ultracentrifugal Analyses of Native Silk Proteins, Especially Fibroin Extracted from the Middle Silk Gland of the Mature Silkworm.* The Journal of Cell Biology, 1970. **46**: p. 1-16.

117. Tashiro, Y. and E. Otsuki, *Studies on the posterior silk gland of the silkworm Bombix Mori IV. Ultracentrifugal Analyses of Native Silk Proteins, Especially Fibroin Extracted from the Middle Silk Gland of the Mature Silkworm.* J. Cell Biol., 1970. **46**(1): p. 1-16.

118. Le Bon, C., T. Nicolai, and D. Durand, D., Intl. J. Food Sci. Technol., 1999. **34**: p. 451-465.

119. Le Bon, C., T. Nicolai, and D. Durand, Macromolecules, 1999. **32**: p. 6120-6127.
120. Matsumoto, A., J. Chen, A. L. Collette, U-J. Kim, G. H. Altman, P. Cebe and D. Kaplan, *Mechanisms of Silk Fibroin Sol Gel Transitions.* The Journal of Physical Chemistry B, 2006. **110**(43): p. 21630-21638.
121. Christel Le Bon., T. Nicolai, and D. Durand, *Growth and structure of aggregates of heat-denatured b-Lactoglobulin.* International Journal of Food Science and Technology 1999. **34**: p. 451–465.
122. Nicolai T., *In Food Colloids : Self assembly and material science*. Dickinson, E.; Leser, M. E., Eds ed. 2009: RSC publishing, Cambridge.
123. Kim, U.-J., J. Park, C. Li, H-J. Jin, R. Valluzzi, and D. L. Kaplan, Biomacromolecules, 2004. **5**: p. 786-792.
124. Guiyang Li, S. Zhengzhong, X. Xun, C. Xin, W. Honghai, C. Lijuan and Y. Tongyin, *The natural silk spinning process: A nucleation-dependent aggregation mechanism?* Eur. J. Biochem., 2001. **268**: p. 6600-6606.
125. Reed J., and Reed T., *A Set of Constructed Type Spectra for the Practical Estimation of Peptide Secondary Structure from Circular Dichroism.* Analytical Biochemistry 1997. **254**: p. 36–40.
126. Brenner, T., R. Johannsson, and T. Nicolai, *Characterization of fish myosin aggregates using static and dynamic light scattering.* Food Hydrocolloids, 2009. **23**(2): p. 296-305.
127. Levitz, P., E. Lecolier,, A. Mourchid, A. Delville, and S. Lyonnard, *Liquid-solid transition of Laponite suspensions at very low ionic strength: Long-range electrostatic stabilisation of anisotropic colloids.* Europhysics Letters, 2000. **49**(5): p. 672-677.
128. Dijkstra, M., J-P. Hansen, and P. A. Madden, *Statistical model for the structure and gelation of smectite clay suspensions.* Physical Review E, 1997. **55**(3): p. 3044.
129. Jun,M., M. Mary, A. Becker, M. Kato, Z. H. Toshihisa, S. Inoue, S. Nakamura, *Crystallization of silk fibroin from solution.* Thermochimica Acta, 2000. **352-353**: p. 165-169.
130. O'Sullivan, C., and G. Guilbgoldlt, *Commercial quartz crystal microbalances-theory and applications.* Biosens. Bioelectron., 1999. **14**: p. 663-670.

131. Noboru, S., and M. Takehisa, *Protein adsorption on self-assembled monolayers with water-soluble non-ionic oligomers using quartz-crystal microbalance.* Mater. Sci. Eng., C, 1998. **6**(4): p. 261-266.

132. Martin, L. and J. Bengt-Harald *Protein Adsorption onto Silica Nanoparticles: Conformational Changes Depend on the Particles' Curvature and the Protein Stability.* Langmuir, 2004. **20**: p. 10639-10647.

Publications

1) **Shailesh Nagarkar**, Taco Nicolai, Christophe Chassenieux and Ashish Lele, "Structure and gelation mechanism of silk hydorgel", manuscript accepted in ***Physical Chemistry Chemical Physics***, 2010. **12**:p. 3834-3844

2) **Shailesh Nagarkar**, Avinash Patil, Ashish Lele, Suresh Bhat, Jayesh Bellare and R. A. Mashelkar, "Some Mechanistic Insights into the Gelation of Regenerated Silk Fibroin Sol", ***Industrial and Engineering Chemistry research,*** 2009**. 48**: p. 8014-8023.

Conference proceedings

1) ***Shailesh Nagarkar****, *Ashish Lele, Dominique Durand, Christophe Chassenieux, and Taco Nicolai, A rheological and light scattering study of the gelation of silk fibroin protein, presented in* **International Congress on Rheology** ***2008, Monterey, California, U.S.***

2) ***Shailesh Nagarkar****, Ashish Lele*[*]*, Dominique Durand, Christophe Chassenieux, and Taco Nicolai, Mechanistic insights into the gelation of regenerated silk fibroin solution, presented in the* **3rd Indo- Australian conference on Biomaterials, Implants, Tissue Engineering and Regenerative Medicine,** ***2009, Sydney, Australia.***

ACKNOWLEDGMENT

First of all I would like to express my sincere gratitude to Dr. Ashish Lele for his invaluable guidance. I have always been a great admirer of his sincerity and dedication to work. His continuous encouragement and support has always inspired me. I think it was my great fortune that I could work closely with Dr. Lele. More than a Ph.D guide, he has always helped me in many situations personally and professionally. I sincerely thank Dr. Lele for all his well wishes, help and guidance.

I take this opportunity to thank Prof. Jayesh Bellare. It was a previledge to have been associated with him. I sincerely thank him for all the trouble and efforts he has taken for me. I would like to acknowledge the many valuable suggestions given to me by my APS committee members, Prof.Norhona and Prof Srivasatava. I would like thank Prof Juveakar for helping us with microcalorimetry experiments. I would also like to thank Anubhav, Shashi, Parag, Chaitanya, Himanshu, Ajay, Hitesh and all my friends in IIT Bombay for their support.

I would like express my gratitude to Prof. Taco Nicolai and Prof. Christophe Chassenieux from the PCI laboratory, University Du Maine, France, for their invaluable guidance on scattering experiments and data analysis which gave the much required initial momemtum to my Ph.D research. I would also like to thank Mr. Komla Ako and Mr. Phillip Weber, my friends in Cite Univercite at Le Mans, France, for their help, support and encouragement.

I would like to acknowledge Dr. Kanika Trivedi and Dr. Nirmalkumar of CSTRI, Mysore for providing silk cocoons reared under controlled conditions. I would like to thank Mrs. Atre form NCCS, Pune, for help in carrying out confocal microscopy. I am thankful to Prof. S. Mazumdar, TIFR, Mumbai for providing access to and for helping me with CD experiments. I would like to thank Mr. Mhatre and all the farmers who have helped me in appreciating sericulture in India. I would like to sincerely thank Dr. Suresh Bhat, Dr. Guruswamy, Dr. Premnath, Dr. Badiger, Dr. Ranade, Mr. Deenadayalan, Mr Harshawardhan, Dr. Neelima and Mrs. Sangeeta for their help and support. I would like to specially acknowledge Dr. Asmita Parbhune for her help in understanding protein chemistry throughout my Ph.D programme, and especially in the beginning stages.

It is my pleasure to thank all present and past PSE-918 lab mates Girish, Sachin, Nitin, Sai, Leena, Rasika, Namrata, Jawahar, Chandu, Mohan, Harsha, Grace, Shubhangi, Suhas, Ashok, Ganapathy, Vipin, Kamendra, Aarti, Anurag, Samruddhi, Kalyani, Nikita,

Purv, Amit, Amruta, Leena, Nandkishore, Venu, Srinivas, Girish, Jeff, Saad and Palak for always maintaining a healthy research atmosphere and for their moral support. I would specially like to thank Avinash for helping me during the long duration fibroin gelation studies. I would like to thank Mr. Shukla for his help and support. I would like thanks to my friends Prashant, Umesh, Kailash, Sharad, Nilesh, Sanjay B., Sanjay T., Parag, Sachin, Sridevi, Sneha for their moral support. I would like thank Khedekar mavashi, without whose support it would have been impossible for me to stay in the NCL residential campus during my Ph.D.

I would like to acknowledge CSIR, India for awarding me the Senior Research Fellowship, and the French Embassy in New Delhi for financial help.

And finally, I would like to express cordial thanks to my family for supporting and encouraging me during every step of this long journey.

Date:-

Signature:-